藥學博士學位論文

The molecular property of Ninjurin1
and its role in bone development

뼈 발생 과정에서 Ninjurin1 단백질의 기능 및
분자적 특성 연구

2017 年 2 月

서울大學校 大學院

藥學科 醫藥生命科學專攻

裵 成 振

The molecular property of Ninjurin1
and its role in bone development

뼈 발생 과정에서 Ninjurin1 단백질의 기능 및 분자적 특성 연구

指導敎授 金 奎 源

이 論文을 藥學博士學位論文으로 提出함

2016年 11月

서울大學校 大學院

藥學科 醫藥生命科學 專攻

裵 成 振

裵 成 振 의 藥學博士學位論文을 認准함

2016年 12月

委 員 長 　　서 영준　　(印)

副委員長 　　이 정 원　　(印)

委　　員 　　하 기 태　　(印)

委　　員 　　이 호 영　　(印)

委　　員 　　김 규 원　　(印)

ABSTRACT

The molecular property of Ninjurin1

and its role in bone development

Sung-Jin Bae

Division of Pharmaceutical Bioscience

College of Pharmacy

The Graduate School

Seoul National University

Osteoclasts (OCs) are bone-resorbing cells that originate from hematopoietic stem cells and develop through the fusion of mononuclear myeloid precursors. Dysregulation of OC development causes skeletal disorders such as osteopetrosis, osteoporosis, and rheumatoid arthritis. Although the molecular mechanisms underlying osteoclastogenesis have been well established, the means by which OCs maintain their survival during OC development remain unknown. In the present study, it was found that Ninjurin1 (Ninj1), a cell surface

protein, supports OC development by enhancing the survival of prefusion OCs (preOCs). Ninj1 expression was dynamically regulated during osteoclastogenesis. In addition, $Ninj1^{-/-}$ mice exhibit mild osteopetrosis owing to impaired OC development. However, typical markers of OC differentiation such as *Nfatc1*, *c-Fos*, *integrinß3*, *Oscar*, and *Calcr* were unaffected by *Ninj1* deficiency. Furthermore, other important events of OC development such as transmigration, fusion, and actin ring formation were also not impaired by the absence of *Ninj1*. Instead, *Ninj1* deficiency increased Caspase-9-dependent intrinsic apoptotic cell death in preOCs. Furthermore, overexpression of *Ninj1* enhanced the survival of mouse macrophage/preOC RAW264.7 cells in osteoclastogenic culture, which suggests that Ninj1 is important for the survival of preOCs. Finally, analysis of publicly available microarray datasets revealed a potent correlation between high *NINJ1* expression and bone disorders in humans. Regarding to Ninj1 molecular property, it was revealed that Ninj1 assembles into a homomeric protein complex composed of two to six monomeric Ninj1 molecules, and the intracellular region of Ninj1 encompassing Leu^{101} to Ala^{110} is important for Ninj1 assembly. Furthermore, Ninj1 is an *N*-glycosylated protein, and the *N*-glycosylation enhances homomer formation and regulates

protein stability and plasma membrane sorting. These findings suggest that Ninj1 plays an important role in bone homeostasis by enhancing the survival of preOCs and might represent a potent therapeutic target for destructive bone disorders. Moreover, targeting of *N*-glycosylation in Ninj1 might be a regulatory strategy for modulation of Ninj1 function(s).

TABLE OF CONTENTS

LIST OF FIGURES

LIST OF TABLES

LIST OF ABBREVIATIONS

7AAD;   7-amino-actinomycin D

BM;   bone marrow

BMM;   bone marrow macrophage

BSA;   bovine serum albumin

CFSE;   carboxyfluorescein succinimidyl ester

Csf1r;   colony-stimulating factor 1 receptor (M-CSF receptor)

CT;   computer tomography

EAE;   experimental autoimmune encephalopathy

FACS;   fluorescence activated cell sorter

FRET;   Förster resonance energy transfer

GEO;   gene expression omnibus

homomer;   homo-oligomer

ITAM;   Immunoreceptor tyrosine-based activation motif

KO;   knock-out

M-CSF;   macrophage colony-stimulating factor

MEM;   modified Eagle medium

Ninj1;   Ninjurin1

OB;   osteoblast

OC;   osteoclast

OPC;   osteoclast progenitor cell

PCR;   polymerase chain reaction

PFA;   paraformaldehyde

preOC;   prefusion osteoclast

qRT-PCR;   quantitative reverse transcription PCR

RANK;   receptor activator of nuclear factor κB

RANKL;   receptor activator of nuclear factor κB ligand

SNP;   single nucleotide polymorphism

TNF-α;   tumor necrosis factor-alpha

TRAP;   tartrate-resistant acid phosphatase

WT;   wild-type

INTRODUCTION

1. Bone and osteoblast

Bone is a highly specialized, hard form of connective tissue whose extracellular matrix is calcified (Gartner and Hiatt, 2001). Bone forms most of the skeleton and is the chief supporting tissue of the body (Steele and Bramblett, 1988). Novel functions of bones are: (1) support for the body, (2) protection for various organs, (3) the mechanical basis for movement, (4) storage for minerals, especially for calcium, (5) a continuous supply of new blood cells (Moore et al., 2013).

Ossification is bone-forming process. From the fetal stage, all bones are developed by two different ossification: intramembranous ossification and endochondral ossification (Gartner and Hiatt, 2001). Intramembranous ossification occurs during the formation of flat bones such as skull, and bony tissues by intramembranous ossification are formed directly from mesenchyme. Endochondral ossification occurs in long bone such as femur, tibia, and humerus, and these bones are developed via cartilage originating from mesenchyme (Currey, 2013).

Ossification is tightly regulated by osteoblasts (OBs). OBs are bone-forming cells and carry out three major roles: (1) secretion of bone matrix which mineralizes to form new bone, (2) regulation of osteoclast (OC) differentiation, (3) supporting hematopoietic cell growth and differentiation (Rosen et al., 2009). They are derived from osteoprogenitor cells which arise from mesenchymal stem cells (Figure 1). OB commitment, differentiation, and function are governed by several transcription factors including Runx2 and Osterix (Marie, 2008). Genetic ablation of Runx2 resulted in failure of osteoblastogenesis, and bone formation was completely blocked in Osterix knockout mice (Rutkovskiy et al., 2016). Dysregulation of OB differentiation and function cause(s) inadequate mineral deposition in bone and excessive mineralization of bone, which are manifested as osteoporosis and osteopetrosis, respectively (Del Fattore et al., 2008; Zuo et al., 2012).
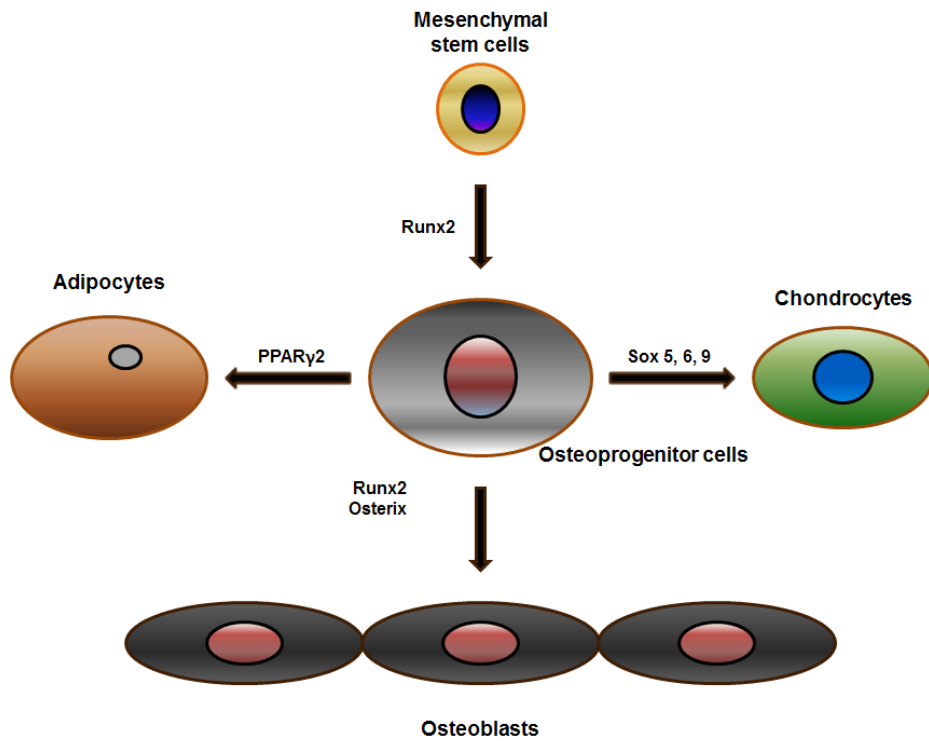
Figure 1. Differentiation of mesenchymal lineage cells and fate-determining transcription factors.

2. Osteoclast

Bone remodeling depends on the balance between bone formation by OBs and bone resorption by OCs. OCs are bone-resorbing cells originating from monocyte/macrophage precursor cells of myeloid lineage derived from hematopoietic progenitor cells (Figure 2). In the bone microenvironment (Figure 3), OC differentiation is mediated by two essential cytokines, M-CSF and RANKL, produced by OBs, stromal cells, and T lymphocytes (Edwards and Mundy, 2011). M-CSF sustains the survival of OC precursors and mature OCs, and RANKL promotes OC differentiation via induction of NFATc1, master transcription factor of osteoclastogenesis (Boyle et al., 2003; Edwards and Mundy, 2011). As a result, the OCs have unique morphological features such as multinucleation, accomplished by fusion of mononuclear OC precursor cells, and actin ring cytoskeleton, composed of podosome belts (Saltel et al., 2008; Vignery, 2005). Therefore, fine movements and well-organized actin ring cytoskeletons are prerequisite not only for cell-cell fusion but for resorptive function in OCs (Saltel et al., 2008). Dysregulation of OC development and function leads to pathological bone disorders such as osteopetrosis,

Paget's disease, rheumatoid arthritis and postmenopausal osteoporosis (Layfield, 2007; Makras et al., 2015; Sato and Takayanagi, 2006; Sobacchi et al., 2013).
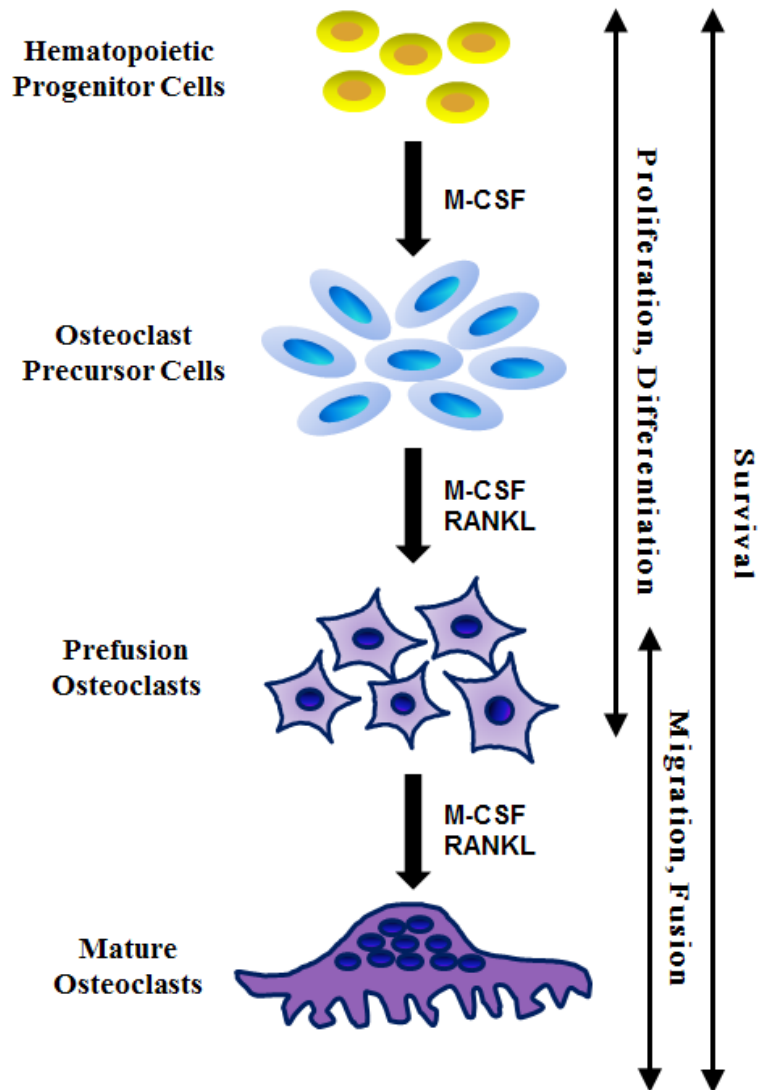
Figure 2. Differentiation of OC and related factors.
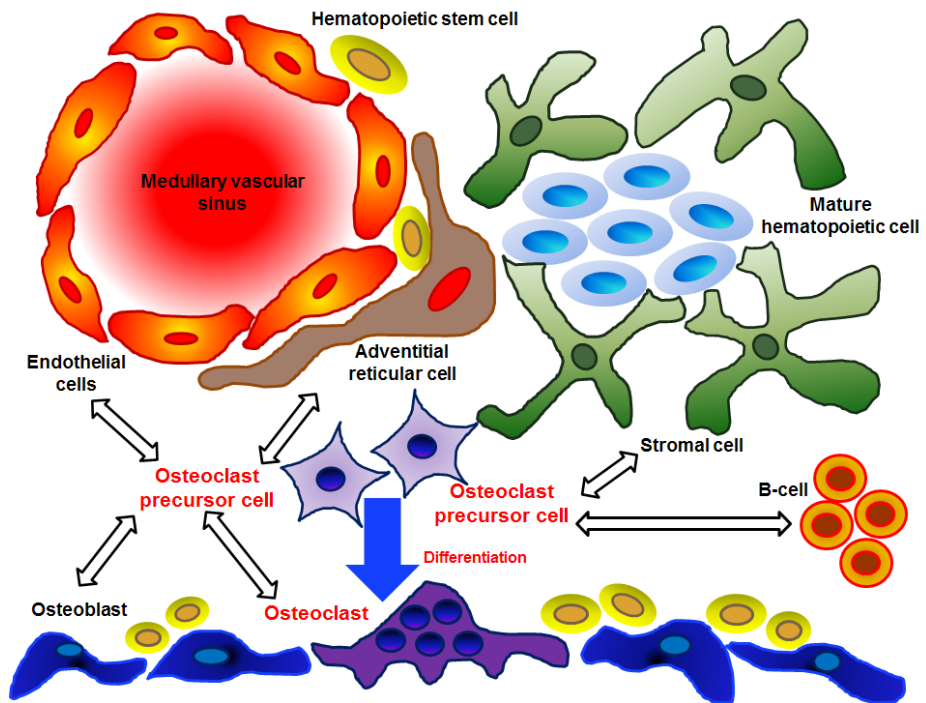
Figure 3. Schematic diagram of bone microenvironment.

3. Ninjurin1

Ninjurin1 (Ninj1) is a transmembrane protein and identified in neurons and Schwann cells after sciatic nerve injury (Araki and Milbrandt, 1996). Ninj1 is composed of two transmembrane regions, one intracellular region, and two extracellular regions of N- and C-termini (Figure 4). In addition, 12 amino acid residues, from Pro^{26} to Asn^{37} positioned in the extracellular region of the N-terminus, were identified as a domain with homophilic binding affinity in a *trans*-interaction (Araki et al., 1997). Furthermore, it was reported that Ninj1 is expressed in perivascular macrophages nearby hyaloid vessels and induces apoptosis of vascular endothelial cells by enhanced secretion of Angiopoietin2 and Wnt7b (Lee et al., 2009). In addition, it was also reported that Ninj1 is expressed in myeloid cells, such as monocytes, macrophages, and microglia in EAE induced rat brain and mouse spinal cord which subsequently modulates the infiltration of inflammatory myeloid cells (Ahn et al., 2014b; Ahn et al., 2009). Ifergan et al. (2011) also showed that Ninj1 is expressed in monocytes and dendritic cells located in multiple sclerosis lesions of the human brain, suggesting that the function of Ninj1 is conserved in mice and humans. Moreover, it

was reported that Ninj1 is upregulated by lipopolysaccharide (LPS) and regulates LPS-induced inflammation in macrophages (Jennewein et al., 2015; Shin et al., 2016). Ninj1 also plays a role in other cells and tissues. For example, *Ninj1*^{-/-} mice are resistant to erectile dysfunction in a streptozotocin-induced diabetic model (Yin et al., 2014). Furthermore, Ninj1 prevents p53-mediated cellular senescence by reducing *p53* translation (Cho et al., 2013).
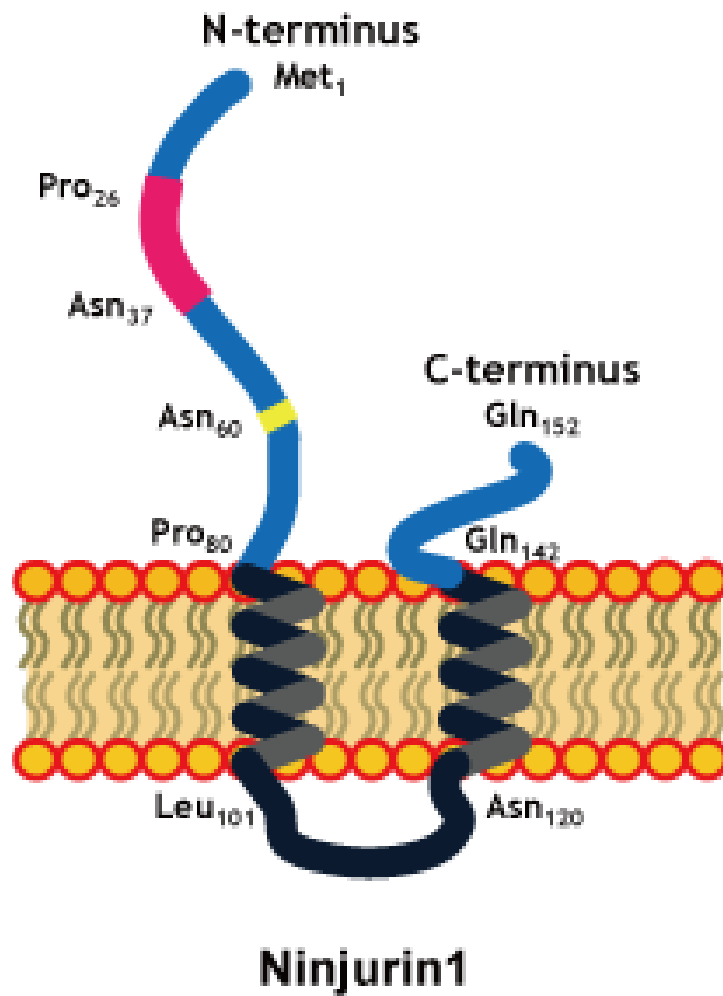
Figure 4. Diagrammatic description of Ninj1.

4. Homomeric protein complex

In a living cell, individual proteins are constantly and physically interacting with other proteins (Marsh and Teichmann, 2015). Protein interactions can be classified as permanent and transient interactions based on their strength and persistence (Nooren and Thornton, 2003). Multi-subunits of quaternary complexes are composed of permanently interacting proteins. Homomers are oligomeric quaternary complexes composed of identical protein subunits. Most proteins form homomers (Kühner et al., 2009; Levy et al., 2006; Marsh and Teichmann, 2014). Homomeric oligomerization is proposed to advantages including the formation of an active site, enhanced protein stability, increased binding affinity to the other biological molecules (Perica et al., 2012). Dysregulated interactions in the assembly of a homomeric complex can result in detrimental status such as Alzheimer's disease and Creutzfeldt-Jakob disease (Dobson, 2003).

PURPOSE OF THIS STUDY

Ninj1 has been known as a transmembrane protein which enhances macrophage adhesiveness to endothelium. Moreover, it was revealed that Ninj1 promotes LPS-induced inflammation through direct binding to LPS in macrophages. However, the role of Ninj1 in OCs, myeloid lineage descent, has not yet been elucidated. Furthermore, previous studies have focused on cellular phenomena so that the precise mechanisms and molecular property need to be elucidated.

Here, I found that Ninj1 is expressed in OCs and dynamically regulated during OC differentiation. $Ninj1^{-/-}$ mice show mild osteopetrosis related to the defective OC development. In addition, *Ninj1* deficiency leads to increased apoptosis in preOCs resulting in reduced numbers of mature OCs. Furthermore, high *NINJ1* expression is associated with human bone disorders, such as rheumatoid arthritis and postmenopausal osteoporosis. Regarding the Ninj1 molecular property, I found that Ninj1 assembles into a homomeric protein complex via a *cis*-interaction, which is composed of six monomeric

Ninj1 molecules. It has been revealed that the intracellular region of Ninj1 encompassing Leu^{101} to Ala^{110} is important for the Ninj1 assembly. I further demonstrated that Ninj1 is an *N*-glycosylated protein, and that *N*-glycosylation enhances homomer formation and membrane targeting. These findings suggest that Ninj1 has a novel role in OC development and bone homeostasis and might represent a potent therapeutic target for destructive bone disorders, and that targeting of *N*-glycosylation might be a regulatory strategy for modulation of Ninj1 function(s).

MATERIALS AND METHODS

1. Ethics statement

All mice were housed in animal care facility of Seoul National University under specific pathogen-free condition and animal procedures conducted in this study were approved by the Institutional Animal Care and Use Committees of Seoul National University.

2. Animals

$Ninj1^{-/-}$ mice were described previously (Ahn et al., 2014b). All animal studies were performed with male mice to exclude sex hormonal effects. The PCR primer sequences for genotyping are as following: wild-type (forward), 5'-AGG GAG CTA CGG CCA TAT CTC-3'; wild-type (reverse), 5'- GGA TCT GCC AGG CAA GCA-3'; neomycin (forward), 5'-CGA ATT CGA ACA CGC AGA TG-3'; neomycin (reverse), 5'- GTG CCC AGT CAT AGC CGA AT-3'.

3. Radiologic analysis

Hind limbs were isolated from 6-week-old or 12-week-old mice and scanned individually by radiology apparatus. Simple plain radiologic images were obtained by IVIS Spectrum CT (PerkinElmer, Waltham, MA) with Living Image Software 4.4.0. (PerkinElmer), and microCT images were acquired by Quantum GX microCT (PerkinElmer) at 10-μm isotropic resolution and processed with Caliper Viewer 1.3.0 (PerkinElmer). Trabecular bone was measured in the 1-mm region in length encompassing the region of distal metaphysis away from the proximal edge of the growth plate in the distal end of femurs and of the proximal metaphysis away from the distal edge of the growth plate in the proximal end of tibias and analyzed with Inveon Research Workplace (Siemens, Malvern, PA).

4. Plasmid construction, transfection and retroviral infection

The coding region of mouse Ninj1 was PCR amplified and cloned into indicated vectors. For Lifeact-mCherry, sense and antisense

oligonucleotides of Lifeact sequence (Riedl et al., 2008) were synthesized and cloned into pMX-IRES-Puromycin^R with PCR-amplified mCherry. CFP and YFP used in a FRET assay are A206K monomeric variants. CFP-fused YFP, used as FRET-positive control, is composed of N-terminal CFP, 18 amino acids linker, and C-terminal YFP. Retroviral packaging was performed by transfecting Platinum A or E with linear polyethylenimine (Polysciences, Warrington, PA). Cultured media containing viral particles were collected after 48 hours and filtered through 0.45-μm syringe filters. Subsequently, target cells were cultured in virus containing media with 5 μg/mL of polybrene (hexadimethrine bromide; Sigma-Aldrich, St. Louis, MO). Sequences of Ninj1 and Scrambled siRNA were described previously (Shin et al., 2016). For knockdown experiments, RAW264.7 cells were transfected with either Ninj1 or Scrambled siRNA using Lipofectamine RNAiMAX (Invitrogen, Carlsbad, CA). All mammalian expression vectors of plasmid and retrovirus are summarized in Table 1 and 2, respectively.

5. Reagents

In experiments of OC development, recombinant mouse M-CSF, GM-CSF, IL-4, and RANKL were purchased from BioLegend (San Diego, CA). Lipofectamine RNAiMax and AF488-phalloidin were purchased from Invitrogen. Anti-Ninj1$_{1-15}$ antibody used for immunoblot assay was described previously (Ahn et al., 2014b). Anti-NFATc1 antibody was purchased from Pierce and anti-Oscar antibody was obtained from R&D Systems (Minneapolis, MS). Antibodies against Integrinβ3, c-Fos, cleaved Caspase-3, -8, -9 and cleaved PARP were purchased from Cell Signaling Technology (Mountain View, CA). For investigating Ninj1 homomer, antibodies were obtained against FLAG-tag (Sigma-Aldrich), DDDDK-tag (Abcam, Cambridge, UK), c-Myc (Santa Cruz, Dallas, TX), Myc-tag (MBL, Nagoya, Japan), GFP (Santa Cruz), α-tubulin (Sigma-Aldrich), actin (Sigma-Aldrich), and vinculin (Sigma-Aldrich). The previously described anti-Ninj1 Ab$_{1-15}$ (Ahn et al., 2014b) was used for immunoprecipitation and immunoblot assays. Antibody-conjugated magnetic agaroses were obtained against FLAG (Sigma-Aldrich), DDDDK-tag (MBL), Myc-tag (MBL), GFP (MBL). Polybrene and blasticidine S hydrochloride were obtained from

Sigma-Aldrich. Puromycin hydrochloride and G418 sulfate were purchased from Cayman Chemical (Ann Arbor, MI) and Enzo Life Sciences (Farmingdale, NY), respectively. For FACS analysis, Fc block, PE-anti-mouse CD115 antibody, APC-anti-mouse CD117 antibody, and V450-anti-mouse CD11b antibody were purchased from BD Biosciences (Bedford, MA). Anti-TRAP antibody, biotin-anti-RANK antibody, and APC/Cy7 streptavidin were obtained from BioLegend.

6. *In vitro* osteoclastogenesis

Bone marrow cells were obtained from femurs and tibias of 7-week-old *Ninj1*$^{-/-}$ mice or their WT littermates and used for differentiation into macrophages or OCs. In brief, bone marrow cells were isolated by flushing the diaphysis of femurs and tibias with PBS and incubated overnight in α–MEM supplemented with 10% FBS to remove non-hematopoietic lineage cells. After discarding adherent cells, floating cells were further incubated in α-MEM supplemented with 10% FBS and M-CSF (30 ng/mL). After 3 days, non-adherent cells were removed and BMMs were used as OC precursor cells. For generation of OCs, BMMs were further cultured in α-MEM supplemented with 10%

FBS and M-CSF (30 ng/mL) and RANKL (100 ng/mL) for indicated days.

7. Cell culture

To isolate cells from liver and spleen, both tissues were grinded by gentleMACS dissociator (Miltenyi Biotec, Bergisch Gladbach, Germany) and centrifuged at 50 g for 3 minutes. Supernatants were collected and filtered through 100-µm cell strainer to dissociate as single cells. Dissociated cells were counted and subjected to formaldehyde cross-linking assay. RAW264.7 cells were purchased from Korean Cell Line Bank and maintained in Dulbecco's MEM (DMEM) with 10% FBS. For OC differentiation, RAW264.7 cells were cultured in α-MEM supplemented with 10% FBS and RANKL (30 ng/mL). MC3T3-E1 cells were obtained from the American Type Culture Collection (ATCC; Manassas, VA) and maintained in α-MEM supplemented with 10% FBS and treated with osteogenic stimuli as indicated. RAW264.7 cells were transduced using a retrovirus containing IRES-GFP or Ninj1-FLAG-IRES-GFP and GFP expressing cells were sorted by FACSAria III (BD Biosciences). Expression of

Ninj1-FLAG was confirmed by immunoblot assay and cells were conducted to Annexin V and 7AAD analysis. In this case, APC-Annexin V (Biolegend) was applied instead of FITC-Annexin V. HEK293T and NIH3T3 cells were obtained from the ATCC and Korean Cell Line Bank (Seoul, Korea), respectively, and maintained in DMEM with 10% FBS. For inhibition of *N*-glycosylation, cells were incubated with tunicamycin (1 μg/mL, Cayman chemical) for 24 hours. Tunicamycin was dissolved in dimethyl sulfoxide (1 mg/mL).

8. TRAP activity staining and measurement of TRAP activity

TRAP activity assay was performed using TRAP Staining Kit (Kamiya Biomedical Company, Tukwila, WA) according to manufacturer's protocol. For TRAP activity staining, cultured cells were fixed with 4% PFA, washed with distilled water, and incubated with chromogenic substrates in tartrate-containing buffer for 1 hour at 37℃. Following colorization, TRAP-positive multinucleated cells (nuclei 3 or more) were counted and images were obtained with Axiocam MRc installed to Axiovert 200M (Zeiss, Oberkochen,

Germany). OC-conditioned media and protein lysates were conducted to measure TRAP activity. To measure TRAP activity in conditioned media, OC culture media were refreshed 24 hours prior to collection at indicated days. Collected media were immediately centrifuged to remove cell debris. Supernatants were incubated with the chromogenic substrates in tartrate-containing buffer for 3 hours at 37℃. To measure TRAP activity in protein lysates, cells were lysed in an extraction buffer containing 100 mM Tris pH 8.0, 150 mM NaCl, 1% NP-40, and proteinase inhibitor cocktail (Calbiochem, San Diego, CA), and lysates were subjected to TRAP activity assay. Following incubation, residual activity was inhibited by 4% NaF for 30 minutes and an absorbance at 540 nm was measured using microplate reader (Spectra Fluor; Tecan, San Jose, CA).

9. FACS analysis

To identify OPCs, bone marrow cells were incubated with mouse Fc Block (anti-mouse CD16/CD32) in 3% BSA/PBS for 30 minutes. Then, cells were stained with antibodies for PE-anti-mouse CD115, APC-anti-mouse CD117, and V450-anti-mouse CD11b for 1 hour, and

analyzed by FACS. To characterize OC precursor cells, bone marrow cells were cultured with M-CSF (30 ng/mL) for 3 days. Differentiated BMMs were preincubated with mouse Fc Block and streptavidin in 3% BSA/PBS for 30 minutes. Subsequently, cells were stained with PE-anti-mouse CD115, V450-anti-mouse CD11b, and biotin-anti-RANK antibody followed by incubation with APC/Cy7 streptavidin. Stained cells were subjected to FACS analysis. To discriminate apoptotic cells, BMMs cultured with M-CSF and RANKL were collected and stained with FITC-Annexin V and 7AAD at indicated days. Subsequently, stained cells were analyzed using FACS. FACS-based FRET assay was adopted from previously described methods (Banning et al., 2010). NIH3T3 cells were retrovirally transduced with WT or Asn^{60} mutant CFP- and YFP-Ninj1 as indicated. Transduced cells were cultured with proper antibiotics for 3 days and subjected to FACS analysis. To identify CFP and YFP, cells were exposed to 405-nm violet laser combined with 448/45 bandpass filter and 488-nm blue laser with 527/32 bandpass filter, respectively. FRET signal was acquired through 528/45 bandpass filter excited by 405-nm violet laser. FRET-positive cells from YFP emission by 405-nm laser were gated first and the remaining FRET-positive cells from CFP emission by 405-nm laser

were gated again (cerulean and brown pentagonal gate in Figures, respectively). All flow cytometric assays were performed using FACSVerse (BD Biosciences) and analyzed with FACSuite 1.0.5 (BD Biosciences).

10. Confocal microscopy

To visualize the multinucleated giant cells, BMMs were cultured on glass coverslips with M-CSF (50 ng/mL) + IL-4 (100 ng/mL) or GM-CSF (50 ng/mL) + IL-4 (100 ng/mL). At day 6, cells were washed with PBS and stained with CFSE (5 μM) for 5 minutes. Subsequently, cells were fixed with 4% PFA and counterstained with Hoechst 33342. To assess the transmigration of preOCs, Lifeact-mCherry was retrovirally transduced into BMMs. Transduced BMMs were selected and further cultured with M-CSF (30 ng/mL) and RANKL (100 ng/mL) for 3 days. Then, cells were detached and overlaid on a confluent monolayer of GFP-expressing MC3T3-E1 cells. Serial images were stacked for 10- to 14-μm depth by 0.4-μm interval. To measure the actin ring cytoskeletons and size of OCs, BMMs were cultured on glass coverslips with M-CSF (30 ng/mL) and RANKL (100 ng/mL) for 6

days and fixed with 4% PFA. Following permeabilization with 0.05% Triton X-100, cells were stained with AF488-phalloidin to visualize F-actin. The area surrounded by actin ring cytoskeleton was calculated with ImageJ 1.47t (National Institutes of Health, Bethesda, MD). Interaction between CFP and YFP was examined using a photobleaching FRET method (Broussard et al., 2013). CFP, YFP, CFP-fused YFP, CFP-Ninj1, and YFP-Ninj1 were retrovirally transduced into NIH3T3 cells singly or in combination as indicated. Transduced cells were cultured with proper antibiotics for 3 days and replated on glass coverslips. Adherent cells were fixed with 4% PFA/PBS and subjected to confocal microscopy. CFP and YFP were excited with 405- and 514-nm laser, respectively. Emission from CFP and YFP were detected in the spectral window of 459–510 nm and 520–580 nm, respectively. Images were acquired before and after YFP quenching by 514-nm laser. The intensity of CFP was measured using ZEN 2012 (Zeiss) and restoration of CFP intensity was assessed as FRET positive. All images except for FRET images were obtained using LSM 700 confocal microscope (Zeiss) and processed with ZEN 2012 (Zeiss). FRET images were obtained using an LSM 710 confocal microscope (Zeiss) and processed using ZEN 2012 (Zeiss).

11. Proliferation assay

Measurement of cell growth by MTS was described previously (Park et al., 2014). In brief, 1×10^4 BMMs/well were seeded on 96-well plates and cultured with M-CSF (30 ng/mL) and RANKL (100 ng/mL) singly or in combination as indicated. At the indicated time, 20 μl of substrate solution was added to each well, and incubated for 3 hour at 37℃. Reaction was stopped by adding 25 μL of 10% SDS and an absorbance at 492 nm was measured using microplate reader (Spectra Fluor; Tecan). Data are expressed as fold ratio to day 0.

12. Protein cross-linking with formaldehyde

PFA was dissolved for 4% (w/v) in PBS for 1 hour at 80℃. The solution was filtered through 0.22-μm cellulose acetate filter, aliquoted, and stored at -80℃. For protein cross-linking, 2×10^7 cells were suspended in 0.5 mL of PFA/PBS as indicated and incubated at room temperature with mild agitation. After 30 minutes, residual activity of formaldehyde was quenched with 1 mL of cold 125mM glycine/PBS.

Then, cells were lysed and subjected to immunoprecipitation followed by immunoblot assay.

13. Immunoblot assay

Cells were lysed in RIPA buffer containing 25 mM Tris pH 7.4, 150 mM NaCl, 5 mM $MgCl_2$, 0.5% NP-40, phosphatase inhibitor cocktail (Sigma-Aldrich), and proteinase inhibitor cocktail (Calbiochem). Protein concentration was determined by BCA assay. Lysates (20 to 40 µg) were resolved on polyacrylamide gel and then immunoblotted as described previously (Shin et al., 2016). To identify the *N*-glycosylation of Ninj1, 50 µg of lysates were resolved on 16% 3C tricine-SDS polyacrylamide gel (Schagger, 2006).

14. RNA isolation and qRT-PCR

Total RNA was isolated with TRIzol reagent (Invitrogen) and cDNA was obtained from 2 µg of total RNA using MMLV reverse transcriptase (Promega Corporation, Madison, WI). Quantitative real-time PCR was then performed using StepOnePlus real-time PCR system (Applied Biosystems, Foster City, CA) with RealHelix qPCR

kit (NanoHelix, Seoul, Korea). Relative mRNA expression levels were calculated using the comparative 2-ΔΔCt method. Gapdh and/or Hprt served as an internal control. Data are expressed as relative mRNA expression. Primer sequences and conditions for PCR are summarized in Table 1.

15. Microarray analysis

I compiled 4 publicly available gene expression datasets of human samples from the GEO (accession no.GSE1964, GSE7158, GSE7524 and GSE27390). Raw feature data from 3 data sets (GSE7158, GSE7524, GSE27390) were normalized using MAS5 method (R package affy). Dataset GSE1964 was downloaded from GEO as already normalized. The average expression values were calculated for samples. *NINJ1* gene with absolute fold change at least 1.3 between compared groups was assigned as differentially expressed. The *t*-test was calculated to evaluate statistical significance between the compared groups using SigmaPlot version 12.5.0. (Systat Software Inc., San Jose, CA).

16. Statistical analysis

Data are presented as the mean ± SD. Data were calculated and analyzed with SigmaPlot 12.5.0. (Systat Software Inc.). The two-tailed Student t-test was used to determine the significance of differences between two groups. Data in Figure 18C and 20B were analyzed by Mann-Whitney U test. Data in Figure 29C and 29D were analyzed by paired t-test and one-tailed Student t test, respectively. Differences with $P < 0.05$ were considered as significant.

Insert	Vector	Length (bp)
FLAG-Ninj1	pCMV Tag2b	501
FLAG-Ninj1(1-110)	pCMV Tag2b	396
FLAG-Ninj1(Δ101-110)	pCMV Tag2b	471
FLAG-Ninj1(N60Q)	pCMV Tag2b	501
FLAG-Ninj1(N60A)	pCMV Tag2b	501
FLAG-NINJ1	pCMV Tag2b	519
GFP-Ninj1	pCS2+	1191
GFP -Ninj1(1-100)	pCS2+	1035
GFP -Ninj1(1-110)	pCS2+	1065
GFP -Ninj1(1-120)	pCS2+	1095
GFP -Ninj1(1-140)	pCS2+	1155
GFP -Ninj1(21-152)	pCS2+	1134
GFP -Ninj1(41-152)	pCS2+	1074
GFP -Ninj1(61-152)	pCS2+	1014
GFP -Ninj1(101-152)	pCS2+	894
GFP-Ninj1(Δ101-110)	pCS2+	1161
GFP-NINJ1	pCS2+	1191

Table 1. List of plasmid vectors.

Insert	Vector	Length (bp)
DsRed	pMX	678
GFP	pMX	720
Lifeact-mCherry	pMX-IRES-Puromycin[R]	774
Oscar(SP-L)-Myc	pMX-IRES-Puromycin[R]	1050
Oscar(SP-S)-Myc	pMX-IRES-Puromycin[R]	1032
Ninj1-FLAG	pMX-IRES-GFP	549
Ninj1-FLAG	pMX-IRES-Blasticidine[R]	549
Ninj1-FLAG(1-70)	pMX-IRES-Blasticidine[R]	303
Ninj1-FLAG(1-113)	pMX-IRES-Blasticidine[R]	432
Ninj1-FLAG(71-152)	pMX-IRES-Blasticidine[R]	342
FLAG-Ninj1	pMX-IRES-Blasticidine[R]	501
FLAG-Ninj1(N60Q)	pMX-IRES-Blasticidine[R]	501
FLAG-Ninj1(N60A)	pMX-IRES-Blasticidine[R]	501
Myc-Ninj1	pMX-IRES-Neomycin[R]	498
Myc-Ninj1(N60Q)	pMX-IRES-Neomycin[R]	498
Myc-Ninj1(N60A)	pMX-IRES-Neomycin[R]	498
CFP	pMX-IRES-Blasticidine[R]	720
CFP-fused YFP	pMX-IRES-Blasticidine[R]	1491
CFP-fused YFP	pMX-IRES-Puromycin[R]	1491
CFP-Ninj1	pMX-IRES-Puromycin[R]	1191
CFP-Ninj1(N60Q)	pMX-IRES-Puromycin[R]	1191
CFP-Ninj1(N60A)	pMX-IRES-Puromycin[R]	1191
YFP	pMX-IRES-Puromycin[R]	720
YFP-Ninj1	pMX-IRES-Puromycin[R]	1065
YFP-Ninj1(N60Q)	pMX-IRES-Puromycin[R]	1155
YFP-Ninj1(N60A)	pMX-IRES-Puromycin[R]	1095

Table 2. List of retroviral vectors.

Gene	Forward (5' → 3')	Reverse (5' → 3')
Gapdh	CAGTGCCAGCCTCGTCCCGTAGA	CTGCAAATGGCAGCCCTGGTGAC
Hprt	GTAATGATCAGTCAACGGGGGAC	CCAGCAAGCTTGCAACCTTAACCA
Ninj1	TCTTCATTACGGCCTTCGGG	CCCTTAAAGTCTCTGGGCGTT
Nfatc1	CCCGTCACATTCTGGTCCAT	CAAGTAACCGTGTAGCTGCACAA
c-Fos	CGGGTTTCAACGCCGACTA	TTGGCACTAGAGACGGACAGA
Itgb3	GATGACATCGAGCAGGTGAAAGAG	CCGGTCATGGATAGTGATGAGTAG
Oscar	TCTGCCCCCTATGTGCTATCA	AGGAGCCAGAACCTTCGAAAC
Calcr	GCCTCCCCATTTACATCTGC	CTCCTCGCCTTCGTTGTTG
c-Src	GGACAGCGGCGGTTTCTACATC	AGCTGCTGCAGGCTGTTGA
Atp6v0d2	GAAGCTGTCAACATTGCAGA	TCACCGTGATCCTTGCAGAAT
Dcstamp	CAAGGAACCCAAGGAGTCGT	ACCCAAGTCTCAGACACACTG
Itgav	GTGTCCGACCACCTCAAGAA	GTGGTGAACTTGGAGCGGA
Cd44	TGGTGATCAACGGTGGCAAT	GGGGTCTCTGATGGTTCCTTG
Trap	CGACCATTGTTAGCCACATACG	CACATAGCCCACACCGTTCTC
Ctsk	AATACGTGCAGCAGAACGGAGGC	CTCGTTCCCCACAGGAATCTCTCTGTAC
Mmp9	CAGGGAGATGCCCATTTCG	GGGCACCATTTGAGTTTCCA

Table 3. List of primer sequences for qRT-PCR.

RESULTS

1. OCs express high amount of Ninj1 and deletion of *Ninj1* induces bone abnormality in mice

Previous reports have revealed that Ninj1 is expressed in myeloid cells including monocytes, macrophages, and microglia in EAE-induced rat brain and mouse spinal cord (Ahn et al., 2014b; Ahn et al., 2009). Ifergan et al. (2011) also have shown that Ninj1 is expressed in monocytes and dendritic cells in inflamed CNS lesion. Based on these results, I further investigated Ninj1 expression in myeloid lineage cells and found that Ninj1 is highly expressed in mature OCs (Figure 5A). This result suggests that Ninj1 might be involved in regulation of bone homeostasis *in vivo*. Assessment of the hind limbs of 6- or 12-week-old *Ninj1*$^{-/-}$ mice by plain radiology indicated that the metaphysis and diaphysis intensities were stronger than those of WT littermates. Furthermore, femur morphologies were linear rather than concave (Figure 5B).

A

	BMM (M-CSF)	BMM (M-CSF + IL-1β)	BMM (M-CSF + TNF-α)	BMDC (GM-CSF)	BMDC (Flt3L)	Osteoclast (M-CSF+RANKL)	BMM + IL-4	Giant Cell (GM-CSF+IL-4)	Giant Cell (M-CSF+IL-4)
Ninj1									
α-Tubulin									

B

$Ninj1^{+/+}$ $Ninj1^{-/-}$

6 weeks-old

12 weeks-old
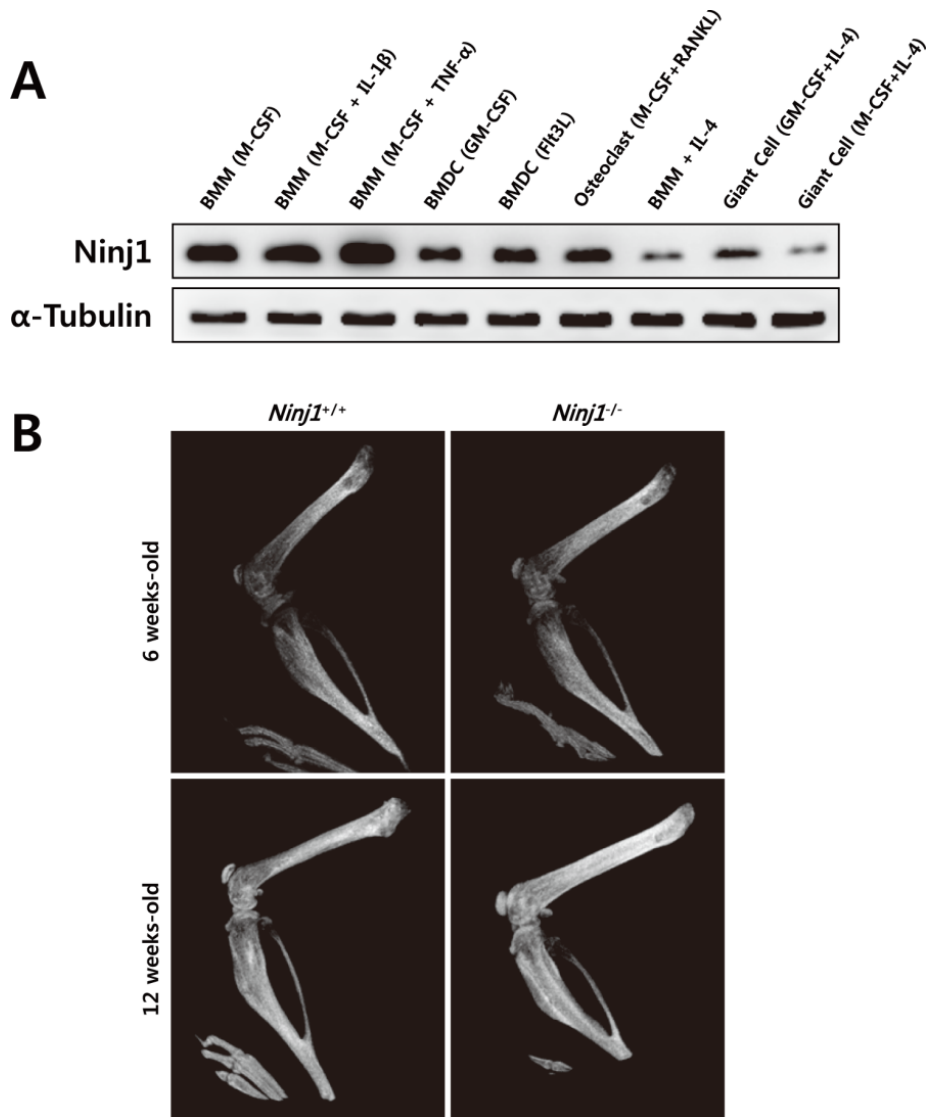
Figure 5. The expression of Ninj1 in various myeloid lineage cells and radiologic images of hind limbs.

33

(A) Ninj1 expression was assessed in *in vitro* differentiated myeloid lineage cells by immunoblot assay. (B) Representative plain X-ray images of hind limbs from *Ninj1*-deficient 6- and 12-week-old mice and their corresponding WT littermate mice.

2. *Ninj1* deficiency induces mild osteopetrosis in mice

To further investigate *Ninj1* deficiency-associated bone abnormalities, I compared distal femurs and proximal tibias from 6- or 12-week-old WT and *Ninj1*$^{-/-}$ male mice by microCT analysis. As expected, a clear trabecular bone mass increase was observed not only in femurs, but also in tibias of *Ninj1*$^{-/-}$ mice (Figure 6A,7A). Quantitative measurements revealed increases of bone parameters, such as the trabecular tissue volume (Bone Volume/Total Volume), thickness, and number in *Ninj1*$^{-/-}$ mice. In contrast, the bone surface area (Bone Surface Area/Bone Volume) and the space between trabecular architectures (Trabecular Spacing) were decreased (Figure 6B,7B). These data indicate that *Ninj1* deficiency stimulates osteopetrosis in mice.
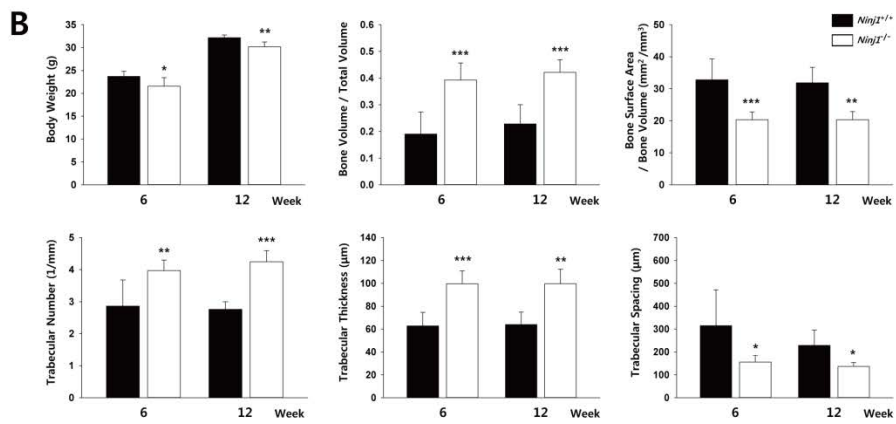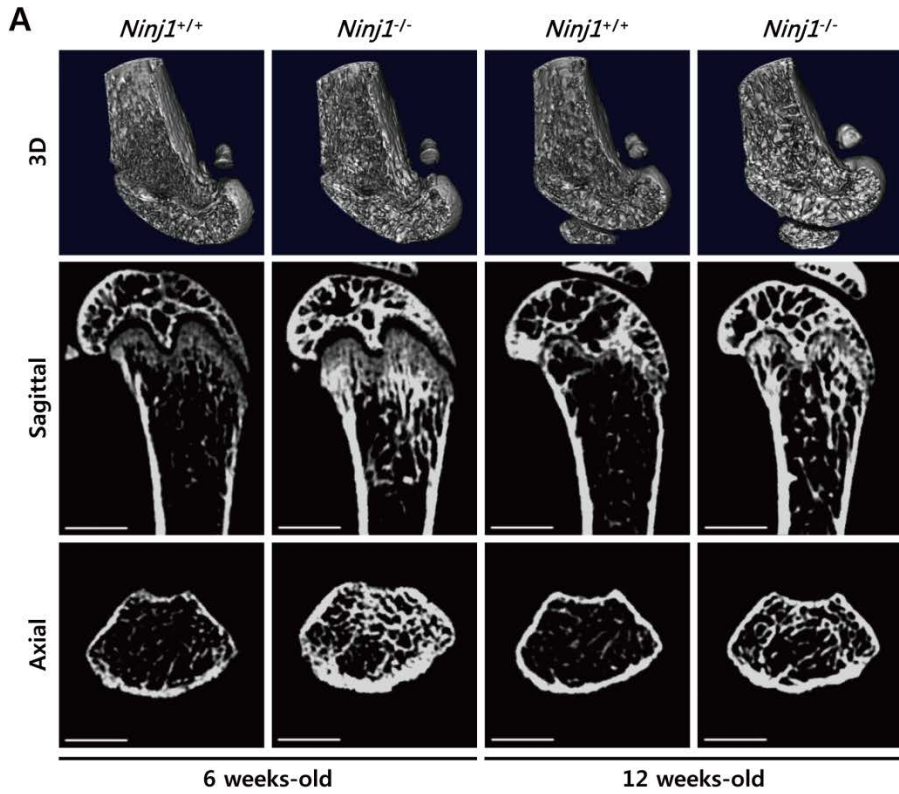
Figure 6. microCT analysis of distal femur.

(A) Representative microCT images of distal femurs from *Ninj1*-deficient 6- or 12-week-old mice and their corresponding WT littermate mice. Scale bars, 1 mm. (C) microCT-determined trabecular bone parameters of distal femurs from 6- or 12-week-old WT (n = 5, n = 4, respectively) and *Ninj1*-deficient mice (6-weeks-old; n = 7, 12-weeks-old; n = 6). All quantitative data are shown as the mean ± SD, *$P <$ 0.05, **$P < 0.01$, ***$P < 0.001$.
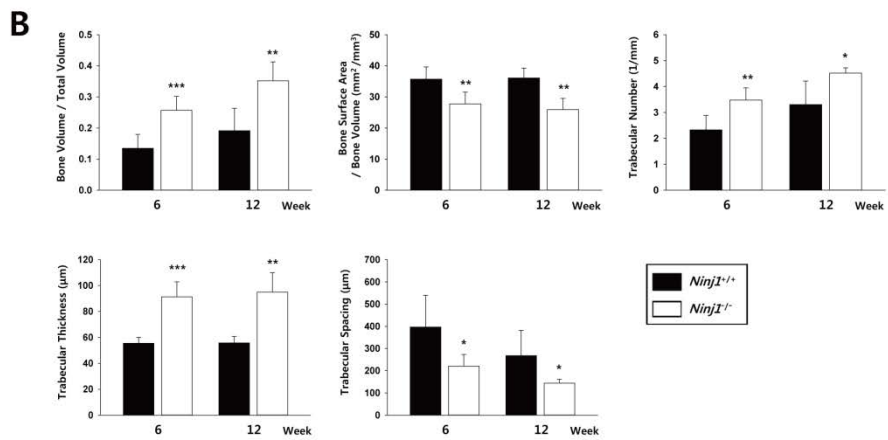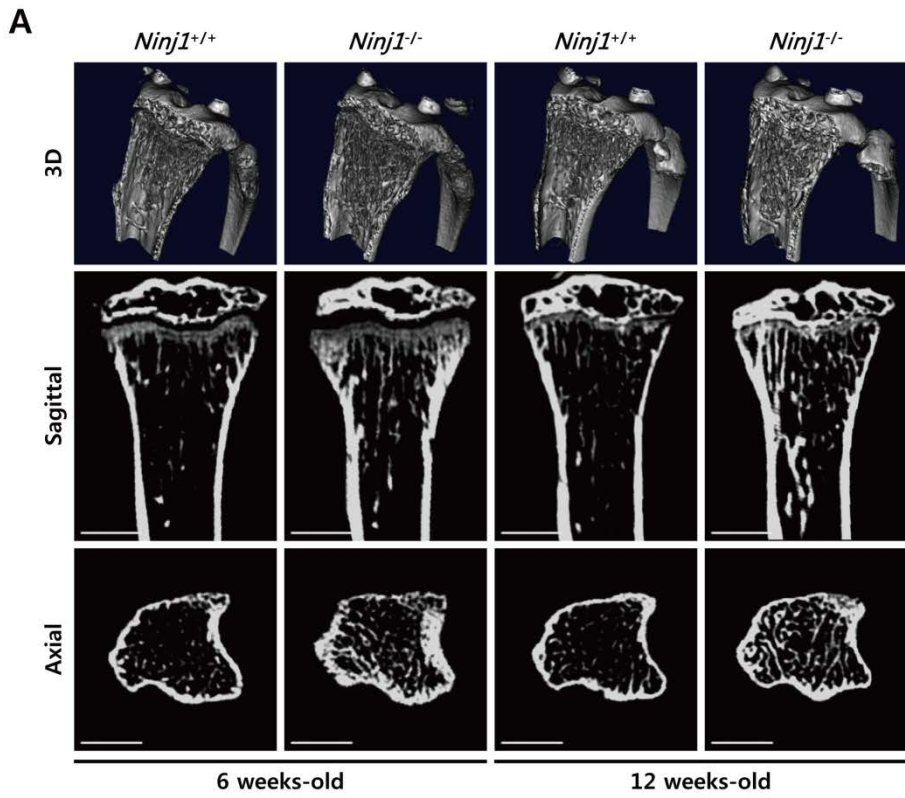
Figure 7. microCT analysis of proximal tibia.

(A) Representative microCT images of proximal tibias from *Ninj1*-deficient 6- or 12-week-old mice and their corresponding WT littermate mice. Scale bars, 1 mm. (C) microCT-determined trabecular bone parameters of proximal tibias from 6- or 12-week-old WT (n = 5, n = 4, respectively) and *Ninj1*-deficient mice (6-weeks-old; n = 7, 12-weeks-old; n = 6). All quantitative data are shown as the mean ± SD, *$P < 0.05$, **$P < 0.01$, ***$P < 0.001$.

3. Ninj1 is expressed in OCs, not in OBs

OBs are bone-producing cells and balance bone metabolism together with OCs (Long, 2012). To determine whether OBs express Ninj1, I cultured the murine OB cell line MC3T3-E1, challenged with several osteogenic stimuli or in osteoblastogenic condition. qRT-PCR and immunoblot assays identified no substantial Ninj1 expression in OBs but high expression in OCs (Figure 8). These data suggest that the mild osteopetrotic phenotype in Ninj1-deficient mice might result from dysregulated OC development.
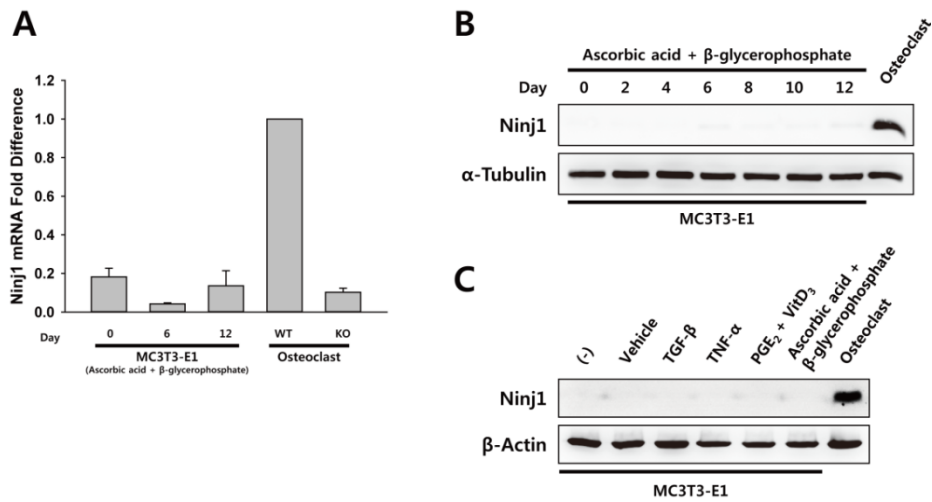
Figure 8. Expression of Ninj1 in osteoblasts.

(A) mRNA expression of *Ninj1* in MC3T3-E1 cells by osteoblastogenic culture. WT and *Ninj1*^{-/-} OCs were used as positive and negative control, respectively. (B) Protein expression of Ninj1 in MC3T3-E1 cells by osteoblastogenic culture. Lysate from WT OCs was used as Ninj1-positive control. (C) Ninj1 expression by various osteogenic stimuli in MC3T3-E1 cells was measured by immunoblot assay. Lysate from WT OCs was used as Ninj1-positive control.

41

4. Ninj1 expression is dynamically regulated during osteoclastogenesis

Previous results revealed that mature OCs express high Ninj1, but not OBs. Thus, I focused on OCs and assessed Ninj1 expression during OC development. Mature OCs differentiated from OC precursor cells passing through preOCs. To evaluate the expression of Ninj1 during osteoclastogenesis, mature OCs were induced from BMMs and RAW264.7 cells which are used as OC precursor cells. Ninj1 was upregulated from days 0 to 2, and downregulated at days 3 and 4, and restored from days 5 to 7 in BMMs cultured with M-CSF and RANKL (Figure 9A). Similar results were obtained in RAW264.7 cells cultured with RANKL. Ninj1 was upregulated at day 1, and downregulated from days 3 to 4, and restored from days 5 to 6 (Figure 9B).
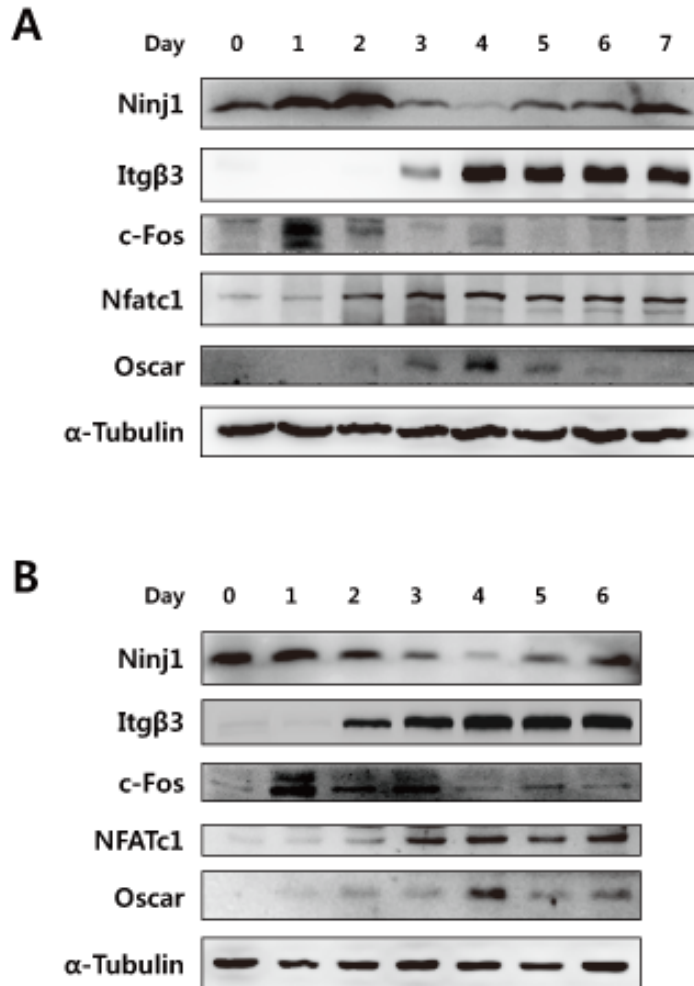
Figure 9. Ninj1 expression during OC development.

(A) BMMs were cultured with M-CSF and RANKL for 7 days to differentiate into OCs. (B) RAW264.7 cells were cultured with RANKL for 6 days to differentiated into OCs. Itgβ3, c-Fos, Nfatc1, and Oscar

were used for OC differentiation markers.

5. *Ninj1* deficiency reduces multinucleated OCs

I then investigated whether the mild osteopetrotic phenotype of *Ninj1*$^{-/-}$ mice represents a defect of OC development. Bone marrow cells from WT and *Ninj1*$^{-/-}$ mice were cultured with M-CSF and RANKL and stained for TRAP activity. As expected, the number of TRAP$^+$ multinucleated cells was significantly decreased in *Ninj1*$^{-/-}$ cells and the size of multinucleated cells were also reduced by *Ninj1* deficiency (Figure 10). Similar results were obtained in RAW264.7 cells. The number of TRAP$^+$ multinucleated cells was substantially reduced in siNinj1 transfected cells (Figure 11).
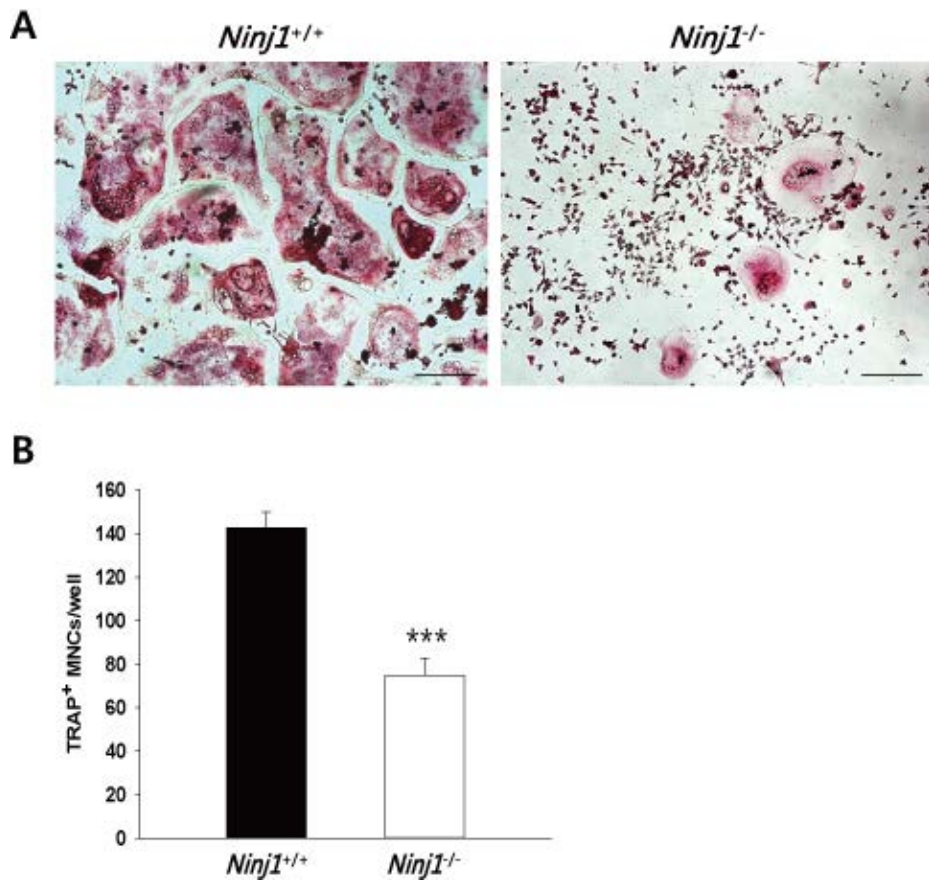
Figure 10. *Ninj1*^{-/-} bone marrow cells produce less multinucleated OCs.

(A,B) WT and *Ninj1*^{-/-} bone marrow cells were cultured with M-CSF for 3 days and non-adherent cells were discarded. Adherent cells were continuously cultured with M-CSF and RANKL for 7 days more. Differentiated cells were stained for TRAP activity. (A) Representative

images of TRAP activity staining. Scale bars, 200 μm. (B) Quantitation of TRAP-positive multinucleated OCs (nuclei 3 or more). All quantitative data are the mean ± SD, ***$P < 0.001$.
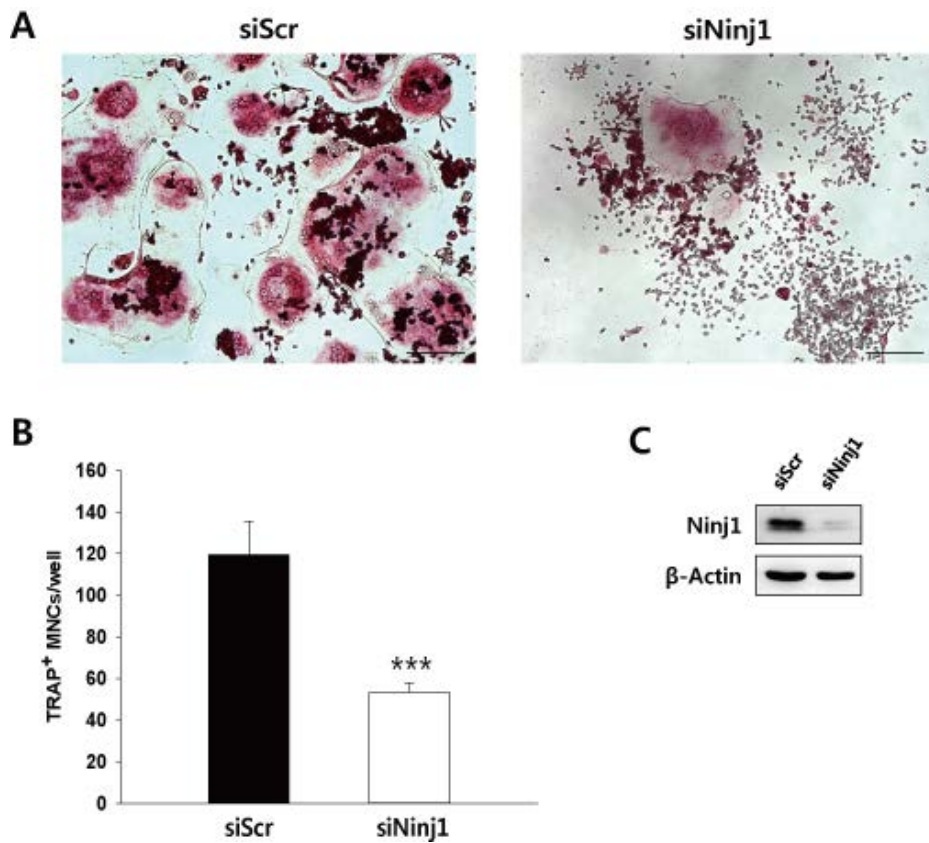
Figure 11. *Ninj1* deficiency impairs OC development derived from RAW264.7 cells.

(A–C) RAW264.7 cells were transfected with siScr or siNinj1 and cultured with RANKL to generate mature OCs. At day 6, the cells were stained for TRAP activity. (A) Representative images of TRAP activity staining. Scale bars, 200 μm. (B) Quantitation of TRAP-positive

multinucleated OCs (nuclei 3 or more). (C) Downregulation of Ninj1 by siRNA was assessed by immunoblot assay at day 1. All quantitative data are the mean ± SD, ***$P < 0.001$.

6. Ninj1 is dispensable for OC differentiation

In bone microenvironment, OC precursor cells, common ancestor of macrophages, differentiate into mononuclear preOCs, immature multinucleated OCs, and finally bone-resorptive mature OCs (Nakamura et al., 2012). Thus, I examined the expression of typical OC differentiation markers to assess whether *Ninj1* deficiency influences OC differentiation. Notably, mRNA expressions of *Nfatc1* and *c-Fos*, transcription factors for OC differentiation, were unchanged at day 2 and another OC-specific gene expressions including *Itgb3*, *Oscar*, and *Calcr* were comparable in *Ninj1*$^{-/-}$ cells (Figure 12). Similarly, protein expression of OC markers was also unaffected by *Ninj1* deficiency (Figure 13). These data suggest that *Ninj1* deficiency disturbs OC development independent from the differentiation process.
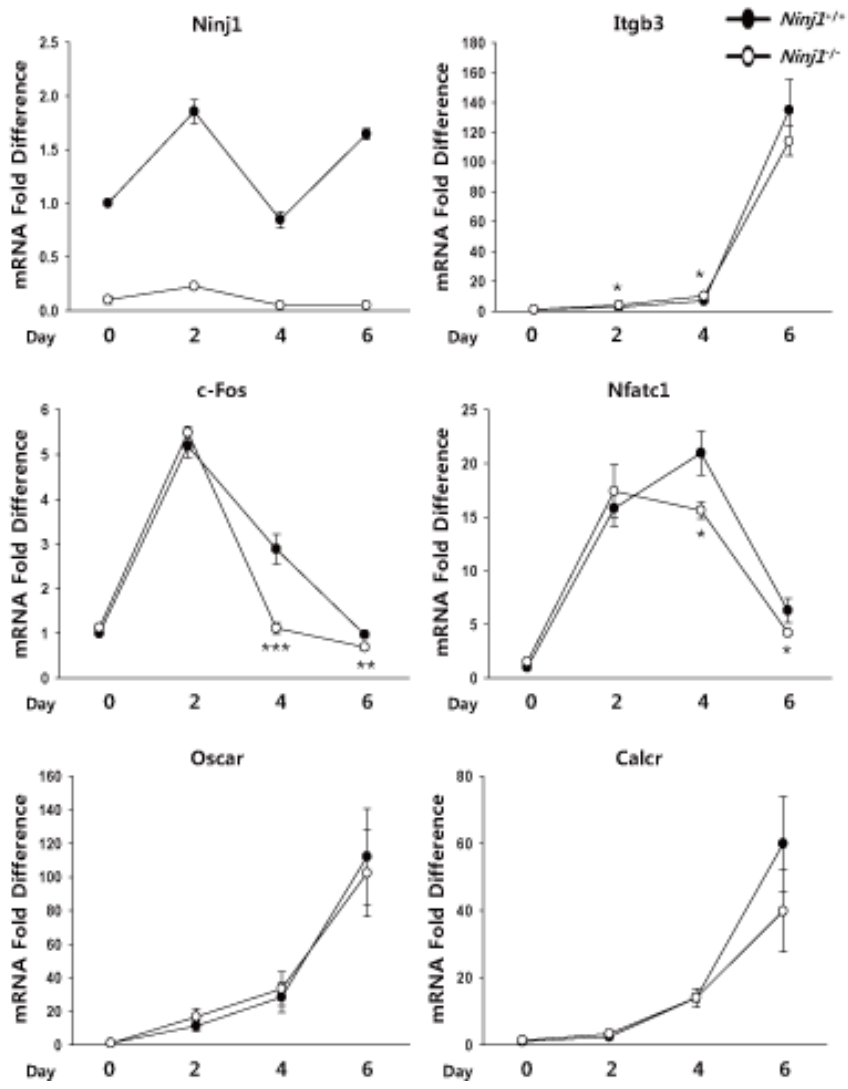
Figure 12. Gene expressions of OC markers.

mRNA expressions of Ninj1 and typical OC differentiation markers including *Nfatc1*, *c-Fos*, *Itgb3*, *Oscar*, and *Calcr* were analyzed by

qRT-PCR and relative mRNA expressions are shown as the mean ± SD,

*$P < 0.05$, **$P < 0.01$, ***$P < 0.001$.
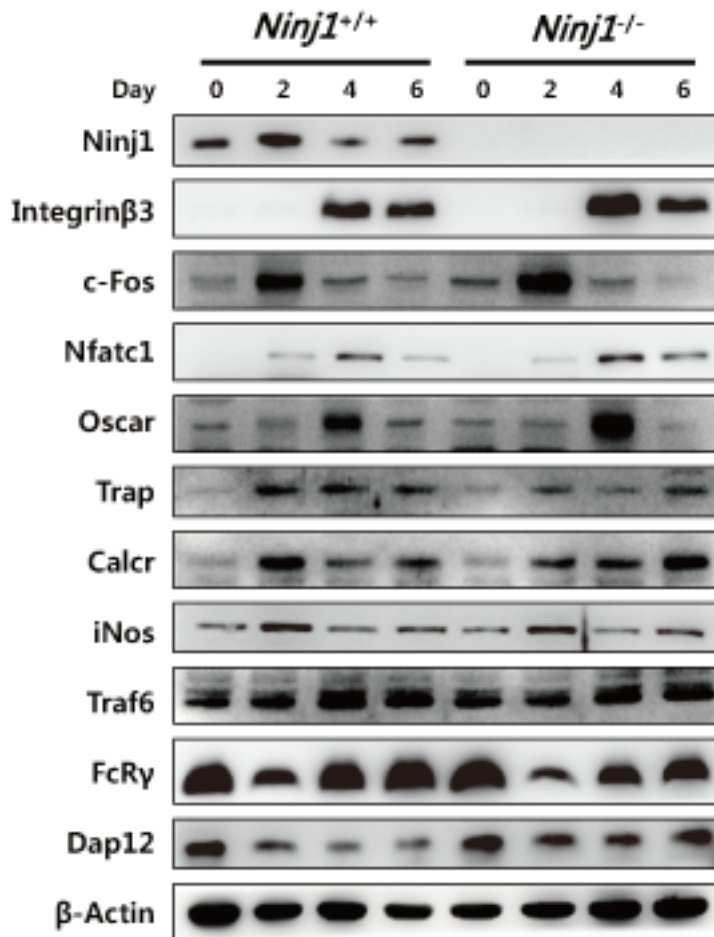
Figure 13. Protein expressions of osteclast markers.

Ninj1, typical OC differentiation markers, and OC-associated proteins were analyzed by immunoblot assay.

7. *Ninj1* deletion augments development of OPCs

The proportion of OPCs in bone marrow is important to the early stage of osteoclastogenesis (Arai et al., 1999). It is suspected that the decreased multinucleated OCs might be an outcome of reduced progenitor cells in bone marrow. Thus, I analyzed the proportion of OPCs in bone marrow cells from WT and $Ninj1^{-/-}$ mice by FACS. $Csf1r^{+}$ cells were gated first and further analyzed by c-Kit and Cd11b (Figure 14A). Notably, OPCs (red square in Figure 14A, defined as $Csf1r^{+}$c-Kit^{+} $Cd11b^{dull}$) were 1.37-fold more abundant in $Ninj1^{-/-}$ mice (Figure 14B). These data suggest that Ninj1 might have a role for negative modulation of OPC development in mice.
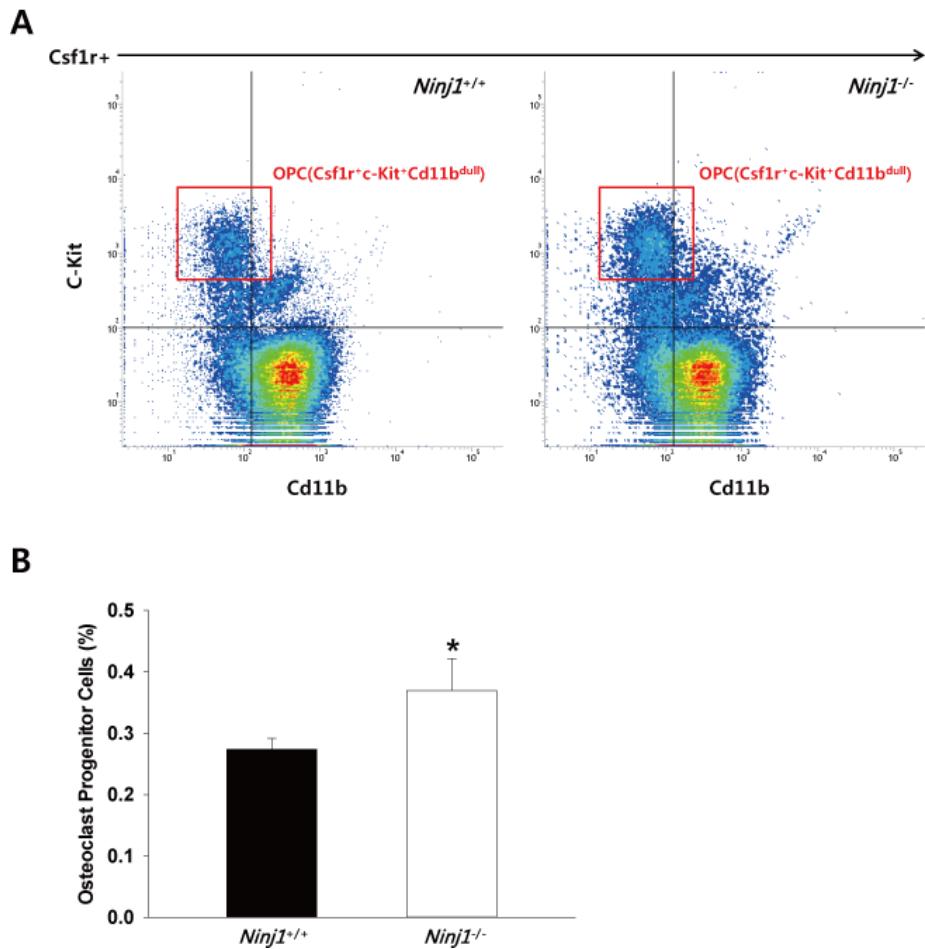
Figure 14. Analysis of OPCs in bone marrow.

(A,B) Bone marrow cells were analyzed by FACS. (A) Representative density plots of $Csf1r^+$ bone marrow cells. (B) The percent frequency of OPCs (red box, $Csf1r^+c\text{-}Kit^+Cd11b^{dull}$) in (A) is shown as the mean $\pm$ SD, $*P < 0.05$.

8. *Ninj1*-deficient OC precursor cells develop normally from OPCs.

The expression level of M-CSF receptor and RANK in OC precursor cell is another important aspect in the early stage of osteoclastogenesis (Arai et al., 1999; Mochizuki et al., 2006). To characterize the OC precursor cells, I evaluated BMMs which are used as OC precursor cells in *in vitro*. Flow cytometric analysis and immunoblot assay revealed the expression levels of Csf1r, Rank, and Cd11b were comparable in two groups (Figure 15). Similar results were obtained by qRT-PCR (Figure 16). These data suggest that Ninj1 is dispensable for differentiation of OC precursor cells.
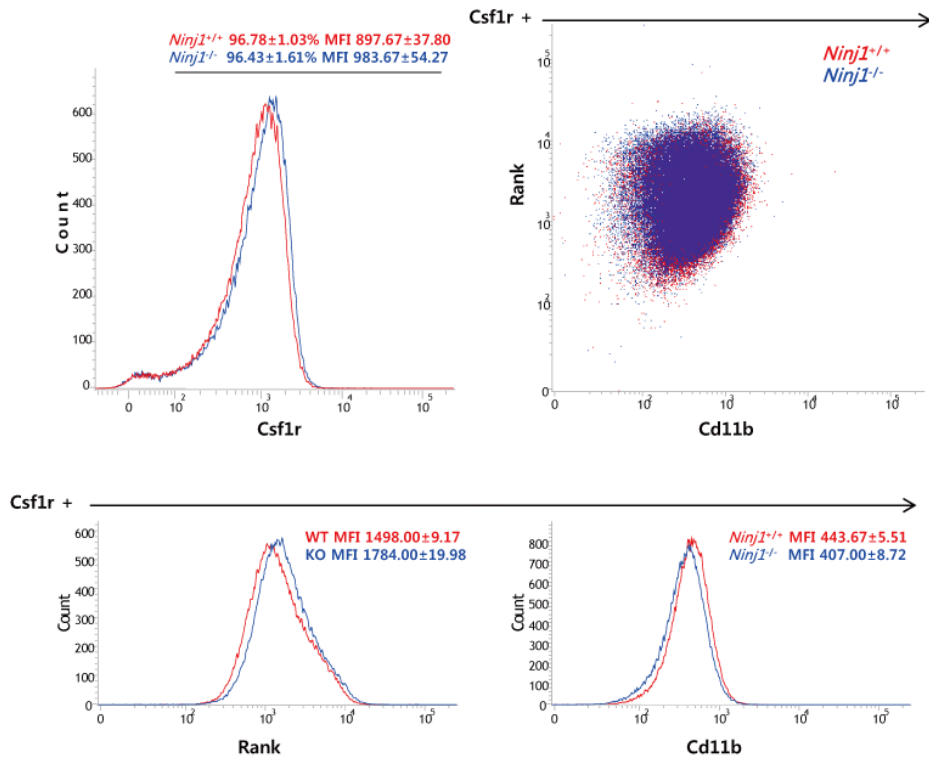
Figure 15. Typical marker expressions in BMMs.

BMMs were analyzed by FACS. The expression of Csf1r is shown in whole cells (upper left) and Csf1r+-gated cells were analyzed by Rank (y axis) and Cd11b (x axis) (upper right). Individual histograms of Rank and Cd11b expressions in Csf1r+-gated BMMs are shown in lower panel.
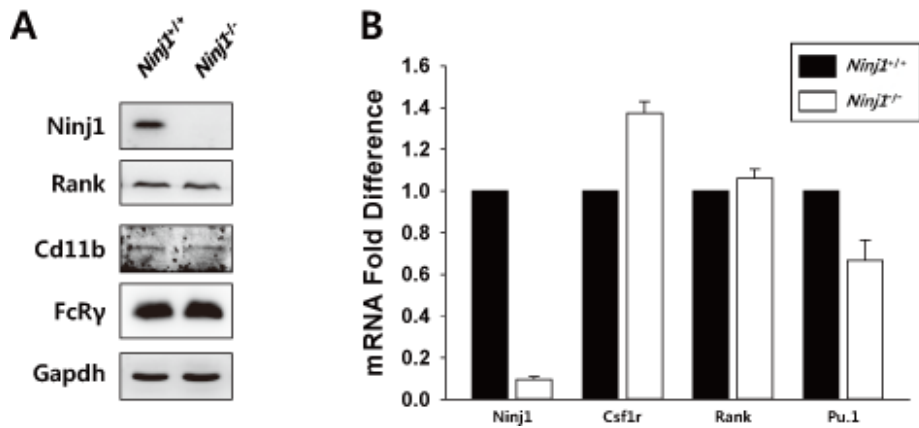
Figure 16. Expressions of Ninj1 and OC precursor markers in bone marrow macrophages.

(A) Protein expressions of Rank, Cd11b, and FcRγ in BMMs were analyzed by immunoblot assay. (B) mRNA expressions of *Ninj1* and OC precursor markers including *Csf1r*, *Rank*, and *Pu.1* were analyzed and relative mRNA expressions are shown as the mean ± SD.

9. Ninj1 is expendable for preOC migration

OCs transmigrate OB layer to adhere to mineralized matrix (Saltel et al., 2008). Previously, it was reported that Ninj1 enhances transendothelial migration of macrophages (Ahn et al., 2014a). To address this possibility in OCs, I compared the capability of transmigration in preOCs (Saltel et al., 2006; Zou et al., 2010). BMMs were transduced with Lifeact-mCherry and cultured with M-CSF and RANKL for 3 days to generate mononuclear preOCs. Then, the cells were replaced on a confluent monolayer of osteoblast-like MC3T3-E1 cells expressing GFP. During continuous culture with osteoclastogenic cytokines, Z-plane images were acquired after 30 minutes and 12 hours by confocal microscopy. Both groups of preOCs transmigrated completely through the OB layer and spread well (Figure 17).
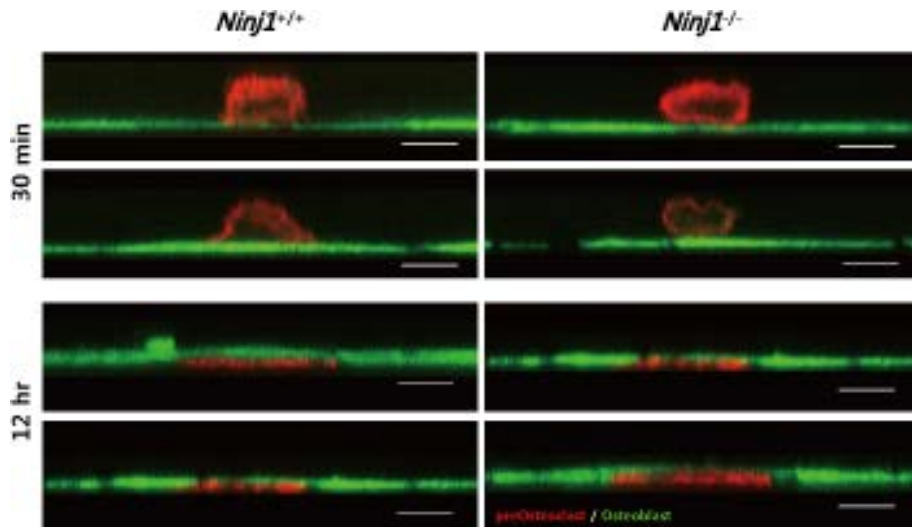
Figure 17. Transmigration of preOCs via OB monolayer.

BMMs, transduced with Lifeact-mCherry, were cultured with M-CSF
and RANKL for 3 days to generate preOCs. Lifeact-mCherry labeled
preOCs were overlaid on GFP-expressing MC3T3-E1 OB monolayer
with continued presence of the osteoclastogenic cytokines. Z-plane
images were acquired after 30 minutes (upper) and 12 hours (lower) by
confocal microscopy. Scale bars, 10 μm.

10. Macrophage fusion is enhanced by *Ninj1* deficiency

Mononuclear cell fusion is a critical step in OC development and defective preOC fusion stimulates osteopetrosis in mice (Xing et al., 2012). Thus, I suspected that *Ninj1* deficiency interrupted cell-cell fusion itself. Accordingly, I cultured BMMs with M-CSF + IL-4 and GM-CSF + IL-4 for 6 days (Yagi et al., 2007). In culture of M-CSF + IL-4, multinucleated giant cells and their nuclei were similar between groups, whereas in GM-CSF + IL-4 culture, 1.44-fold more multinucleated giant cells and significant nuclei increases were observed in *Ninj1*$^{-/-}$ cells (Figure 18A–C). Because *Ninj1* deficiency might affect the efficacy of IL-4 in macrophages, I assessed Arginase-1 induction by IL-4 in BMMs; however, no between-group differences were observed (Figure 18D). In addition, genes associated with migration and/or fusion of preOCs including *c-Src*, *Itgav*, *Cd44*, *Atp6v0d2*, and *Dcstamp* were significantly increased in *Ninj1*$^{-/-}$ preOCs (Figure 19). As accelerated myeloid cell fusion reduces bone mass by improving osteoclastogenesis (Fujita et al., 2012; Iwasaki et al., 2008), these results suggest that enhanced *Ninj1*$^{-/-}$ cell fusion might attenuate osteopetrosis severity in *Ninj1*$^{-/-}$ mice and that Ninj1 has an inhibitory

role for myeloid cell fusion.
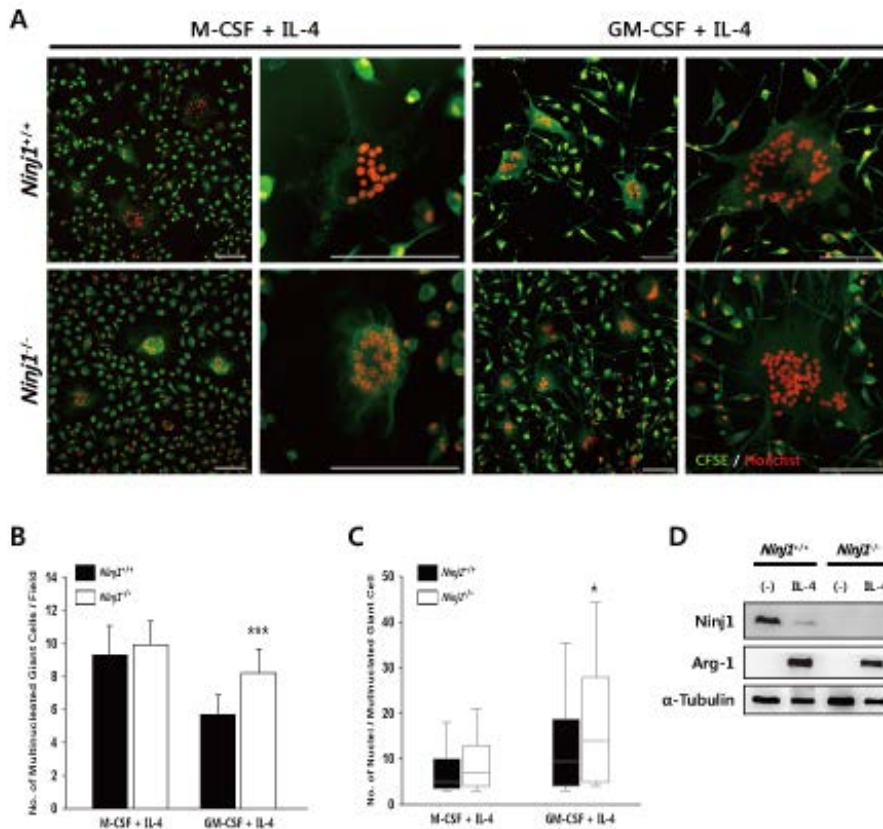
Figure 18. *Ninj1^{-/-}* macrophages generate more multinucleated giant cells.

(A–C) Multinucleated giant cells were induced by culturing BMMs with M-CSF + IL-4 (left in A) and GM-CSF + IL-4 (right in A) followed by staining with CFSE (green) and Hoechst (red). (A) Representative images of multinucleated giant cells. Scale bars, 100 μm. (B) Numbers of multinucleated cells are shown as the mean ± SD,

***$P < 0.001$. (C) Numbers of nuclei in multinucleated cells are presented as median-quartile boxplot, *$P < 0.05$. (D) Cytokine-starved BMMs were cultured with or without IL-4 (10 ng/mL) for 24 hours. The expressions of Arg-1 and Ninj1 were evaluated by immunoblot assay.
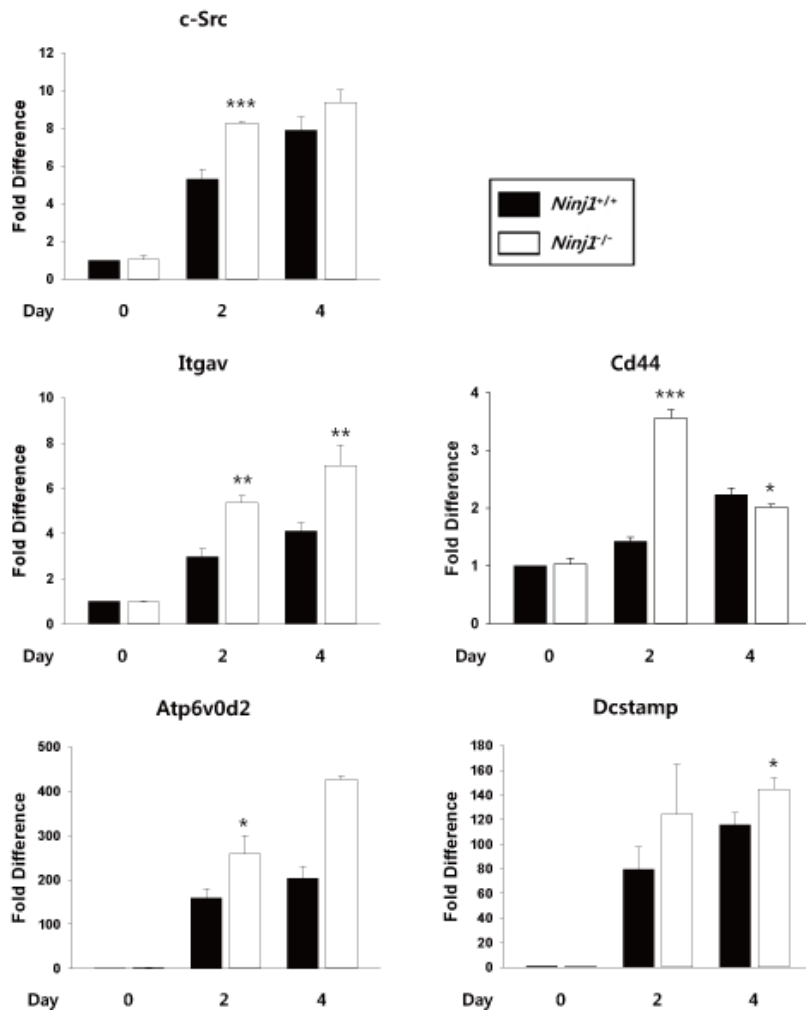
Figure 19. mRNA expressions of motility- and/or fusion-associated genes.

BMMs were cultured with M-CSF and RANKL and mRNA expressions of *c-Src*, *Itgav*, *Cd44*, *Atp6v0d2*, and *Dcstamp* were

analyzed by quantitative real-time PCR and relative mRNA expressions

are shown as the mean $\pm$ SD, $*P < 0.05$, $**P < 0.01$, $***P < 0.001$.

11. Ninj1 deletion reduces mature OC area

The OC actin ring cytoskeleton isolates the degradative microenvironment from the general extracellular space; failure of actin ring formation contributes to osteopetrosis development (Teitelbaum, 2011). Thus, I assessed actin cytoskeletons in mature OCs. BMMs were cultured with M-CSF and RANKL on glass coverslips. After 6 days, cells were stained with phalloidin to visualize F-actin. However, actin ring appearance was indistinguishable between $Ninj1^{-/-}$ and WT OCs, with similar proportions of actin ring forming cells (Figure 20A). Conversely, mature $Ninj1^{-/-}$ OCs were smaller than WT OCs, exhibiting a 0.73-fold smaller area surrounded by the actin ring (Figure 20B). As $Ninj1^{-/-}$ myeloid cells showed no defect in cell-cell fusion or actin ring formation, these data suggest that the area reduction in $Ninj1^{-/-}$ OCs might be associated with the diminished preOC population.
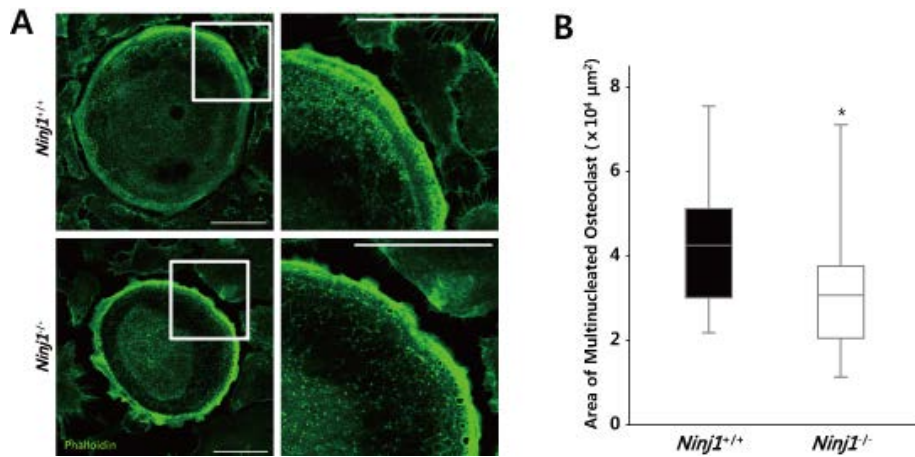
Figure 20. *Ninj1*-deficient OCs have smaller area surrounded by actin ring.

(A,B) BMMs were cultured on glass coverslips with M-CSF and RANKL for 6 days. Cells were stained with AF488-Phalloidin. (A) Representative images of actin-ring formed OCs (left) and highly magnified images of insets in left (right). Scale bars, 50 μm. (B) The area of actin-ring formed OCs is shown as median-quartile boxplot, *$P < 0.05$.

12. Lack of Ninj1 attenuates TRAP activity in cultured media

Bone matrix resorption is a novel OC function dependent upon degradative enzyme quantity and mobilization (Teitelbaum, 2007). Specifically, TRAP directly reflects OC resorptive function (Yu et al., 2009). Thus, I assessed TRAP activity during OC development by culturing BMMs with M-CSF and RANKL (Park et al., 2013; Watanabe et al., 2014). TRAP activities in conditioned media were significantly reduced in $Ninj1^{-/-}$ culture (Figure 21A), whereas cell lysate activities were comparable to WT (Figure 21B). In addition, similar TRAP and other OC enzyme mRNA expression pattern, including Cathepsin K and MMP-9, were found (Figure 21C). This discordance of TRAP activity in $Ninj1^{-/-}$ cell-cultured media reflects reduced numbers of TRAP-producing cells. Together, these data suggest that $Ninj1^{-/-}$cells dropped out prior to OC maturation and that Ninj1 might be important for cell population maintenance.
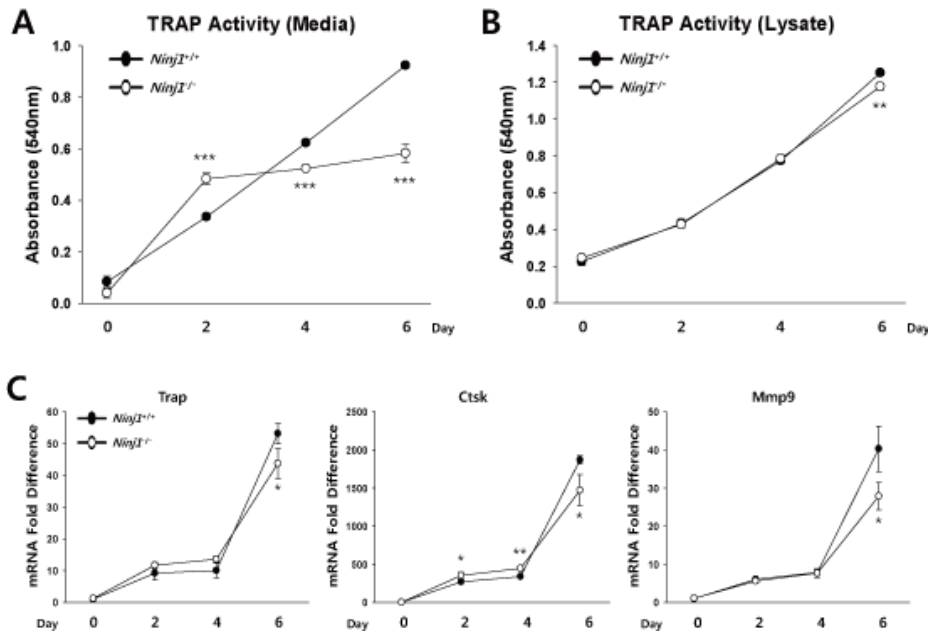
Figure 21. TRAP activity in conditioned media is reduced in *Ninj1*$^{-/-}$ cell culture media.

(A,B) BMMs were cultured with M-CSF and RANKL for indicated days. An absorbance for TRAP activity was measured at 540 nm. (A) Conditioned media were collected at indicated days and subjected to TRAP activity assay. An absorbance is shown as the mean ± SD ($n = 3$, triplicate in each experiment), ***$P < 0.001$. (B) Cell lysates were harvested at indicated days and subjected to TRAP activity assay. An absorbance is shown as the mean ± SD ($n = 3$, triplicate in each

experiment), **$P < 0.01$. (C) mRNA expressions of resorption related OC markers including TRAP (*Trap*), Cathepsin K (*Ctsk*) and MMP-9 (*Mmp9*) were analyzed by qRT-PCR. Relative mRNA expressions are shown as the mean ± SD, *$P < 0.05$, **$P < 0.01$.

13. Ninj1 is important for maintenance of cell population during preOC stage

The previous data collectively suggest that *Ninj1* deficiency might influence cell population by modulating proliferation and/or survival. The OC number is influenced by precursor cell propagation and precursor, prefusion, and mature OC death. Thus, I monitored cell population following M-CSF and RANKL treatment singly or in combination. *Ninj1*$^{-/-}$ BMMs grew faster during the first 2 days than WT cells with combination treatment. From day 2 to 4, however, the number of *Ninj1*$^{-/-}$ cells diminished rapidly (Figure 22A). The expansion of *Ninj1*$^{-/-}$ BMMs was significant in culture with M-CSF (Figure 22B) and neither phenomenon was observed upon RANKL treatment (Figure 22C). These data indicate that M-CSF-dependent *Ninj1*$^{-/-}$ myeloid cell amplification might ameliorate mature OC reduction *in vitro* and osteopetrosis *in vivo* and that *Ninj1*$^{-/-}$ cell reduction is related to the osteoclastogenic condition.
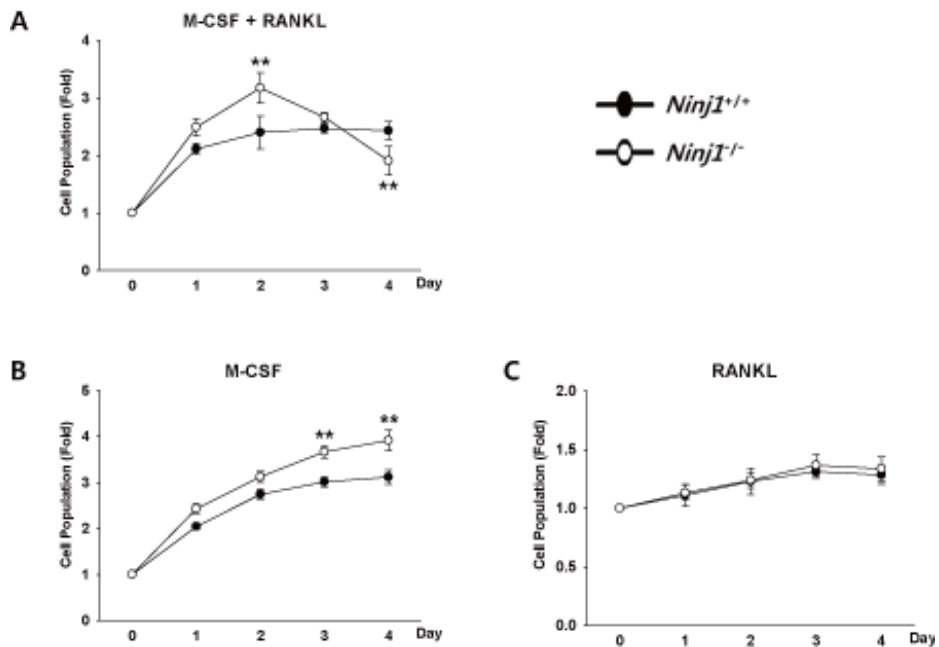
Figure 22. *Ninj1* deficiency reduces preOC population.

(A) BMMs were cultured with M-CSF and RANKL. An absorbance by MTS was measured at 492 nm and relative cell population was shown as the mean ± SD ($n = 3$, triplicate in each experiment), **$P < 0.01$. (B) BMMs were cultured with M-CSF and relative cell growth, evaluated at indicated time points, was shown as the mean ± SD ($n = 3$, triplicate in each experiment). (C) BMMs were cultured with RANKL and relative cell growth, evaluated at indicated days, was shown as the mean ± SD ($n = 3$, triplicate in each experiment), **$P < 0.01$.

14. Ninj1 enhances preOC survival during osteoclastogenesis

To verify that the population diminishment is related to apoptosis, cells stained with Annexin V and 7AAD were analyzed by FACS. Annexin V^+ populations in $Ninj1^{-/-}$ cells were 1.82-, 1.75-, and 1.51-fold greater than WT cells at days 2, 3, and 4, respectively; over half of Annexin V^+ cells were also $7AAD^+$, indicating irreversible apoptosis (Figure 23). Similar results were obtained in RAW264.7 cells following Ninj1 siRNA treatment at days 2 and 3 (1.61- and 1.90-fold increase, respectively) (Figure 24). Moreover, increased apoptosis in $Ninj1$-deficient cells occurred specifically by RANKL and those phenomena were not induced by TNF-α (Figure 25). These results indicate that Ninj1 sustains preOC survival and inhibits apoptosis following OC differentiation.
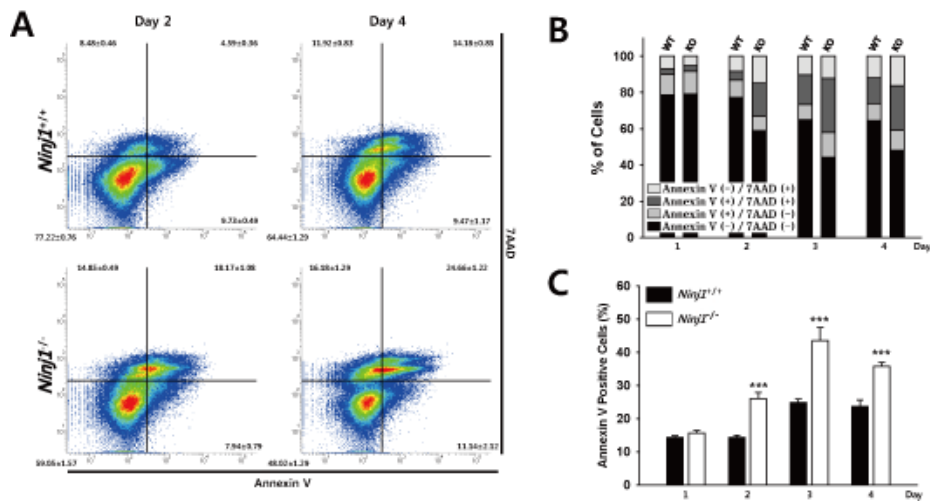
Figure 23. Lack of Ninj1 induces apoptosis during osteoclastogenesis.

(A–C) BMMs were cultured with M-CSF and RANKL. Cells were harvested and stained with FITC-Annexin V and 7AAD at indicated days followed by FACS analysis. (A) Representative density plots at days 2 and 4. (B) FACS-determined statistical stacked bars ($n = 4$). (C) FACS-determined percent frequency of Annexin V$^+$ cells are shown as the mean ± SD ($n = 4$).
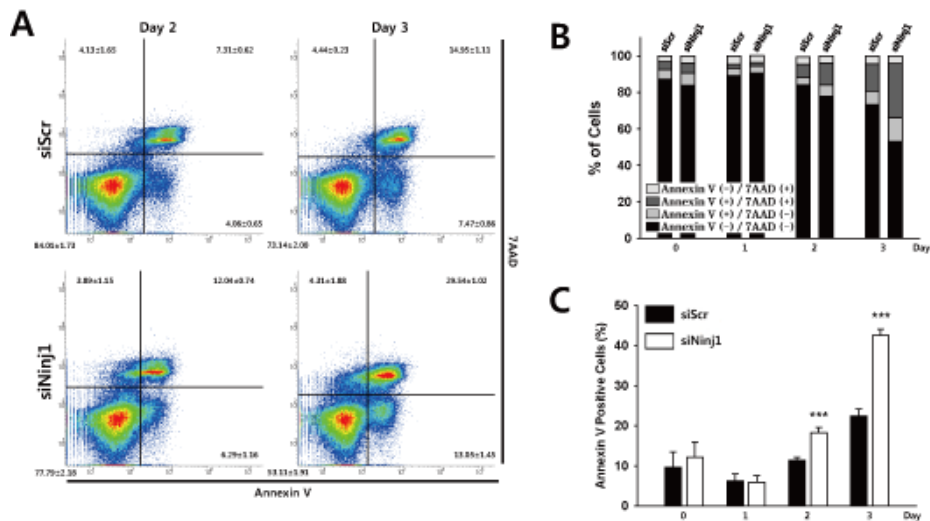
Figure 24. Ninj1 insufficient RAW264.7 cells drop out by apoptosis during osteoclastogenesis.

(A–C) RAW264.7 cells were transfected with siScr or siNinj1 and cultured with RANKL. Cells were harvested and stained with FITC-Annexin V and 7AAD at indicated days followed by FACS analysis. (A) Representative density plots at days 2 and 3 analyzed by FACS. (B) FACS-determined statistical stacked bars ($n = 4$). (C) FACS-determined percent frequency of Annexin V$^+$ cells. Data are shown as the mean ± SD ($n = 4$), ***$P < 0.001$.
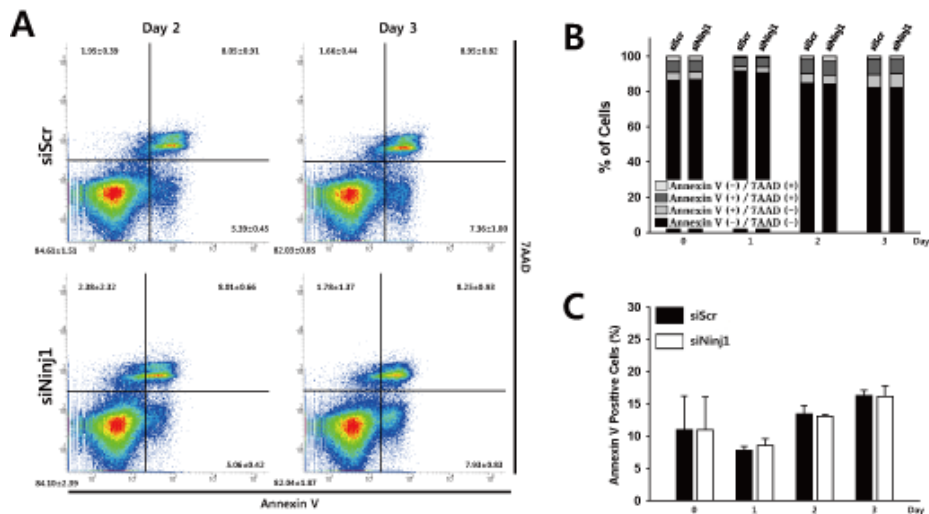
Figure 25. Analysis of TNF-α-induced apoptosis in RAW264.7 cells.

(A–C) RAW264.7 cells were transfected with siScr or siNinj1 and cultured with TNF-α. Cells were harvested and stained with FITC-Annexin V and 7AAD at indicated days followed by FACS analysis. (C) Representative density plots of days 2 and 3 analyzed by FACS. (D) FACS-determined statistical stacked bars ($n = 3$). (E) FACS-determined percent frequency of Annexin V^+ cells. Data are shown as the mean $\pm$ SD ($n = 3$).

15. *Ninj1* deficiency induces Caspase-9-dependent intrinsic apoptosis in preOCs

Apoptosis is classified to the intrinsic pathways which are initiated by dysregulation of pro- or anti-apoptotic proteins followed by sequential activation of Caspase-9 and Caspase-3, and the extrinsic pathways which are initiated by liganded death receptors followed by sequential activation of Caspase-8 and Caspase-3 (Garrido and Kroemer, 2004; Kroemer et al., 2009). To identify the type of apoptosis induced by *Ninj1* deficiency, BMMs were cultured with M-CSF and RANKL, and cell lysates were subjected to immunoblot assay. Cleaved Caspase-3 was observed from day 2 in *Ninj1*$^{-/-}$ cells and amount of it was augmented following differentiation. Interestingly, the only cleaved Caspase-9, not cleaved Caspase-8, was observed with cleaved Caspase-3 and cleaved PARP in *Ninj1*$^{-/-}$ cells (Figure 26A). Similarly, active form of Caspase-9 and Caspase-3 were stronger in siNinj1 transfected RAW264.7 cells than in control cells and still, cleaved Caspase-8 was not detected (Figure 26B). Finally, I confirmed whether apoptosis of *Ninj1*-deficient cells might affect viability of neighborhood cells or depend on cell-autonomous manner. Thus, GFP- or DsRed-

labeled RAW264.7 cells were transfected with siScr or siNinj1 and an equal number of GFP$^+$ and DsRed$^+$ transfectants were cultured together with RANKL. The ratio of GFP$^+$ to DsRed$^+$ cells was determined following culture by FACS. siNinj1 transfectants did not exacerbate viability of siScr transfectants, and conversely, siScr treated cells did not rescue survival of siNinj1 transfected cells neither (Figure 27). These data indicate that Ninj1 is a prerequisite for preventing induction of Caspase-9-dependent apoptosis in preOCs.
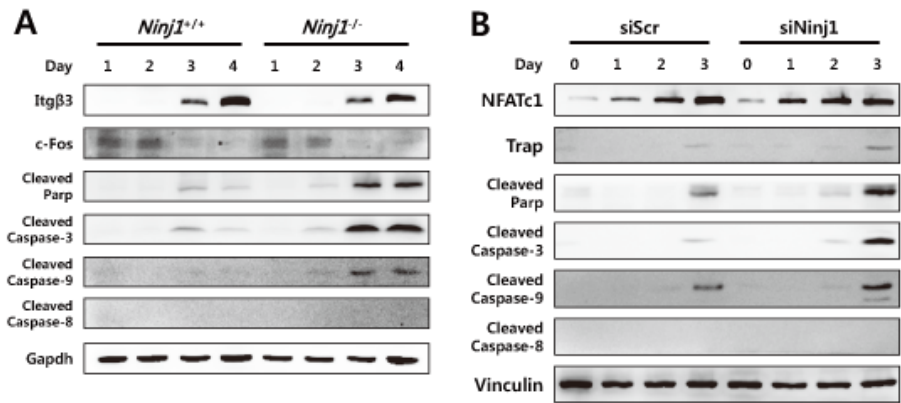
Figure 26. Ninj1 suppresses Caspase-9-dependent intrinsic apoptosis in preOCs.

(A) BMMs were cultured with M-CSF and RANKL for indicated days. Cell lysates were subjected to immunoblot analysis. (B) RAW264.7 cells transfected with siScr or siNinj1 were cultured with RANKL. Cells were harvested at indicated days and subjected to immunoblot assay.
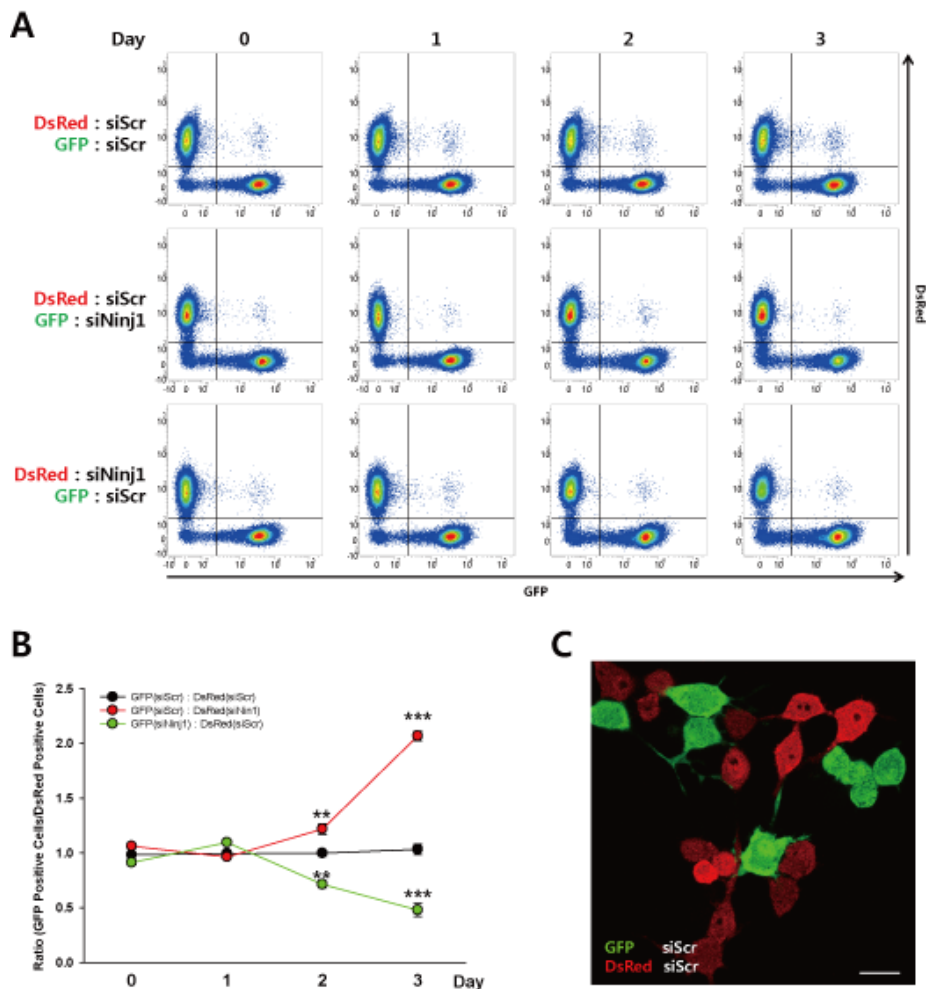
Figure 27. *Ninj1* deficiency-induced apoptosis occurs cell-autonomously.

(A–C) RAW264.7 cells were stably transduced with GFP or DsRed using a retrovirus. GFP$^+$ or DsRed$^+$ RAW264.7 cells were transfected

with scrambled siRNA or Ninj1 siRNA as indicated. Equal numbers of each fluorescence protein labeled cells were co-cultured with RANKL and analyzed by FACS. (A) Representative density plots at indicated days. (B) The ratio of GFP$^+$ to DsRed$^+$ cells was determined using FACS and data are shown as the mean ± SD ($n = 3$, triplicate in each experiment), **$P < 0.01$, ***$P < 0.001$. (C) Representative image of mixed culture. Scale bar, 20 μm.

16. A high level of Ninj1 improves preOC survival

Next, I suspected whether incremental Ninj1 expression would attenuate spontaneous apoptosis during osteoclastogenesis. Thus, I transduced Ninj1 into RAW264.7 cells and examined apoptosis following treatment of RANKL by FACS. Annexin V^+ cells were 0.66- and 0.55-fold reduced by overexpression of Ninj1 at days 2 and 3, respectively (Figure 28). Collectively, these data suggest that upregulation of Ninj1 enhances preOC survival and dysregulated Ninj1 expression might be involved in pathogenesis of bone disease.
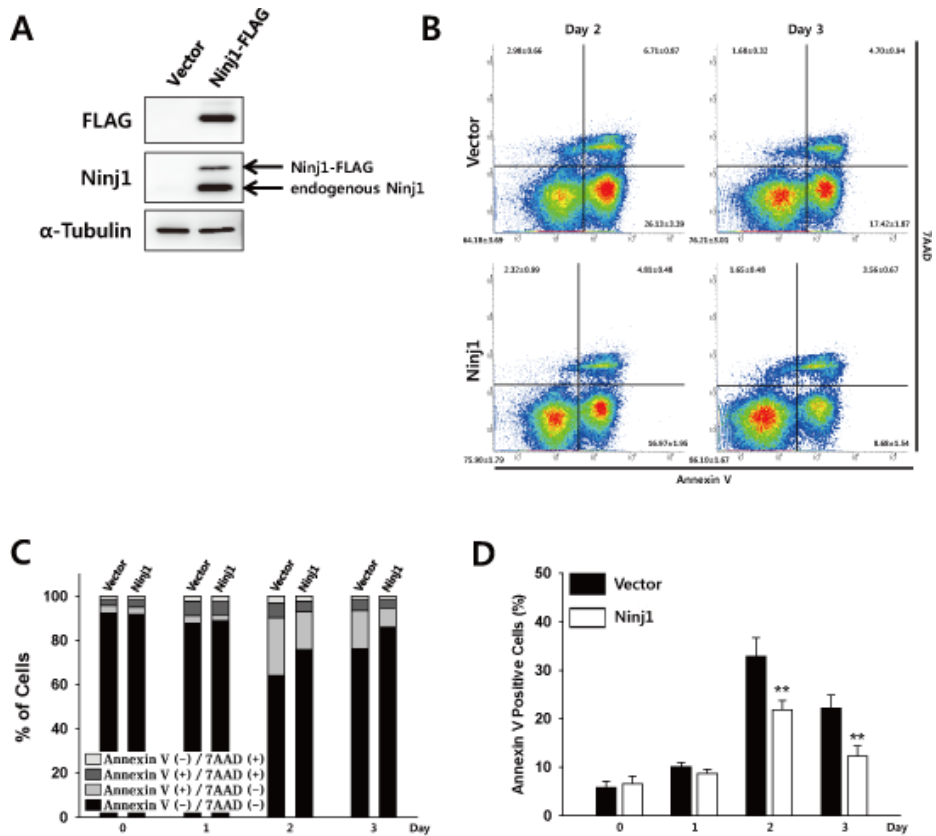
Figure 28. Incremental Ninj1 expression enhances the survival of preOCs.

(A–D) RAW264.7 cells were stably transduced with Ninj1-FLAG or empty vector using a retrovirus and cultured with RANKL. Cells were harvested and stained with APC-Annexin V and 7AAD at indicated days followed by FACS analysis. (A) Stable expression of Ninj1-FLAG

in RAW264.7 cells was validated by immunoblot assay. (B) Representative density plots at days 2 and 3 analyzed by FACS analysis. (C) FACS-determined statistical stacked bars ($n = 4$). (D) FACS-determined percent frequency of Annexin V^+ cells. Data are shown as the mean ± SD (n = 4), **$P < 0.01$.

17. High *NINJ1* expression correlates with human bone disorders

To investigate the potential association between *NINJ1* expression and bone disorders in humans, I mined publicly available datasets in the GEO and analyzed four different microarrays. Gene expression profiles of 10 patients with osteoarthritis (OA) and 9 with rheumatoid arthritis (RA) demonstrated significantly elevated *NINJ1* expression in RA (1.99-fold compared to OA, Figure 29A). Furthermore, comparison of *NINJ1* expression in 8 patients with RA and 15 with early RA revealed 2.60-fold enhancement in early RA, suggesting that *NINJ1* is important for RA onset and/or early progression (Figure 29B). Following three months of anti-TNF (Enbrel) therapy in 2 patients with RA, *NINJ1* expression was significantly reduced (0.46-fold vs. pretreatment, Figure 29C). Furthermore, postmenopausal women with low peak bone mass ($n = 7$) exhibited 1.40-fold higher *NINJ1* expression than those with high peak bone mass ($n = 8$), suggesting that *NINJ1* might be associated with both inflammatory and osteoporotic bone loss (Figure 29D). Together, these data suggest that *NINJ1* has a potent role in the human bone disorder pathogenesis and/or progression.
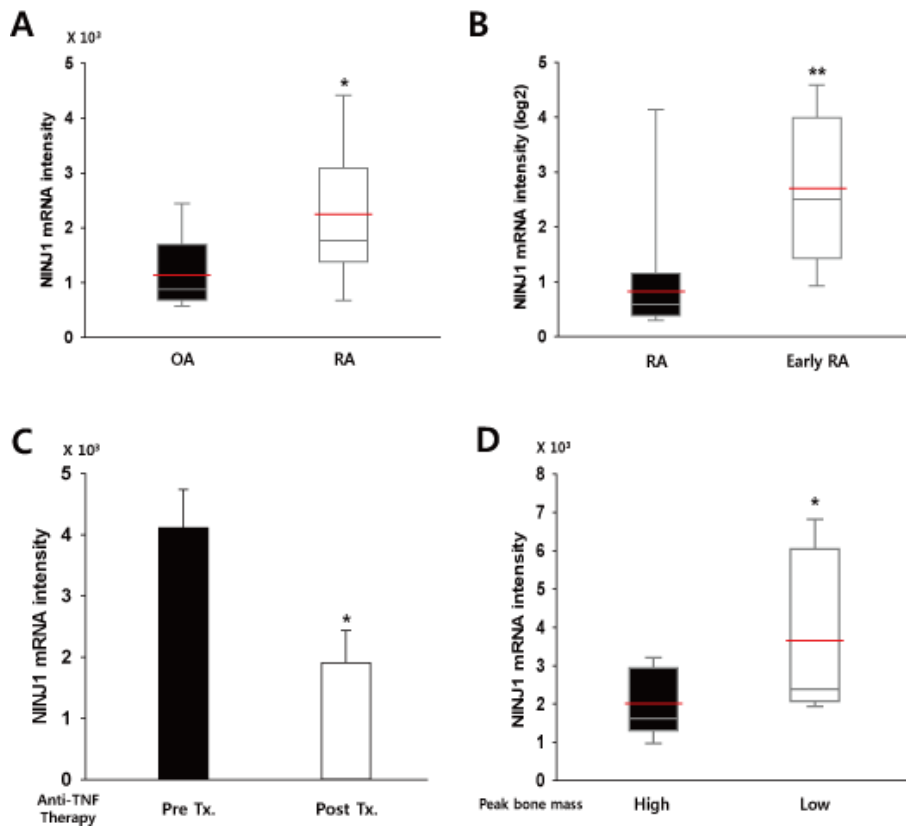
Figure 29. The expression level of *NINJ1* correlates with bone disorders in human.

(A–D) Expression levels of *NINJ1* mRNA were analyzed from gene expression datasets GSE27390 (A), GSE1964 (B), GSE7524 (C), and GSE7158 (D) deposited in GEO. Red bars indicate the mean value. (A) Bone marrow-derived mononuclear cells were obtained from patients

with osteoarthritis (n = 10) and rheumatoid arthritis (n = 9), and *NINJ1* mRNA expressions were analyzed. Data are shown as median-quartile boxplot, $*P < 0.05$. (B) Comparison of *NINJ1* expression in peripheral blood mononuclear cells derived from patients with rheumatoid arthritis (n = 8) and early rheumatoid arthritis (n = 15). Data are shown as median-quartile boxplot, $**P < 0.01$. (C) The change of *NINJ1* mRNA expression in whole blood samples from rheumatoid arthritis patients following anti-TNF therapy was analyzed and data are shown as the mean $\pm$ SD (n = 2), $*P < 0.05$. (D) The difference of *NINJ1* mRNA expression in circulating monocytes derived from postmenopausal women with high (n = 8) and low (n = 7) peak bone mass was analyzed and data are shown as median-quartile boxplot, $*P < 0.05$.

18. Ninj1 might be a co-stimulatory molecule and/or co-receptor for ITAM-mediated signals

Although the importance of M-CSF and RANKL as extracellular stimuli and Ca^{2+}-NFATc1 pathway as an intracellular signaling has been established for OC differentiation, it has been suspected that other regulatory pathway(s) might exist (Humphrey et al., 2005), and recent studies have showed a critical role for the ITAM-containing adapter proteins DAP12 and the FcRγ chain in OC development; mice deficient in both the DAP12 and the FcRγ chain adapter were severely osteopetrotic (Koga et al., 2004; Mocsai et al., 2004). The fact that *Ninj1* deficiency only affects the viability of preOCs and that Ninj1 is dispensable for OC differentiation prompted me to investigate potent relationship between Ninj1 and ITAM-mediated signaling proteins. Regardless of M-CSF, tyrosine phosphorylation of Dap12 and its binding to Syk were elevated in *Ninj1*^{-/-} preOCs (Figure 30A). Furthermore, Ninj1 and Oscar, an FcRγ-associated ITAM receptor, bound successfully to each other (Figure 30B). These results suggest that Ninj1 might have a role in ITAM-mediated signaling as a co-stimulatory molecule and/or co-receptor for ITAM-associated receptor.
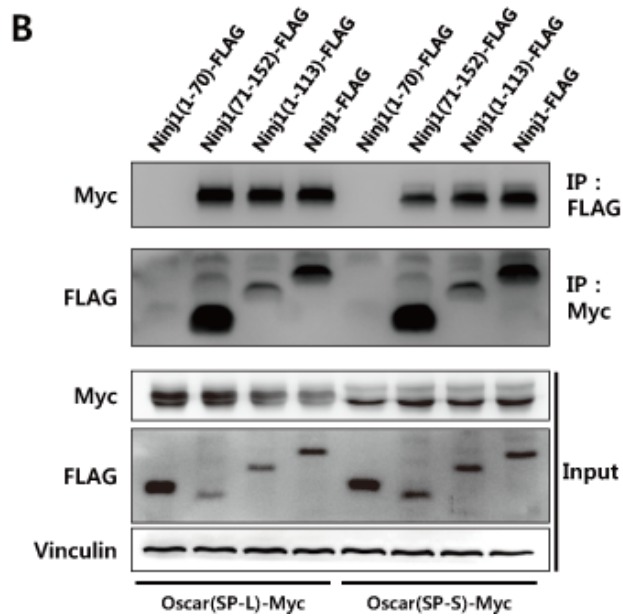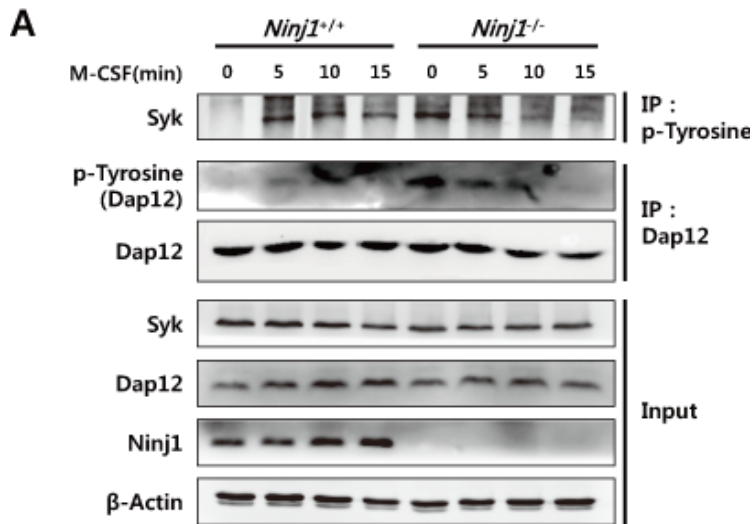
Figure 30. Analysis of the relationships between Ninj1 and ITAM-related signaling proteins.

(A) BMMs were cultured with M-CSF and RANKL for 3 days to differentiate into preOCs and cytokine-starved for 3 hours. Then, cells were re-stimulated with M-CSF and analyzed by immunoblot assay as indicated. (B) Intact or truncated Ninj1 and Oscar were simultaneously transduced into NIH3T3 cells using a retrovirus. Interactions between proteins were analyzed by immunoblot assay following co-immunoprecipitation as indicated.

19. Ninj1 possesses homophilic binding affinity

Ninj1 has been identified as a homophilic adhesion protein (Araki and Milbrandt, 1996), and interruption of Ninj1-mediated homophilic adhesion reduced leukocyte infiltration into EAE-induced lesion (Ahn et al., 2014b; Ifergan et al., 2011). Ninj1 interaction at the molecular level, however, has not been evaluated yet. Thus, to recapitulate Ninj1 homophilic interaction in *in vitro*, I examined Ninj1 homophilic property by co-immunoprecipitation. First, BMMs were transduced with FLAG-tagged Ninj1 and subjected to immunoprecipitation. Endogenous Ninj1 was successfully co-immunoprecipitated with ectopic Ninj1 (Figure 31A), and two different epitope-tagged Ninj1 were co-immunoprecipitated with one another in both case of human NINJ1 and mouse Ninj1 (Figure 31B,C). Furthermore, human and mouse Ninj1 were co-immunoprecipitated with each other (Figure 31D), suggesting that the Ninj1 interaction is conserved between species. As expected, sequence alignment of mouse Ninj1 with human NINJ1 revealed that Ninj1 is highly conserved in human and mouse (Figure 31E; identity, 89.5%; homology, 95.4%). These data suggest that the homophilic property of Ninj1 is conserved.

A

Vector   Ninj1-FLAG

IP : FLAG
IB : Ninj1   → Ninj1-FLAG
  → endogenous Ninj1

IP : FLAG
IB : FLAG

FLAG
Ninj1   Input
β-actin

B

GFP-Ninj1   +   mo   +
FLAG-Ninj1   mo   +   +

GFP   IP : GFP
FLAG

GFP   IP : FLAG
FLAG

GFP   Input
FLAG
Vinculin

C

GFP-NINJ1   +   mo   +
FLAG-NINJ1   mo   +   +

GFP   IP : GFP
FLAG

GFP   IP : FLAG
FLAG

GFP   Input
FLAG
Vinculin

D

GFP-Ninj1   Ms   mo   Ms   Hu   mo   Hu   Hu   mo   Hu   Ms   mo   Ms
FLAG-Ninj1   mo   Hu   Hu   mo   Hu   Hu   mo   Ms   Ms   mo   Ms   Ms

mo: mock vector
Hu: human NINJ1
Ms: mouse Ninj1

GFP   IP : GFP
FLAG

GFP   IP : FLAG
FLAG

GFP   Input
FLAG
Vinculin

E

```
sp|O70131|NINJ1_MOUSE   MESGTEEYELNGDLRPGSPGSPDALPPRWGLRNRPINVNHYANKKSAAESMLDIALLMAN   60
sp|Q92982|NINJ1_HUMAN   MDSGTEEYELNGGLPPGTPGSPDASPARWGWRHGPINVNHYASKKSAAESMLDIALLMAN   60
                        *:************.* **:******* * *** *: ******* *************

sp|O70131|NINJ1_MOUSE   ASQLKAVVEQGNDFAFFVPLVVLISISLVLQIGVGVLLIFLVKYDLNNPAKHAKLDFLNN   120
sp|Q92982|NINJ1_HUMAN   ASQLKAVVEQGPSFAFYVPLVVLISISLVLQIGVGVLLIFLVKYDLNNPAKHAKLDFLNN   120
                        *********** .***:***********************************

sp|O70131|NINJ1_MOUSE   LATGLVFIIVVVNIFITAFGVQKPVMDVAPRQ   152
sp|Q92982|NINJ1_HUMAN   LATGLVFIIVVVNIFITAFGVQKPLMDMAPQQ   152
                        ***********************:**:**:*
```

Figure 31. Recapitulation of Ninj1 homophilic interaction in *in vitro*.

  (A) Ninj1-FLAG was retrovirally transduced into BMMs. Co-immunoprecipitation of endogenous Ninj1 with anti-FLAG antibody was analyzed by immunoblot assay. (B) GFP-Ninj1 and FLAG-Ninj1 were co-transfected into HEK293T cells as indicated. Co-immunoprecipitation of each recombinant Ninj1s was analyzed by immunoblot assay. (C) GFP-NINJ1 and FLAG-NINJ1 were co-transfected into HEK293T cells as indicated. Co-immunoprecipitation of each recombinant NINJ1s was analyzed by immunoblot assay. (D) GFP- and FLAG-tagged human and mouse Ninj1 (NINJ1) were co-transfected into HEK293T cells as indicated. Co-immunoprecipitation of each recombinant Ninj1 (NINJ1) was analyzed by immunoblot assay. (E) Amino acid sequences of human and mouse Ninj1 were aligned and analyzed using FASTA 36.3.8d. Identical amino acids are marked with an asterisk.

20. Ninj1 is a *cis*-interacting protein

To validate that Ninj1 forms a homomeric complex by *cis*-interaction on the same membrane in a single cell, I conducted a FRET assay with confocal microscope (Snapp and Hegde, 2006; Wouters and Bastiaens, 2001). Thus, CFP, YFP, CFP-fused YFP, CFP-Ninj1, and YFP-Ninj1 were transduced into NIH3T3 cells singly or in combination using a retrovirus, and FRET was analyzed by confocal microscopy (Figure 32). Photobleaching of YFP, an acceptor in the CFP-YFP FRET pair, restored CFP intensity in CFP-fused YFP, which was used as a FRET-positive control. CFP- and YFP-Ninj1 transduced cells also showed restoration of CFP intensity after photobleaching whereas this phenomenon was not observed in CFP and YFP doubly transduced cells (Figure 33A). To confirm FRET in living cells, the same FRET constructs were transduced into NIH3T3 cells using a retrovirus, and the cells were validated by FACS-based FRET analysis (Chan, 2004; Siegel et al., 2000). The FACS-determined FRET-positive frequency revealed that approximately 75% of Ninj1-transduced cells were FRET-positive (Figure 33B,C). These data suggest that Ninj1 is a *cis*-interacting protein and may exist as a homomer.
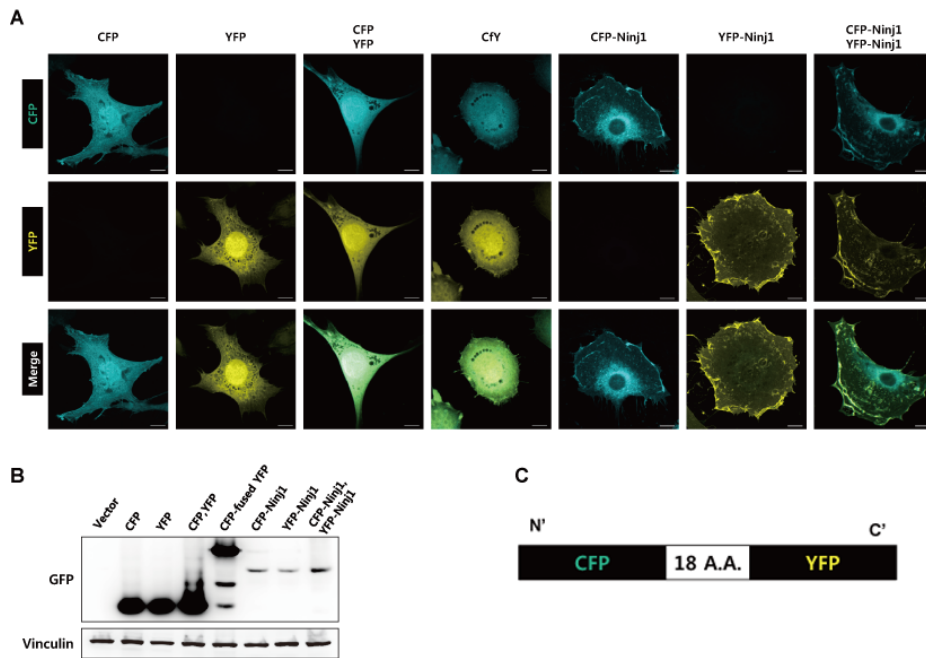
Figure 32. Construction of FRET expression vectors.

(A–B) CFP, YFP, CFP-fused YFP, CFP-Ninj1, and YFP-Ninj1 were singly or doubly transduced into NIH3T3 cells using a retrovirus as indicated. (A) Representative images of FRET vector-transduced cells by confocal microscopy, Scale bars, 10 μm. (B) FRET expression vectors were assessed by immunoblot assay. (C) Schematic diagram of CFP-fused YFP. N' and C' represent N- and C-terminus, respectively.
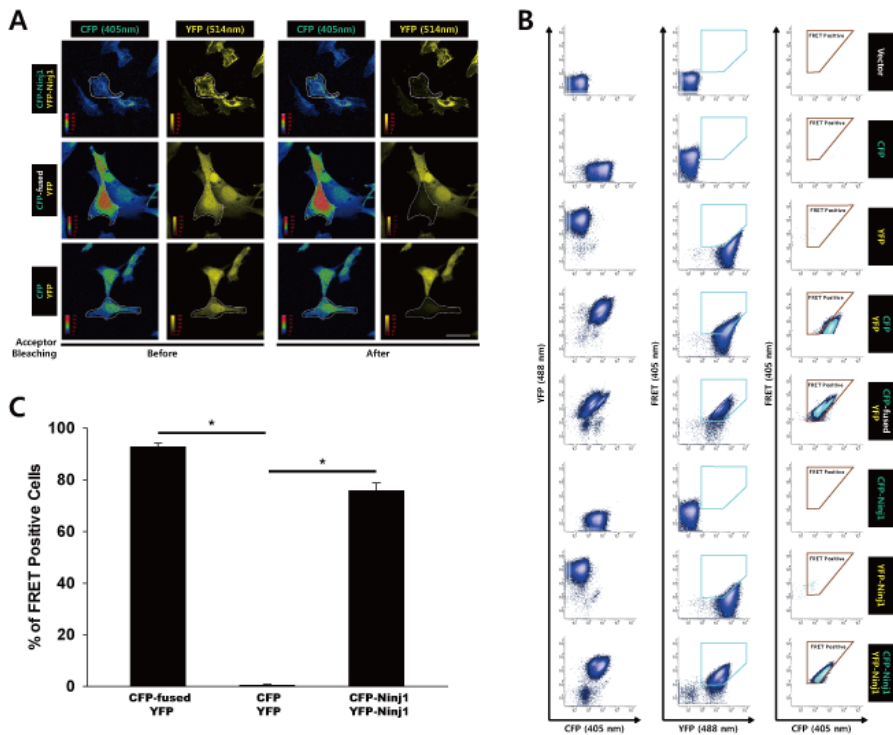
Figure 33. *cis*-Interaction of Ninj1 in single cells.

(A–C) CFP, YFP, CFP-fused YFP, CFP-Ninj1, and YFP-Ninj1 were singly or doubly transduced into NIH3T3 cells using a retrovirus as indicated. (A) Restoration of the CFP intensity by YFP bleaching was evaluated by confocal microscopy, Scale bar, 30 μm. (B) Representative plots of FRET assays by FACS. Cerulean and brown pentagonal gates were used to exclude false-FRET-positive cells by

YFP and CFP, respectively. (C) The percent frequency of FRET-positive cells determined by FACS are shown as the mean $\pm$ SD ($n = 4$), *$P < 0.05$.

21. Ninj1 assembles into a homomeric protein complex

Next, I hypothesized that Ninj1 assembles into a homomeric protein complex in living cells. To evaluate whether Ninj1 is present as a homomer and the number of Ninj1 composing the homomeric complex, proteins in living cells were covalently cross-linked with formaldehyde to stabilize the protein-protein interactions (Bruce, 2012; Klockenbusch and Kast, 2010). Bone marrow cells were isolated from WT and *Ninj1*^{-/-} mice and differentiated into BMMs, which express high levels of Ninj1. Next, the cells were incubated with formaldehyde and subjected to immunoprecipitation followed by immunoblot assay. Immunoprecipitants from formaldehyde cross-linked BMMs showed arithmetically increasing molecular weight-bearing Ninj1 homomers that were augmented by increasing the PFA concentration; these complexes were not present in *Ninj1*^{-/-} BMMs. Moreover, the highest molecular weight was approximately 120 kDa, which was suspected to be a hexameric homomer of Ninj1 (Figure 34A). To determine whether the Ninj1 homomer is present in other types of cells, liver and spleen derived from WT and *Ninj1*^{-/-} mice were dissociated as single cells and subjected to formaldehyde cross-linking. Formaldehyde cross-linked

hepatic and splenic cells showed similar Ninj1 homomers to those of BMMs (Figure 34B,C). Furthermore, exogenous Ninj1, FLAG- and Myc-Ninj1, transduced into NIH3T3 cells, a murine fibroblast cell line, also formed the homomeric Ninj1 complex (Figure 35). These data suggest that Ninj1 assembles into a homomeric protein complex and that the Ninj1 complex is not limited to specific types of cells.
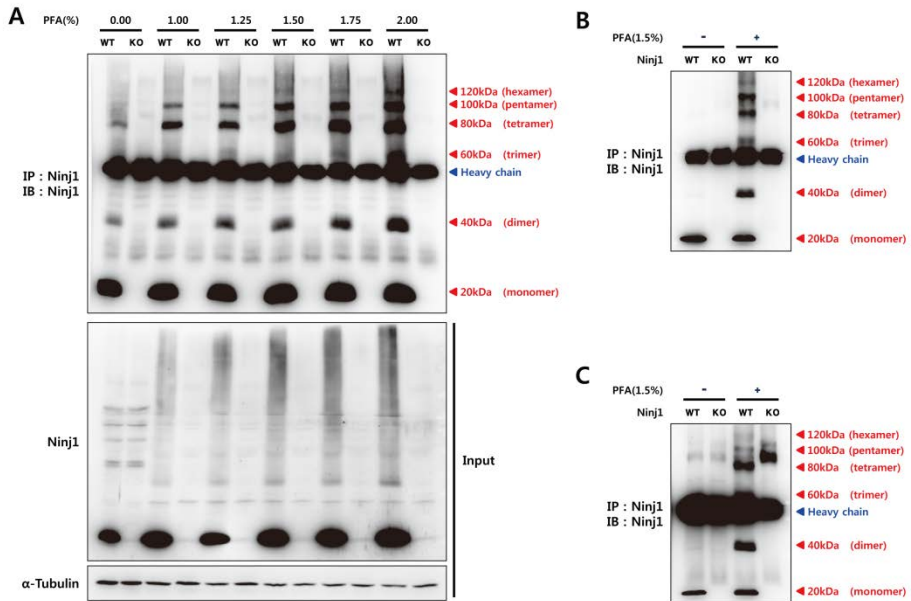
Figure 34. Identification of Ninj1 homomer in living cells.

(A–C) Single cells of BMMs (A), hepatic cells (B), and splenic cells (C) derived from WT and *Ninj1*^{-/-} mice (KO) were suspended and incubated for 30 minutes in PFA/PBS as indicated. Ninj1 homomeric complexes were isolated by immunoprecipitation and assessed by immunoblot assay. Ninj1 homomeric complexes including monomeric form were annotated in red. Heavy chains of antibodies used in immunoprecipitation were marked in blue.
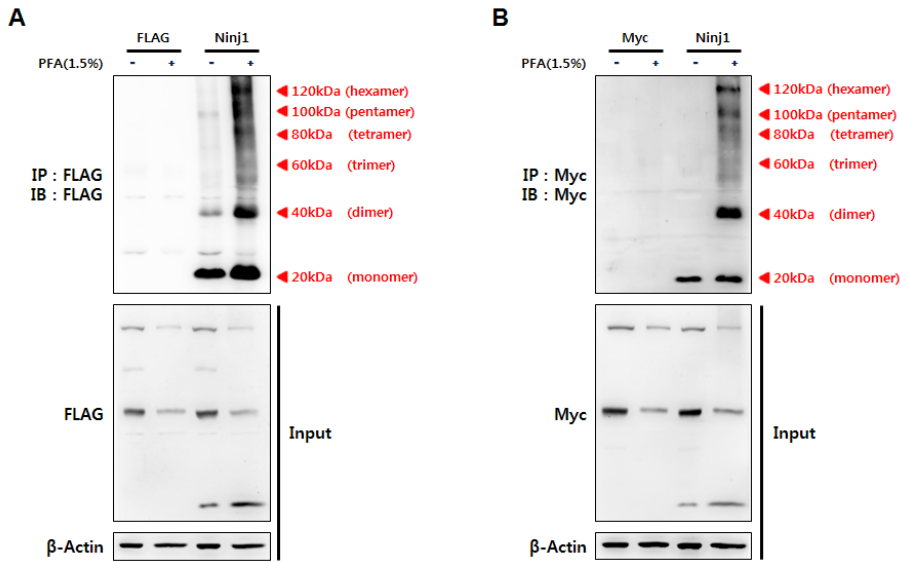
Figure 35. Exogenous Ninj1 assembles into a homomeric protein complex.

(A,B) FLAG-Ninj1 (A) or Myc-Ninj1 (B) was transduced into NIH3T3 cells using a retrovirus. Single cells of either transductants were cross-linked with 1.5% PFA. Ninj1 homomeric complex was immunoprecipitated and assessed by immunoblot assay as indicated.

22. Intracellular region of Ninj1 from Leu^{101} to Ala^{110} is required for Ninj1 assembly

To identify interacting interface(s) for Ninj1 homomer formation, I constructed truncated GFP-Ninj1 from the N-terminus and C-terminus and the established constructs were subjected to a co-immunoprecipitation assay. Deletion of N-terminus by Asn^{60} and C-terminus from Leu^{121} did not affect homophilic affinity, but deletion from Leu^{101} completely abolished binding affinity (Figure 36A). To define the interacting region more precisely, I prepared additional truncated GFP-Ninj1 constructs. GFP-Ninj1 Met^{1}–Phe^{100} still failed to bind with intact FLAG-Ninj1, whereas Met^{1}–Ala^{110} and Lys^{101}–Gln^{152} bound with not only intact FLAG-Ninj1 but also with Met^{1}–Ala^{110} fragmented FLAG-Ninj1 (Figure 36B,C). To evaluate whether Leu^{101}–Ala^{110} is indispensable for the Ninj1 interaction, I further constructed FLAG- and GFP-Ninj1 that contained a deletion from Leu^{101} to Ala^{110} and compared the binding affinity with that of intact Nin1. A co-immunoprecipitation assay revealed complete blockage of the Ninj1 homophilic interaction by deletion of this region (Figure 36D). These data suggest that Ninj1 assembly involves Leu^{101} to Ala^{110} and that this

region might be an isologous interacting interface.
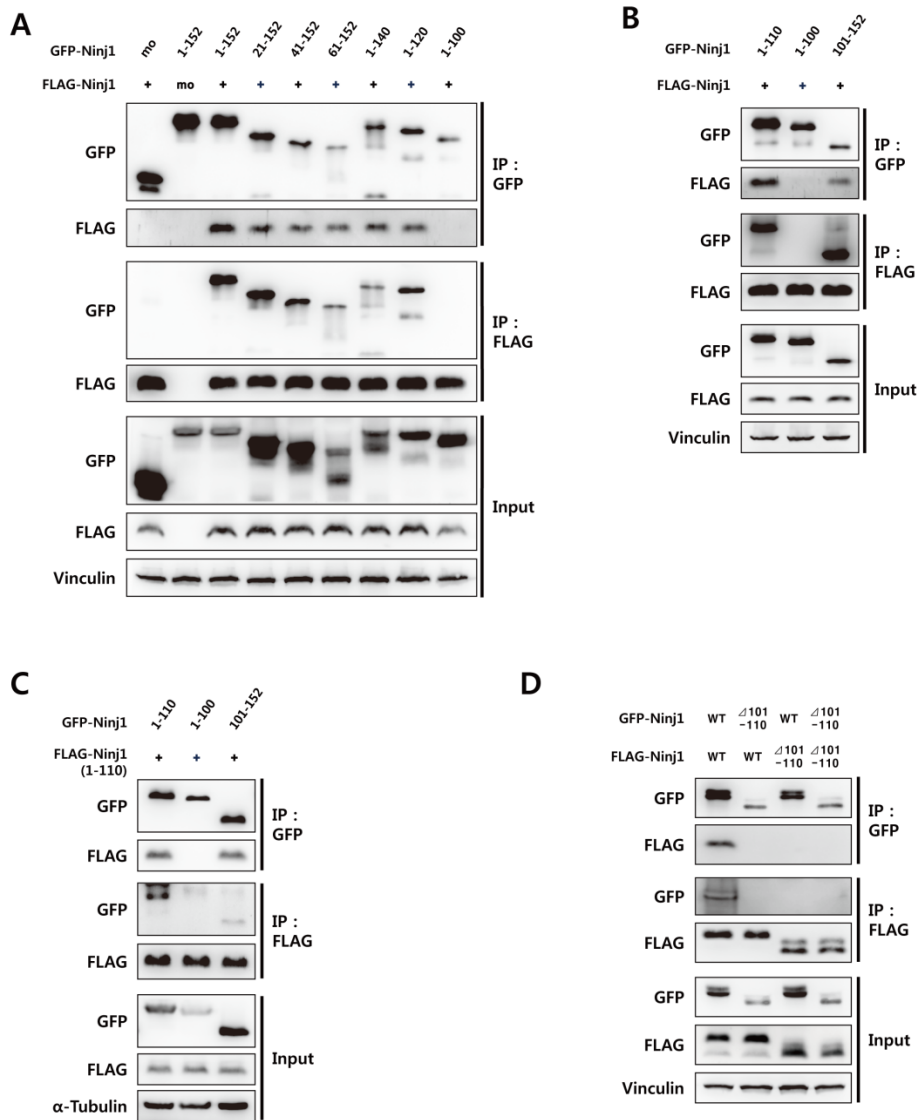
Figure 36. Determination of Ninj1 homomeric assembly region.

(A,B) N-terminus or C-terminus truncated Ninj1 fragments were fused

with GFP and co-transfected with intact FLAG-Ninj1 into HEK293T cells as indicated. Protein lysates were co-immunoprecipitated and analyzed by immunoblot assay. (C) C-terminus truncated FLAG-Ninj1 (1–110) were co-transfected with GFP-Ninj1 fragments into HEK293T cells as indicated. Protein binding was assessed by co-immunoprecipitation followed by immunoblot assay. (D) Leu[101] to Ala[110] deleted GFP- and FLAG-Ninj1 were co-transfected into HEK293T cells as indicated. Protein lysates were co-immunoprecipitated and analyzed by immunoblot assay.

23. Ninj1 is an *N*-linked glycosylated protein

Chadwick et al. (1998) reported that an *N*-glycosylation motif of Ninj1 is conserved in rodents and humans, and I further found that the *N*-glycosylation motif is highly conserved in vertebrates. Moreover, total 99 amino acids sequence carrying the *N*-glycosylation motif and intracellular interacting interface is highly conserved (Table 4). Thus, I evaluated Ninj1 molecular weight derived from various tissues and BMMs. Immunoblot assay revealed differential migration of each Ninj1 derived from different tissues (Figure 37A). To determine whether Ninj1 is *N*-glycosylated *in situ*, I cultured BMMs with tunicamycin, a GlcNAc transferase inhibitor that prevents *N*-glycosylation. Not only Ninj1 but also ICAM-1, which contains 10 *N*-glycosylation motifs, migrated more following incubation with tunicamycin (Figure 37B). To determine whether *N*-glycosylation on Asn[60] is the *N*-glycosylation consensus site, Gln- or Ala- substituted mutants were constructed. Immunoblot assays revealed that both mutants migrated more than WT Ninj1 (Figure 37C,D) and that the degrees of migration were similar to those of tunicamycin-treated WT Ninj1 (Figure 37E). These data demonstrate that Ninj1 is an *N*-

glycosylated protein.

Scientific name	Sequence
Homo sapience	HYASKKSAAESMLDIALLMA**NAS**QLKAVVEQGPSFAFYVPLVVLISISLVLQIGVGVLLIFLVKYDLNNPAKHAKLDFLNNLATGLVFIIVVVNIFITA
Macaca mulatta	HYANKKSAAESMLDIALLMA**NAS**QLKAVVEQGPSFAFYVPLVVLISISLALQIGVGVLLIFLVKYDLNNPAKHAKLDFLNNLATGLVFIIVVVNIFITA
Pan troglodytes	HYANKKSAAESMLDIALLMA**NAS**QLKAVVEQGPSFAFYVPLVVLISISLVLQIGVGVLLIFLVKYDLNNPAKHAKLDFLNNLATGLVFIIVVVNIFITA
Pongo abelii	HYANKKSAAESMLDIALLMA**NAS**QLKAVVEQGPSFAFYVPLVVLISISLALQIGVGVLLIFLVKYDLNNPAKHAKLDFLNNLATGLVFIIVVVNIFITA
Gorilla gorilla gorilla	HYANKKSAAESMLDIALLMA**NAS**QLKAVVEQGPSFAFYVPLVVLISISLALQISVGVLLIFLVKYDLNNPAKHAKLDFLNNLATGLVFIIVVVNIFITA
Mus musculus	HYANKKSAAESMLDIALLMA**NAS**QLKAVVEQGNDFAFFVPLVVLISISLVLQIGVGVLLIFLVKYDLNNPAKHAKLDFLNNLATGLVFIIVVVNIFITA
Rattus norvegicus	HYANKKSAAESMLDIALLMA**NAS**QLKAVVEQGNEFAFFVPLVVLISISLVLQIGVGVLLIFLVKYDLNNPAKHAKLDFLNNLATGLVFIIVVVNIFITA
Cavia porcellus	HYANKKSAAESMLDIALLMA**NAS**QLKAVVEQGPAFSFFVPLVVLISISLVLQIGVGVLLIFLVKYDLNNPAKHAKLDFLNNLATGLVFIIVVVNIFITA
Bos taurus	HYANKKSAAESMLDIALLMA**NAS**QLKAVIEQGPGFAFFIPLVVLISISLALQIAVGVLLIFLVRYDLNNPAKHAKLDFLNNLATGLVFIIVVVNIFITA
Canis lupus familiaris	HYANKKSAAESMLDIALLMA**NAS**QLKAVIEQGPSFTFFVPLVVLITISLALQIGVGVLLIFLVRYDLNNPAKHAKLDFLNNLATGLIFIIVVVNIFITA
Loxodonta africana	HYANKKSAAESMLDIALLMA**NAS**QLKAVIEQGPSFTFFVPLVVLISISLVLQVGVGVLLIFLVKYDLNNPAKHAKLDFLNNLATGLVFIIVVVNIFITA
Oryctolagus cuniculus	HYANKKSAAESMLDIALLMA**NAS**QLKAVVEQGPSFAFFVPLVVLISISLALQIGVGVLLIFLVKYDLNNPAKHAKLDFLNNLATGLVFVIVVVNIFITA
Capra hircus	HYANKKSAAESMLDIALLMP**NAS**QLKAVIEQGTGFAFVIPLVVLISISLVLQIGVGVLLIFLVRYALNNPAKHAKLDFPNTLATGLVFIIVVVNIFITA
Ovis aries	HYANKKSAAESMLDIALLMA**NAS**QLKAVIEQGTGFAFFIPLVVLISISLVLQIGVGVLLIFLVRYDLNNPAKHAKLDFLNNLATGLIFIIVVVNIFITA
Ailuropoda melanoleuca	HYANKKSAAESMLDIALLMA**NAS**QLKAVIEQGPGFAFFVPLVVLISISLVLQIGVGVLLIFLVRYDLNNPAKHAKLDFLNNLATGLVFIIVVVNIFITA
Equus caballus	HYANKKSAAESMLDIALLMA**NAS**QLKAVVEQGPSFAFFFPLVVLISISLLLQICVGVLLIFLVKYDLNNPAKHAKLDFLNNLATGLVFVIVVINIFITA
Felis catus	HYANKKSAAESMLDIALLMA**NAS**QLKAVIEQGPGFAFFVPLVVLISISLVLQIGVGVLLIFLVRYDLNNPAKHAKLDFLNNLATGLVFIIVVVNIFITA
Gallus gallus	HYANKKSAAESMLDIALLMA**NAS**QLKAVIEQGPSFSFYMPLIVLISLSLAMQIMVGVLLIFLVKYDLNNPAKHGKLDFLNNLATGLVFIIVVVNIFITA
Aptenodytes forsteri	HYANKKSAAESMLDIALLMA**NAS**QLKAVMEQGPSFSFYIPLIILISLSLTLQVMVGVLLIFLVKYDLNNPAKHGKLDFLNNLATGLVFIIVVVNIFITA
Alligator mississippiensis	HYANKKSAAESMLDIALLMA**NAS**QLKAVMEQGPSFSFYVPLIVLISMSLVLQVAVGVLLIFLVKYDLNNPAKHNKLDALNNVATGLVFIIVVV
Pelodiscus sinensis	HYANKKSAAESMLDIALLMA**NAS**QLKAVMEQGPSFSFYIPLIILISISLILQIGVGVLLIFLVKYDLNNPAKHAKLDFLNNLATGLVFIIVVVNIFITA
Anolis carolinensis	HYANKKSAAESMLDIALLMA**NAS**QLKAVMEQGPSFSFYIPLIVLISISLTLQVGVGVLLIFLVK ELKNPVKHAKLDFLNNLEQKGA KVVVVNIFITA
Xenopus tropicalis	HYANKKSVAESMLDVALLMA**NAS**QMKAVIDQGPSFSYYVPLLVLISISFVLQVIVGVLLIFIVKYDLNNPAKHYILDILENTATGLVFIIVVVNVLVTA
Danio rerio	HYANKKSAAESMLDIALLMA**NAS**QLKTVLELGPSFSFYIPLITLISISLTLQIIVGILLIFIVKWNLNDSSKHYILNLLENIVTALVFIVVVVNVFITA
Oreochromis niloticus	HYANKKSAAESMLD VALLMA**NAS**QLKAVMQQGPSFTFYVPLIILISISLTLQILVGVLLIFIVKWNLNDQRNHYRLDILENVTTAFVFIIVVINVFITA
Oryzias latipes	HYANKKSAAESMLDVALLMA**NAS**QLKAVMEQGPGFTFYVPLITLISISLILQILVGVMLIFIVKWNLNDQSTHYKLNVMENAATAFVFIIVVVNVFITA

Table 4. Conserved sequences of Ninj1 in vertebrates.

Highly conserved Ninj1 sequences in vertebrates contain the *N*-glycosylation motif and intracellular interacting interface from Leu[101] to Ala[110].
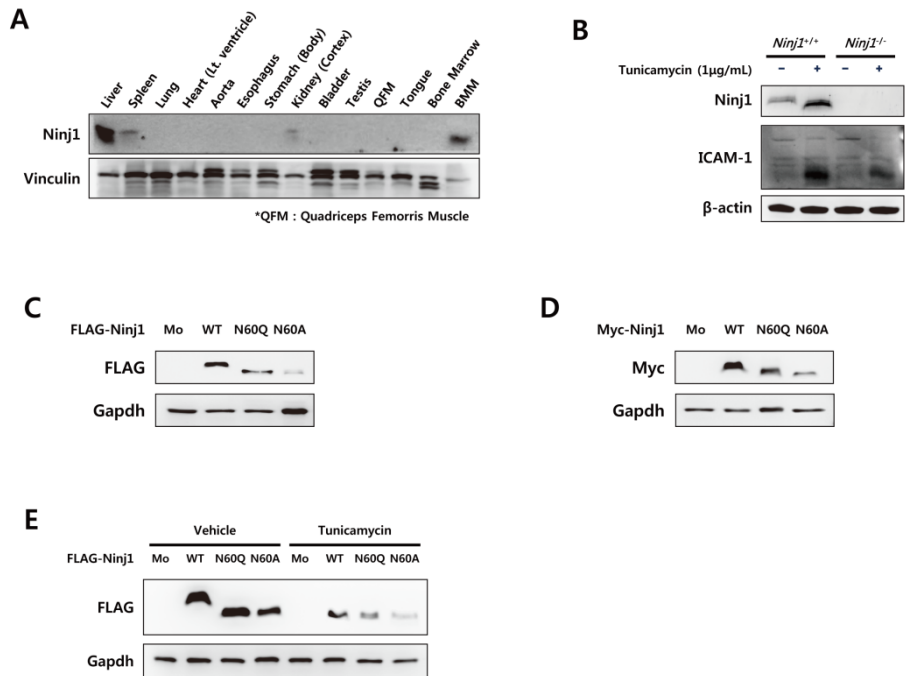
Figure 37. Ninj1 is an *N*-glycosylated protein.

(A) Protein lysates were isolated from indicated tissues, and Ninj1 expression was assessed by immunoblot assay. BMMs were used as Ninj1-positive control. (B) BMMs were cultured with tunicamycin for 24 hours and analyzed by immunoblot assay. *Ninj1*$^{-/-}$ BMMs were used as Ninj1-negative control and ICAM-1 was used as a positive control for *N*-glycosylation inhibition. (C,D) FLAG- and Myc-tagged WT and Asn^{60} mutant Ninj1 were transduced into NIH3T3 cells. Migration of

110

WT and Asn^{60} mutant Ninj1 was analyzed by immunoblot assay. (E) WT and Asn^{60} mutant FLAG-Ninj1 transduced NIH3T3 cells were cultured with tunicamycin for 24 hours and migrations of WT and Asn^{60} mutant FLAG-Ninj1 were analyzed by immunoblot assay.

24. *N*-glycosylation stabilizes the Ninj1 homomeric complex

Formaldehyde cross-linking assay revealed that Ninj1 assembles into a homo-oligomeric complex frequently than into a homo-dimeric complex. However, co-immunoprecipitation with truncated Ninj1 revealed a single homophilic interactive region suspected to be the isologous interaction interface. Trimer or additional oligomers should possess at least two interaction interfaces and more than one of those might be an isologous interaction interface (Levy and Teichmann, 2013). Recently, several groups have reported the role of *N*-glycosylation in protein assembly (Hassinen et al., 2011; Kim et al., 2010; Ryan et al., 2000; Wu et al., 2016). These findings together with the present results prompted me to investigate the involvement of *N*-glycosylation in Ninj1 homomeric complex formation. Thus, WT or Asn[60] mutant CFP- and YFP-Ninj1 were simultaneously transduced into NIH3T3 cells, and FRET-positive cells were analyzed by FACS (Figure 38A). Gln substitution resulted in a 5.9-fold reduction of FRET-positive cells and Ala substitution abrogated FRET similarly to in CFP- and YFP-transduced FRET-negative cells (Figure 38B). Finally, I

conducted formaldehyde cross-linking assays with WT and Asn[60] mutant Ninj1. Consistently with the results of FRET analysis, Ninj1 homomeric complex formation was impaired by Gln substitution, and the Ninj1[N60A] mutant failed to assemble into a homomeric protein complex (Figure 38C). These data suggest that *N*-glycosylation of Ninj1 is a prerequisite for homomeric complex formation.
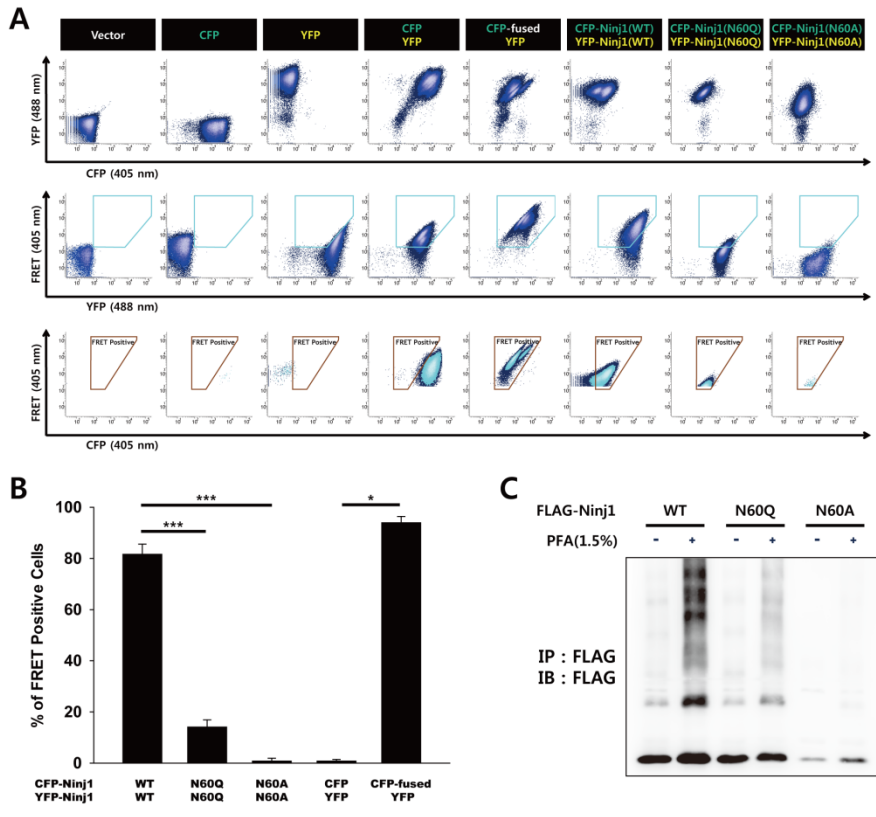
Figure 38. Abrogation of *N*-glycosylation disrupts Ninj1 homomer formation.

(A,B) WT or Asn[60] mutant CFP- and YFP-Ninj1 were simultaneously transduced into NIH3T3 cells using a retrovirus as indicated. (A) Representative plots of FRET assays by FACS. Cerulean and brown pentagonal gates were used to exclude false-FRET-positive cells by

YFP and CFP, respectively. (B) The percent frequency of FRET-positive cells determined by FACS are shown as the mean ± SD ($n = 4$), *$P < 0.05$, ***$P < 0.001$. (C) WT and Asn^{60} mutant FLAG-Ninj1 were transduced into NIH3T3 cells using a retrovirus. Transduced cells were incubated with 1.5% PFA for 30 minutes. Ninj1 homomers were isolated by immunoprecipitation and assessed by immunoblot assay.

25. *N*-glycosylation is important for Ninj1 trafficking and stability

A lot of evidences have been accumulated for regulatory role of *N*-glycosylation related to protein stability and trafficking (Haga et al., 2011; Imjeti et al., 2011; Moharir et al., 2013). To elucidate Ninj1 is the case, WT YFP-Ninj1 and Asn[60] mutants were transduced into NIH3T3 cells with or without WT CFP-Ninj1. WT YFP-Ninj1 normally localized onto plasma membrane. However, Asn[60] mutation impaired cell surface expression of Ninj1. Substantial amount of N60Q mutant still retained in the cytosolic compartment, and N60A mutant completely failed to localize onto plasma membrane (Figure 39 left). Interestingly, simultaneous expression of WT CFP-Ninj1 rescued improperly localized Asn60 mutants (Figure 39 right). Similar results were obtained for the protein stability. The expression levels of Asn[60] mutants were lower than WT (Figure 40A left, black bar in C). On the other hand, simultaneous expression of WT CFP-Ninj1 increased expression levels of Asn60 mutants similar to those of WT (Figure 40A right, white bar in C). Furthermore, amount of endogenous Ninj1 was enhanced by dose-dependent exogenous Ninj1 in RAW264.7 cells

(Figure 40C). Finally, to verify interactions between Ninj1 by partial abrogation of *N*-glycosylation, I revisited FACS-based FRET assay. Asn^{60} mutation of YFP-Ninj1 disturbed Ninj1 interaction partially, however, mutation in CFP-Ninj1 almost disrupted FRET in Ninj1 homomeric complex (Figure 41). These data suggest that Ninj1 homomeric complex formation by *N*-glycosylation improves the protein stability and is indispensable for cell surface expression of Ninj1.
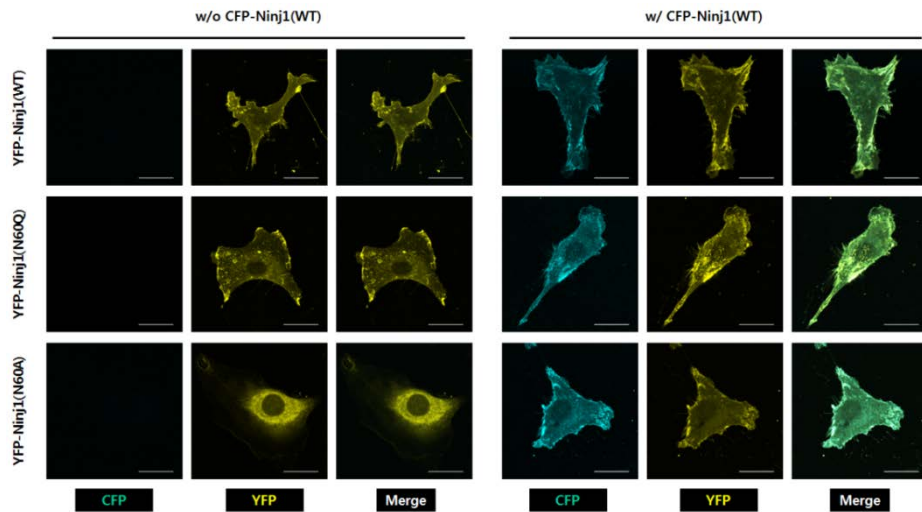
Figure 39. *N*-glycosylation of Ninj1 regulates trafficking onto plasma membrane.

WT or Asn[60] mutants YFP-Ninj1 was transduced into NIH3T3 cells with or without WT CFP-Ninj1 using a retrovirus as indicated. Localization of Ninj1 was analyzed by confocal microscopy. Scale bars, 20 μm.
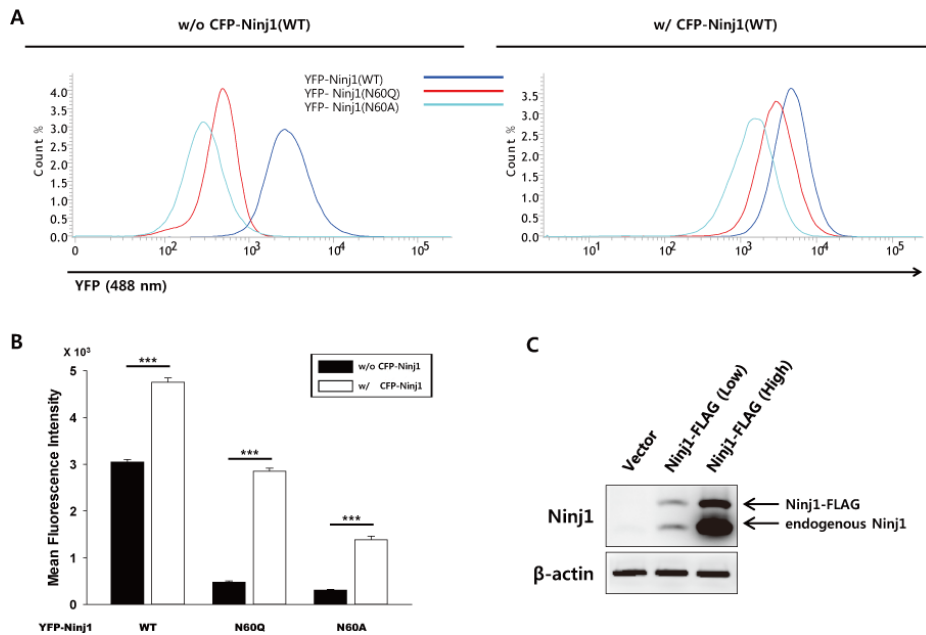
Figure 40. *N*-glycosylation of Ninj1 enhances protein stability.

(A,B) WT YFP-Ninj1 or Asn^{60} mutants were transduced into NIH3T3 cells with or without WT CFP-Ninj1 using a retrovirus as indicated. (A) Expressions of WT YFP-Ninj1 and Asn^{60} mutants were analyzed by FACS. (B) Mean fluorescence intensities of YFP-Ninj1 determined by FACS are shown as the mean ± SD. ***$P < 0.001$. (C) Ninj1-FLAG-IRES-GFP or IRES-GFP was transduced into RAW264.7 cells using a retrovirus. Then, cells were divided to two groups following GFP expression by FACS sorting, and expressions of endogenous Ninj1 and

Ninj1-FLAG were analyzed by immunoblot assay.

A

| CFP-Ninj1(WT) YFP-Ninj1(WT) | CFP-Ninj1(WT) YFP-Ninj1(N60Q) | CFP-Ninj1(WT) YFP-Ninj1(N60A) | CFP-Ninj1(N60Q) YFP-Ninj1(WT) | CFP-Ninj1(N60A) YFP-Ninj1(WT) |

B

Figure 41. Disruption of FRET by partial abrogation of *N*-glycosylation.

(A) WT or Asn^{60} mutant CFP- and YFP-Ninj1 were simultaneously transduced into NIH3T3 cells using a retrovirus as indicated. (A) Representative plots of FRET assays by FACS. Cerulean and brown pentagonal gates were used to exclude the false-FRET-positive cells by YFP and CFP, respectively. (B) The percent frequency of FRET-positive cells determined by FACS is shown as the mean ± SD, ***$P <$ 0.001.

Superior view　　**Oblique view**

Ninjurin1

Asn$_{60}$

N-linked oligosaccharide

Homophilic physical interaction
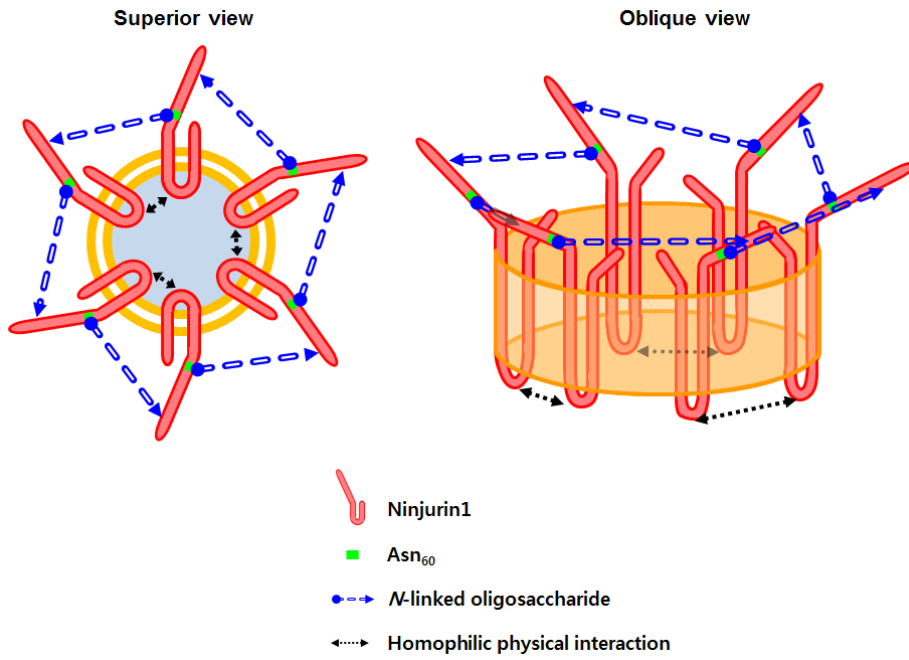
Figure 42. Schematic diagrams of Ninj1 homomer: in the case of homo-hexamer.

	Sample Ascertainment				Genotype Detail				Alleles	
ss#	Population	Individual Group	Chrom. Sample Cnt.	Source	G/G	G/T	T/T	HWP	G	T
ss115761672	YRI		2	IG		1.00000000			0.50000000	0.50000000
ss1334597404	EAS		1008	AF					0.12600000	0.87400001
	EUR		1006	AF					0.18990000	0.81009996
	AFR		1322	AF					0.37520000	0.62480003
	AMR		694	AF					0.12250000	0.87750000
	SAS		978	AF					0.16049999	0.83950001
ss143504239	ENSEMBL_Venter		2	IG		1.00000000			0.50000000	0.50000000
ss164438072	CEU	European	2	IG		1.00000000			0.50000000	0.50000000
ss165467351	YRI	Sub-Saharan African	2	IG		1.00000000			0.50000000	0.50000000
ss166690096	PGP		2	IG			1.00000000			1.00000000
ss1689552788	ExAc_Aggregated_Populations		121410	AF					0.19565110	0.80434889
ss200613142	BUSHMAN_POP		2	IG		1.00000000			0.50000000	0.50000000
	BANTU		2	IG		1.00000000			0.50000000	0.50000000
ss224338661	pilot_1_YRI_low_coverage_panel		118	AF					0.39830509	0.60169494
ss234886125	pilot_1_CEU_low_coverage_panel		120	AF					0.14166667	0.85833335
ss241647114	pilot_1_CHB+JPT_low_coverage_panel		120	AF					0.15833333	0.84166664
ss342276848	ESP_Cohort_Populations		4552	GF	0.07073814	0.33655536	0.59270650	0.00100000	0.23901582	0.76098418
ss491938805	CSAgilent		1317	GF	0.03300000	0.28400001	0.68300003	0.75183000	0.17500000	0.82499999
ss6540754	CEPH		184	AF					0.05000000	0.94999999
ss69296159	HapMap-CEU	European	120	IG	0.03333334	0.23333333	0.73333335	0.52708900	0.15000001	0.85000002
	HapMap-HCB	Asian	90	IG		0.15555556	0.84444445	1.00000000	0.07777778	0.92222220
	HapMap-JPT	Asian	90	IG	0.04444445	0.24444444	0.71111113	0.43857800	0.16666667	0.83333331
	HapMap-YRI	Sub-Saharan African	120	IG	0.10000000	0.58333331	0.31666666	0.09972100	0.39166668	0.60833335
ss76280954	ICMHP		6	IG			1.00000000			1.00000000
ss76894952	HapMap-CEU	European	226	IG	0.04424779	0.22123894	0.73451328	0.15022200	0.15486726	0.84513277
	HapMap-HCB	Asian	86	IG		0.16279070	0.83720928	1.00000000	0.08139535	0.91860467
	HapMap-JPT	Asian	172	IG	0.06976745	0.29069766	0.63953489	0.20032500	0.21511628	0.78488374
	HapMap-YRI	Sub-Saharan African	226	IG	0.13274336	0.47787610	0.38938054	1.00000000	0.37168142	0.62831861
	HAPMAP-ASW		98	IG	0.18367347	0.32653061	0.48979592	0.09972100	0.34693879	0.65306121
	HAPMAP-CHB	Asian	80	IG		0.07500000	0.92500001	1.00000000	0.03750000	0.96249998
	HAPMAP-CHD		170	IG	0.011764711	0.211764711	0.77647060	1.00000000	0.11764706	0.88235295
	HAPMAP-GIH		176	IG	0.01136364	0.29545453	0.69318181	0.34278200	0.15909091	0.84090906
	HAPMAP-LWK		180	IG	0.18888889	0.41111112	0.40000001	0.20032500	0.39444444	0.60555553
	HAPMAP-MEX		100	IG		0.16000000	0.83999997	1.00000000	0.08000000	0.92000002
	HAPMAP-MKK		286	IG	0.03496503	0.44755244	0.51748252	0.05004300	0.25874126	0.74125874
	HAPMAP-TSI		176	IG	0.07954545	0.40909091	0.51136363	1.00000000	0.28409091	0.71590906
	ENSEMBL_Watson		2	IG	1.00000000				1.00000000	
ss97812806	J. Craig Venter		2	IG		1.00000000			0.50000000	0.50000000

Figure 43. Population diversity regarding Ala[110] vs Asp[110].

SNP informations of A110D in human *NINJ1* (rs2275848) were downloaded from dbSNP in NCBI and listed.

124

| ss# | Sample Ascertainment | | | | Genotype Detail | | | | Alleles | |
	Population	Individual Group	Chrom. Sample Cnt.	Source	C/C ▬	C/T ▬	T/T ▬	HWP	C ▬	T ▬
ss1334597457	EAS		1008	AF						1.00000000
	EUR		1006	AF						1.00000000
	AFR		1322	AF					0.00530000	0.99470001
	AMR		694	AF					0.00140000	0.99859995
	SAS		978	AF						1.00000000
ss1689552841	ExAc_Aggregated_Populations		121412	AF					0.00068362	0.99931639
ss342276853	ESP_Cohort_Populations		4550	GF	0.00527473	0.99472529	1.00000000		0.00263736	0.99736261

Figure 44. Population diversity regarding Asn[60] vs Ser[60].

SNP informations of N60S in human *NINJ1* (rs140126462) were downloaded from dbSNP in NCBI and listed.

DISCUSSION

The current study investigated the role of Ninj1 in OC development and cell survival maintenance, providing the first evidence that Ninj1 is important for bone homeostasis by sustaining preOC survival. I show that Ninj1 is expressed in OCs differentiated from bone marrow cells but not in osteoblasts, and that OC and macrophage Ninj1 expression is comparable. Plain X-ray demonstrated strong hind limb intensity and linear rather than concave femur diaphysis in $Ninj1^{-/-}$ mice, which are novel signs of osteopetrosis (Whyte et al., 2008). microCT analysis further demonstrated increased femoral and tibial trabecular bone mass in $Ninj1^{-/-}$ mice, which was prolonged from 6- to 12-weeks. $Ninj1^{-/-}$ mice were reported to be small, have several skeletal deformities such as an asymmetric face or dome-shaped head, and often develop hydrocephalus (Ahn et al., 2014b; Cho et al., 2013), which is frequently developed in patients with autosomal recessive osteopetrosis (Del Fattore et al., 2008; Sobacchi et al., 2013). In addition, $Ninj1^{-/-}$ mice frequently exhibit vertebral column (kyphosis or scoliosis) and orbital bone (cyclopia) deformities and often show cycling behavior,

suggesting the possibility of defective ossicles and/or cochlea (unpublished observations). Collectively, these data suggest that Ninj1 might impact bone homeostasis by modulating OC development and/or function.

OCs accomplish bone resorption by several continuous processes: (1) OC progenitor/precursor cell development from hematopoietic stem cells, (2) OC precursor proliferation, (3) OC precursor differentiation into mononuclear preOCs, (4) preOCs fusion into multinucleated OCs, (5) attachment to calcified matrix and OC polarization followed by matrix degradation, and finally (6) death by apoptosis (Nakamura et al., 2012). The current data show that *Ninj1* deficiency reduces the number of TRAP$^+$ multinucleated OCs derived from bone marrow cells but does not impact differentiation into OCs as defined by OC marker expression, suggesting that *Ninj1* deficiency only minimally disrupts major OC differentiation signaling pathways such as MAPK, AP-1, NFκB, and NFATc1 (Lee and Kim, 2003). The reduction in mature OCs might, therefore, results from a decreased proportion or quality of OPCs in bone marrow, which are derived from hematopoietic stem cells that give rise to common lymphoid and myeloid progenitors in response to various factors (Akashi et al., 2000). Accordingly, M-CSF,

PU.1, MITF, and Bcl-2 mutation lead to osteopetrosis in mice consequential to reduced OPCs (Asagiri and Takayanagi, 2007). Specifically, $Csf1r^+c\text{-}Kit^+Cd11b^{dull}$ cells are potent bone marrow OPCs that effectively differentiate into OCs (Arai et al., 1999). However, $Csf1r^+c\text{-}Kit^+Cd11b^{dull}$ OPCs are clearly increased in *Ninj1*^{-/-} mice. Nonetheless, whereas previous report showed similar peripheral blood cell composition in *Ninj1*^{-/-} and WT mice by complete blood count, the differential count identified a trend toward myeloid cell increase including neutrophils (1.28-fold) and monocytes (1.33-fold) (Ahn et al., 2014b). Combined with the current observations, these data suggest that Ninj1 might instead have a potent role on myelopoiesis. Finally, the essential osteoclastogenic cytokines M-CSF and RANKL bind M-CSF receptor and RANK respectively on OC precursors and their targeted deletion leads to osteopetrosis in mice caused by OC differentiation failure (Dai et al., 2002; Dougall et al., 1999; Li et al., 2000). However, the current data show that Csf1r, Rank, and Cd11b expressions in BMMs are indistinguishable between genotypes indicating that *Ninj1*^{-/-} OC precursor cells develop normally from myeloid progenitors and implying that *Ninj1* deficiency might affect a later stage of osteoclastogenesis.

OC precursors, exposed to M-CSF and RANKL, differentiate into mononuclear preOCs followed by mononuclear cell fusion to generate multinucleated OCs (Vignery, 2005). Disrupting cell fusion through genetic ablation of ATP6v0d2 or DC-STAMP, suspected to be involved in cell-cell recognition (Oursler, 2010), results in severe osteopetrosis in mice from multinucleated OC deficiency. As Ninj1 is a homophilic adhesion protein (Araki and Milbrandt, 1996), *Ninj1* deficiency might also disrupt cell-cell recognition and fusion. However, *Ninj1*^{-/-} BMMs fuse more efficiently than WT BMMs especially in the culture with GM-CSF + IL-4, suggesting that Ninj1 is dispensable for preOC fusion. Also, the frequency of multinucleated cells with actin ring cytoskeleton and the actin ring morphologies are indistinguishable between WT and *Ninj1*^{-/-} cells. Conversely, the area enclosed by the actin ring is significantly reduced in *Ninj1*^{-/-} OCs, suggesting that the participant mononuclear preOC numbers might be decreased by *Ninj1* deficiency prior to this stage. The significant reduction in TRAP activity in the *Ninj1*^{-/-} cell conditioned media but not lysate indicates that Ninj1 deletion might alter the cell population by modulating proliferation and/or survival.

Aberrant OC apoptosis leads to bone homeostasis dysregulation and

bone disease. OC apoptosis is lower in osteoporotic bone and evident in the late stage of Paget's bone disease, which manifests as sclerotic bone lesions (Mollazadeh et al., 2015). The current data revealed that *Ninj1* deficiency induces Caspase-9-dependent intrinsic apoptosis in both primary and RAW264.7 cells in a cell-autonomous manner. Ninj1 reduction accompanied apoptotic features in WT preOCs and Ninj1 overexpression in RAW264.7 cells reduced this spontaneous apoptosis in osteoclastogenic culture. Thus, during osteoclastogenesis, the Ninj1 level influences preOC survival with deficiency exacerbating apoptosis. Conversely, loss of Ninj1 in BMMs accelerates M-CSF-induced cell proliferation. The novel role of Ninj1 in OC/macrophage precursor cell propagation needs to be elucidated.

Recently, a protective role of Ninj1 against different types of cell death was reported. Ninj1 inhibited p53-dependent cellular senescence by reducing p53 translation, potentially regulated by mechanistic targeting of rapamycin (mTOR) kinase (Cho et al., 2013). M-CSF and RANKL promoted OC survival through mTOR kinase via down-regulating Bim expression as a downstream effector of PI3K (Glantschnig et al., 2003). Conversely, p53 inhibited mTOR, resulting in suppression of cell survival (Loayza-Puch et al., 2013). Furthermore,

$p53^{-/-}$ mice exhibit increased OC number and bone resorption (Wang et al., 2006). Thus, Ninj1 might potentially enhance preOC survival by intervening in the p53-mTOR kinase crosstalk. Considering its role as a c-Jun-regulated anti-apoptotic gene, apoptosis was induced by Ninj1 down-regulation in triple-negative breast cancer cells and further accelerated by TNF-α, whereas Ninj1 overexpression ameliorated TNF-α-induced apoptosis in c-Jun knockdown cells (Qiao et al., 2016). Consistently, these data support the protective role of Ninj1 against various types of cell death.

Decreased OC apoptosis is implicated in destructive bone diseases such as RA and osteoporosis (Roux and Brown, 2009). The current data show that increased Ninj1 expression ameliorates spontaneous apoptosis during osteoclastogenesis in RAW264.7 cells and that high *NINJ1* expression correlates with the above disorders. Thus, incremental Ninj1 might play a detrimental role in destructive bone disorders as well as in other pathologic conditions as previously mentioned such as diabetes mellitus (Yin et al., 2014). Accordingly, *NINJ1* is associated with insulin insensitivity and type 2 diabetes incidence in African Americans (Sharma et al., 2016). In humans, diabetes elicits several metabolic and endocrine alterations that result in

osteoporosis (Vestergaard, 2007), and streptozotocin induces osteoporosis following the occurrence of diabetes in mice (Peng et al., 2016). Therefore, an investigation of the precise role of NINJ1 in bone homeostasis in metabolic diseases such as diabetes might yield new insights into the systemic regulation of bone metabolism.

The hallmark of OCs is their unique ability to resorb mineralized calcium apatite or carbonate substrates in bone (Saltel et al., 2008). In the current study, however, I primarily focused on the role of Ninj1 in OC development. In *Ninj1*$^{-/-}$ mice used for the current investigations, *Ninj1* is ubiquitously deleted so that during *in vitro* OC differentiation, most *Ninj1*$^{-/-}$ cells dropped out and a few mature OCs remained. The failure to provide mature OCs rendered defining the role of Ninj1 in those cells difficult. Accordingly, stage-specific *Ninj1* deletion might extend current findings to mature OCs.

To illuminate Ninj1-mediated cell signaling, the current study instead investigated the Ninj1 molecular property of biochemical and biophysical, providing the noble findings that Ninj1 assembles into a homomeric complex and that the intracellular region encompassing Leu^{101} to Ala^{110} and *N*-glycosylation on Asn^{60} are two interaction interfaces (Figure 42). Furthermore, *N*-glycosylation is important for

regulating stability and plasma membrane sorting of Ninj1.

Previous studies have focused on homophilic interaction of Ninj1 between cells (Lee et al., 2010), known as the *trans*-interaction (Held and Mariuzza, 2011). However, many transmembrane proteins assemble into homomers by lateral or *cis*-interaction on the same membrane which appears to play a crucial role in the clustering of proteins (Held and Mariuzza, 2011). Analysis of the Protein Data Bank of Transmembrane Proteins suggests that approximate 65% of membrane proteins are obligate oligomers (Tusnady et al., 2005) and have more than one membrane-spanning subunit (Levy et al., 2006). The present study therefore investigated Ninj1 homomer formation via its *cis*-interaction using FRET, formaldehyde cross-linking, and immunoprecipitation in living cells. Moreover, the Ninj1 homomeric complex was found in various types of cells including macrophages, hepatic cells, splenic cells, and the murine fibroblast cell line NIH3T3.

Protein-Protein interaction have been studied by three major categorized methods: *in vivo*, *in vitro*, and *in silico* methods (Rao et al., 2014). Among them, I investigated Ninj1 homomer formation by FRET, (co-)immunoprecipitation, and formaldehyde cross-linking which are classified into *in vivo*, *in vitro*, and *in vivo* and *in vitro* combined tools,

respectively. I first identified one of interacting interfaces, Leu[101] to Ala[110], in a protein-fragment complementation assay combined with co-immunoprecipitation (Michnick et al., 2011). In the FRET assay using the CFP-YFP pair, Förster distance was measured to be approximately 4.9 nm (Hochreiter et al., 2015; Vogel et al., 2014); thus these results suggest that Ninj1 molecules are located in closer proximity to one another following *N*-glycosylation which evoke FRET phenomenon.

Another versatile method to define protein-protein interaction is covalent cross-linking in intact cells using a chemical cross-linker (Bruce, 2012), and formaldehyde is one of the shortest available cross-linkers in intact living cells (2.3–2.7 Å) (Sutherland et al., 2008). I used a relatively lower PFA concentration (1–2%) and shorter reaction times (30 minutes) to reduce the artificial protein oligomerization. As a result, I identified Ninj1 homomer from a dimer to a hexamer in various types of cells by formaldehyde cross-linking. The number of subunits in a homomeric membrane protein complex varies from a dimer to more than an octamer (Forrest, 2015), and these results show that Ninj1 homomer is composed of six monomeric Ninj1 molecules at least.

Numerous studies demonstrated the regulatory role of *N*-glycosylation in protein stability and trafficking (Haga et al., 2011;

Imjeti et al., 2011; Moharir et al., 2013). These results revealed that *N*-glycosylation in Ninj1 also has two regulatory roles of protein stability and trafficking. Recently, the role of *N*-glycosylation has been extended to protein assembly (Kim et al., 2010; Wu et al., 2016), and Moh et al. (2016) reported that site-specific *N*-glycosylation determines the pentameric or hexameric assembly of recombinant human IgM. The current results revealed that both of endogenous and exogenous Ninj1 are *N*-glycosylated. For the *cis*-interaction, abrogation of *N*-glycosylation significantly reduced Ninj1 homomer formation, suggesting the indispensable role of *N*-glycosylation in the Ninj1 homomeric protein complex. However, it remains unclear whether *N*-glycan mediates carbohydrate–carbohydrate or carbohydrate–peptide interactions. Identification of sugar moieties in Ninj1 would resolve this issue.

I further found that amino acid sequences of Ninj1 are highly conserved not only between rodents and humans, but also in vertebrates (Table 4). Based on the highly conserved Ninj1 amino acid sequences in vertebrate that cover two interacting interfaces, Leu[101] to Ala[110] and an *N*-glycosylation motif, it is likely that the function and molecular properties of the protein are conserved. Diabetes and leprosy were

found to be associated with an Ala[110] single nucleotide polymorphism (SNP) of NINJ1 in humans (Cardoso et al., 2007; Graca et al., 2012; Sharma et al., 2016). Specifically, leprosy patients who carried the Asp[110] SNP (rs2275848, Figure 43) had a lower risk of developing a disability than patients with Ala[110]. Based on the present results and the high homology in vertebrates including human and mouse, that discrepancy might result from dysregulated Ninj1 homomer formation. Moreover, a missense SNP of N60S (rs140126462, Figure 44), an *N*-glycosylation motif, was reported, and I am currently investigating the effects of both SNPs in NINJ1 homomeric complex formation and its related biological function(s).

This work has provided several novel findings. First, Ninj1 is expressed in OCs but not in osteoblasts and *Ninj1*^{-/-} mice show mild osteopetrosis. Second, *Ninj1* deficiency reduces multinucleated OC numbers. Third, *Ninj1*^{-/-} preOCs are vulnerable to Caspase-9-dependent intrinsic apoptosis. Finally, high *NINJ1* expression correlates with human bone disorders such as RA and postmenopausal osteoporosis. Regarding to Ninj1 molecular property, Ninj1 assembles into a homomeric protein complex composed of six monomeric Ninj1 molecules, and the intracellular region of Ninj1 encompassing Leu[101] to

Ala^{110} is important for Ninj1 assembly. Furthermore, Ninj1 is an *N*-glycosylated protein and the *N*-glycosylation is a prerequisite for homomer formation. These findings suggest that Ninj1 plays an important role in bone homeostasis by enhancing the survival of preOCs and might represent a potent therapeutic target for destructive bone disorders. Moreover, targeting of *N*-glycosylation in Ninj1 might be a regulatory strategy for modulation of Ninj1 function(s).

The current investigations have illuminated a novel function of Ninj1 in bone homeostasis and the molecular property. These findings provide a foundation for further studies to elucidate the novel role(s) of Ninj1 in human being.

REFERENCES

Ahn, B.J., Le, H., Shin, M.W., Bae, S.J., Lee, E.J., Lee, S.Y., Yang, J.H., Wee, H.J., Cha, J.H., Seo, J.H.*, et al.* (2014a). Ninjurin1 enhances the basal motility and transendothelial migration of immune cells by inducing protrusive membrane dynamics. J Biol Chem *289*, 21926-21936.

Ahn, B.J., Le, H., Shin, M.W., Bae, S.J., Lee, E.J., Wee, H.J., Cha, J.H., Lee, H.J., Lee, H.S., Kim, J.H.*, et al.* (2014b). Ninjurin1 deficiency attenuates susceptibility of experimental autoimmune encephalomyelitis in mice. J Biol Chem *289*, 3328-3338.

Ahn, B.J., Lee, H.J., Shin, M.W., Choi, J.H., Jeong, J.W., and Kim, K.W. (2009). Ninjurin1 is expressed in myeloid cells and mediates endothelium adhesion in the brains of EAE rats. Biochem Biophys Res Commun *387*, 321-325.

Akashi, K., Traver, D., Miyamoto, T., and Weissman, I.L. (2000). A clonogenic common myeloid progenitor that gives rise to all myeloid lineages. Nature *404*, 193-197.

Arai, F., Miyamoto, T., Ohneda, O., Inada, T., Sudo, T., Brasel, K., Miyata, T., Anderson, D.M., and Suda, T. (1999). Commitment and differentiation of osteoclast precursor cells by the sequential expression of c-Fms and receptor activator of nuclear factor κB (RANK) receptors. J Exp Med *190*, 1741-1754.
Araki, T., and Milbrandt, J. (1996). Ninjurin, a novel adhesion molecule, is induced by nerve injury and promotes axonal growth. Neuron *17*, 353-361.

Araki, T., Zimonjic, D.B., Popescu, N.C., and Milbrandt, J. (1997). Mechanism of Homophilic Binding Mediated by Ninjurin, a Novel Widely Expressed Adhesion Molecule. J Biol Chem *272*, 21373-21380.

Asagiri, M., and Takayanagi, H. (2007). The molecular understanding of osteoclast differentiation. Bone *40*, 251-264.

Banning, C., Votteler, J., Hoffmann, D., Koppensteiner, H., Warmer, M., Reimer, R., Kirchhoff, F., Schubert, U., Hauber, J., and Schindler, M. (2010). A flow cytometry-based FRET assay to identify and analyse protein-protein interactions in living cells. PLoS One *5*, e9344.

Boyle, W.J., Simonet, W.S., and Lacey, D.L. (2003). Osteoclast differentiation and activation. Nature *423*, 337-342.

Broussard, J.A., Rappaz, B., Webb, D.J., and Brown, C.M. (2013). Fluorescence resonance energy transfer microscopy as demonstrated by measuring the activation of the serine/threonine kinase Akt. Nat Protoc *8*, 265-281.

Bruce, J.E. (2012). In vivo protein complex topologies: sights through a cross-linking lens. Proteomics *12*, 1565-1575.

Cardoso, C.C., Martinez, A.N., Guimaraes, P.E., Mendes, C.T., Pacheco, A.G., de Oliveira, R.B., Teles, R.M., Illarramendi, X., Sampaio, E.P., Sarno, E.N., *et al.* (2007). Ninjurin 1 asp110ala single nucleotide polymorphism is associated with protection in leprosy nerve damage. J Neuroimmunol *190*, 131-138.

Chadwick, B.P., Heath, S.K., Williamson, J., Obermayr, F., Patel, L., Sheer, D., and Frischauf, A.-M. (1998). The Human Homologue of theninjurinGene Maps to the Candidate Region of Hereditary Sensory Neuropathy Type I (HSNI). Genomics *47*, 58-63.

Chan, F.K.-M. (2004). Monitoring molecular interactions in living cells using flow cytometric analysis of fluorescence resonance energy transfer. Methods Mol Biol *261*, 371-381.

Cho, S.J., Rossi, A., Jung, Y.S., Yan, W., Liu, G., Zhang, J., Zhang, M., and Chen, X. (2013). Ninjurin1, a target of p53, regulates p53 expression and p53-dependent cell survival, senescence, and radiation-induced mortality. Proc Natl Acad Sci U S A *110*, 9362-9367.

Currey, J.D. (2013). Bones: Structure and Mechanics (Princeton University Press).

Dai, X.-M., Ryan, G.R., Hapel, A.J., Dominguez, M.G., Russell, R.G., Kapp, S., Sylvestre, V., and Stanley, E.R. (2002). Targeted disruption of the mouse colony-stimulating factor 1 receptor gene results in osteopetrosis, mononuclear phagocyte deficiency, increased primitive progenitor cell frequencies, and reproductive defects. Blood *99*, 111-120.

Del Fattore, A., Capariello, A., and Teti, A. (2008). Genetics, pathogenesis and complications of osteopetrosis. Bone *42*, 19-29.

Dobson, C.M. (2003). Protein folding and misfolding. Nature *426*, 884-890.

Dougall, W.C., Glaccum, M., Charrier, K., Rohrbach, K., Brasel, K., De Smedt, T., Daro, E., Smith, J., Tometsko, M.E., and Maliszewski, C.R. (1999). RANK is essential for osteoclast and lymph node development. Gene Dev *13*, 2412-2424.

Edwards, J.R., and Mundy, G.R. (2011). Advances in osteoclast biology: old findings and new insights from mouse models. Nat Rev Rheumatol *7*, 235-243.

Forrest, L.R. (2015). Structural Symmetry in Membrane Proteins. Annu Rev Biophys *44*, 311-337.

Fujita, K., Iwasaki, M., Ochi, H., Fukuda, T., Ma, C., Miyamoto, T., Takitani, K., Negishi-Koga, T., Sunamura, S., Kodama, T.*, et al.* (2012). Vitamin E decreases bone mass by stimulating osteoclast fusion. Nat Med *18*, 589-594.

Garrido, C., and Kroemer, G. (2004). Life's smile, death's grin: vital functions of apoptosis-executing proteins. Curr Opin Cell Biol *16*, 639-646.

Gartner, L.P., and Hiatt, J.L. (2001). Color Textbook of Histology (W.B. Saunders).

Glantschnig, H., Fisher, J., Wesolowski, G., Rodan, G., and Reszka, A. (2003). M-CSF, TNFα and RANK ligand promote osteoclast survival

by signaling through mTOR/S6 kinase. Cell Death Differ *10*, 1165-1177.

Graca, C.R., Paschoal, V.D., Cordeiro-Soubhia, R.M., Tonelli-Nardi, S.M., Machado, R.L., Kouyoumdjian, J.A., and Baptista Rossit, A.R. (2012). NINJURIN1 single nucleotide polymorphism and nerve damage in leprosy. Infect Genet Evol *12*, 597-600.

Haga, Y., Ishii, K., and Suzuki, T. (2011). N-glycosylation is critical for the stability and intracellular trafficking of glucose transporter GLUT4. J Biol Chem *286*, 31320-31327.

Hassinen, A., Pujol, F.M., Kokkonen, N., Pieters, C., Kihlstrom, M., Korhonen, K., and Kellokumpu, S. (2011). Functional organization of Golgi N- and O-glycosylation pathways involves pH-dependent complex formation that is impaired in cancer cells. J Biol Chem *286*, 38329-38340.

Held, W., and Mariuzza, R.A. (2011). Cis-trans interactions of cell surface receptors: biological roles and structural basis. Cell Mol Life Sci *68*, 3469-3478.

Hochreiter, B., Garcia, A.P., and Schmid, J.A. (2015). Fluorescent proteins as genetically encoded FRET biosensors in life sciences. Sensors (Basel) *15*, 26281-26314.

Humphrey, M.B., Lanier, L.L., and Nakamura, M.C. (2005). Role of ITAM-containing adapter proteins and their receptors in the immune system and bone. Immunol Rev *208*, 50-65.

Ifergan, I., Kebir, H., Terouz, S., Alvarez, J.I., Lecuyer, M.A., Gendron, S., Bourbonniere, L., Dunay, I.R., Bouthillier, A., Moumdjian, R.*, et al.* (2011). Role of Ninjurin-1 in the migration of myeloid cells to central nervous system inflammatory lesions. Ann Neurol *70*, 751-763.

Imjeti, N.S., Lebreton, S., Paladino, S., De La Fuente, E., Gonzalez, A., and Zurzolo, C. (2011). N-Glycosylation instead of cholesterol mediates oligomerization and apical sorting of GPI-APs in FRT cells. Mol Biol Cell *22*, 4621-4634.

Iwasaki, R., Ninomiya, K., Miyamoto, K., Suzuki, T., Sato, Y., Kawana, H., Nakagawa, T., Suda, T., and Miyamoto, T. (2008). Cell fusion in osteoclasts plays a critical role in controlling bone mass and osteoblastic activity. Biochem Biophys Res Commun *377*, 899-904.

Jennewein, C., Sowa, R., Faber, A.C., Dildey, M., von Knethen, A., Meybohm, P., Scheller, B., Drose, S., and Zacharowski, K. (2015). Contribution of Ninjurin1 to Toll-like receptor 4 signaling and systemic inflammation. Am J Respir Cell Mol Biol *53*, 656-663.

Kühner, S., van Noort, V., Betts, M.J., Leo-Macias, A., Batisse, C., Rode, M., Yamada, T., Maier, T., Bader, S., and Beltran-Alvarez, P. (2009). Proteome organization in a genome-reduced bacterium. Science *326*, 1235-1240.

Kim, H., Kang, H., Jang, M., Chang, J.H., Miao, Y., Jiang, L., and Hwang, I. (2010). Homomeric interaction of AtVSR1 is essential for its function as a vacuolar sorting receptor. Plant Physiol *154*, 134-148.

Klockenbusch, C., and Kast, J. (2010). Optimization of formaldehyde cross-linking for protein interaction analysis of non-tagged integrin beta1. J Biomed Biotechnol *2010*, 927585.

Koga, T., Inui, M., Inoue, K., Kim, S., Suematsu, A., Kobayashi, E., Iwata, T., Ohnishi, H., Matozaki, T., and Kodama, T. (2004). Costimulatory signals mediated by the ITAM motif cooperate with RANKL for bone homeostasis. Nature *428*, 758-763.

Kroemer, G., Galluzzi, L., Vandenabeele, P., Abrams, J., Alnemri, E.S., Baehrecke, E.H., Blagosklonny, M.V., El-Deiry, W.S., Golstein, P., Green, D.R.*, et al.* (2009). Classification of cell death: recommendations of the Nomenclature Committee on Cell Death 2009. Cell Death Differ *16*, 3-11.

Layfield, R. (2007). The molecular pathogenesis of Paget disease of bone. Expert Rev Mol Med *9*, 1-13.

Lee, H.J., Ahn, B.J., Shin, M.W., Choi, J.H., and Kim, K.W. (2010).

Ninjurin1: a potential adhesion molecule and its role in inflammation and tissue remodeling. Mol Cells *29*, 223-227.

Lee, H.J., Ahn, B.J., Shin, M.W., Jeong, J.W., Kim, J.H., and Kim, K.W. (2009). Ninjurin1 mediates macrophage-induced programmed cell death during early ocular development. Cell Death Differ *16*, 1395-1407.

Lee, Z.H., and Kim, H.-H. (2003). Signal transduction by receptor activator of nuclear factor kappa B in osteoclasts. Biochemical and biophysical research communications *305*, 211-214.

Levy, E.D., Pereira-Leal, J.B., Chothia, C., and Teichmann, S.A. (2006). 3D complex: a structural classification of protein complexes. PLoS Comput Biol *2*, e155.

Levy, E.D., and Teichmann, S. (2013). Structural, evolutionary, and assembly principles of protein oligomerization. Prog Mol Biol Transl Sci *117*, 25-51.

Li, J., Sarosi, I., Yan, X.-Q., Morony, S., Capparelli, C., Tan, H.-L., McCabe, S., Elliott, R., Scully, S., and Van, G. (2000). RANK is the intrinsic hematopoietic cell surface receptor that controls osteoclastogenesis and regulation of bone mass and calcium metabolism. Proc Natl Acad Sci U S A *97*, 1566-1571.

Loayza-Puch, F., Drost, J., Rooijers, K., Lopes, R., Elkon, R., and Agami, R. (2013). p53 induces transcriptional and translational programs to suppress cell proliferation and growth. Genome Biol *14*, R32.

Long, F. (2012). Building strong bones: molecular regulation of the osteoblast lineage. Nat Rev Mol Cell Biol *13*, 27-38.

Makras, P., Delaroudis, S., and Anastasilakis, A.D. (2015). Novel therapies for osteoporosis. Metabolism *64*, 1199-1214.

Marie, P.J. (2008). Transcription factors controlling osteoblastogenesis. Arch Biochem Biophys *473*, 98-105.

Marsh, J.A., and Teichmann, S.A. (2014). Protein flexibility facilitates quaternary structure assembly and evolution. PLoS Biol *12*, e1001870.

Marsh, J.A., and Teichmann, S.A. (2015). Structure, dynamics, assembly, and evolution of protein complexes. Annu Rev Biochem *84*, 551-575.

Michnick, S.W., Ear, P.H., Landry, C., Malleshaiah, M.K., and Messier, V. (2011). Protein-fragment complementation assays for large-scale analysis, functional dissection and dynamic studies of protein–protein interactions in living cells. Methods Mol Biol *756*, 395-425.

Mochizuki, A., Takami, M., Kawawa, T., Suzumoto, R., Sasaki, T., Shiba, A., Tsukasaki, H., Zhao, B., Yasuhara, R., Suzawa, T.*, et al.* (2006). Identification and Characterization of the Precursors Committed to Osteoclasts Induced by TNF-Related Activation-Induced Cytokine/Receptor Activator of NF- B Ligand. J Immunol *177*, 4360-4368.

Mocsai, A., Humphrey, M.B., Van Ziffle, J.A., Hu, Y., Burghardt, A., Spusta, S.C., Majumdar, S., Lanier, L.L., Lowell, C.A., and Nakamura, M.C. (2004). The immunomodulatory adapter proteins DAP12 and Fc receptor gamma-chain (FcRgamma) regulate development of functional osteoclasts through the Syk tyrosine kinase. Proc Natl Acad Sci U S A *101*, 6158-6163.

Moh, E.S., Lin, C.-H., Thaysen-Andersen, M., and Packer, N.H. (2016). Site-Specific N-Glycosylation of Recombinant Pentameric and Hexameric Human IgM. J Am Soc Mass Spectr *27*, 1-13.

Moharir, A., Peck, S.H., Budden, T., and Lee, S.Y. (2013). The role of N-glycosylation in folding, trafficking, and functionality of lysosomal protein CLN5. PLoS One *8*, e74299.

Mollazadeh, S., Fazly Bazzaz, B.S., and Kerachian, M.A. (2015). Role of apoptosis in pathogenesis and treatment of bone-related diseases. J Orthop Surg Res *10*, 15.

Moore, K.L., Dalley, A.F., and Agur, A.M.R. (2013). Clinically Oriented Anatomy (Wolters Kluwer Health).

Nakamura, I., Takahashi, N., Jimi, E., Udagawa, N., and Suda, T. (2012). Regulation of osteoclast function. Mod Rheumatol *22*, 167-177.

Nooren, I.M.A., and Thornton, J.M. (2003). Structural Characterisation and Functional Significance of Transient Protein–Protein Interactions. J Mol Biol *325*, 991-1018.

Oursler, M.J. (2010). Recent advances in understanding the mechanisms of osteoclast precursor fusion. J Cell Biochem *110*, 1058-1062.

Park, J.H., Seo, J.H., Wee, H.J., Vo, T.T., Lee, E.J., Choi, H., Cha, J.H., Ahn, B.J., Shin, M.W., Bae, S.J.*, et al.* (2014). Nuclear translocation of hARD1 contributes to proper cell cycle progression. PLoS One *9*, e105185.

Park, K.H., Park, B., Yoon, D.S., Kwon, S.-H., Shin, D.M., Lee, J.W., Lee, H.G., Shim, J.-H., Park, J.H., and Lee, J.M. (2013). Zinc inhibits osteoclast differentiation by suppression of Ca 2+-Calcineurin-NFATc1 signaling pathway. Cell Commun Signal *11*, 74.

Peng, J., Hui, K., Hao, C., Peng, Z., Gao, Q.X., Jin, Q., Lei, G., Min, J., Qi, Z., Bo, C.*, et al.* (2016). Low bone turnover and reduced angiogenesis in streptozotocin-induced osteoporotic mice. Connect Tissue Res, 1-13.

Perica, T., Marsh, J.A., Sousa, F.L., Natan, E., Colwell, L.J., Ahnert, S.E., and Teichmann, S.A. (2012). The emergence of protein complexes: quaternary structure, dynamics and allostery. Biochem Soc T *40*, 475-491.

Qiao, Y., He, H., Jonsson, P., Sinha, I., Zhao, C., and Dahlman-Wright, K. (2016). AP-1 Is a Key Regulator of Proinflammatory Cytokine TNFalpha-mediated Triple-negative Breast Cancer Progression. J Biol Chem *291*, 5068-5079.

Rao, V.S., Srinivas, K., Sujini, G.N., and Kumar, G.N. (2014). Protein-protein interaction detection: methods and analysis. Int J Proteomics *2014*, 147648.

Riedl, J., Crevenna, A.H., Kessenbrock, K., Yu, J.H., Neukirchen, D., Bista, M., Bradke, F., Jenne, D., Holak, T.A., Werb, Z.*, et al.* (2008). Lifeact: a versatile marker to visualize F-actin. Nat Methods *5*, 605-607.

Rosen, C.J., Ackert-Bicknell, C., Rodriguez, J.P., and Pino, A.M. (2009). Marrow Fat and the Bone Microenvironment: Developmental, Functional, and Pathological Implications. Crit Rev Eukaryot Gene Expr *19*, 109-124.

Roux, S., and Brown, J.P. (2009). Osteoclast apoptosis in rheumatic diseases characterized by a high level of bone resorption (osteoporosis, rheumatoid arthritis, myeloma and Paget's disease of bone). Curr Rheumatol Rev *5*, 98-110.

Rutkovskiy, A., Stensløkken, K.-O., and Vaage, I.J. (2016). Osteoblast Differentiation at a Glance. Med Sci Monit Basic Res *22*, 95-106.

Ryan, M.C., Notterpek, L., Tobler, A.R., Liu, N., and Shooter, E.M. (2000). Role of the Peripheral Myelin Protein 22 N-Linked Glycan in Oligomer Stability. J Neurochem *75*, 1465-1474.

Saltel, F., Chabadel, A., Bonnelye, E., and Jurdic, P. (2008). Actin cytoskeletal organisation in osteoclasts: a model to decipher transmigration and matrix degradation. Eur J Cell Biol *87*, 459-468.

Saltel, F., Chabadel, A., Zhao, Y., Lafage-Proust, M.H., Clezardin, P., Jurdic, P., and Bonnelye, E. (2006). Transmigration: a new property of mature multinucleated osteoclasts. J Bone Miner Res *21*, 1913-1923.

Sato, K., and Takayanagi, H. (2006). Osteoclasts, rheumatoid arthritis, and osteoimmunology. Curr Opin Rheumatol *18*, 419-426.

Schagger, H. (2006). Tricine-SDS-PAGE. Nat Protoc *1*, 16-22.

Sharma, N.K., Sajuthi, S.P., Chou, J.W., Calles-Escandon, J., Demons,

J., Rogers, S., Ma, L., Palmer, N.D., McWilliams, D.R., Beal, J.*, et al.* (2016). Tissue-Specific and Genetic Regulation of Insulin Sensitivity-Associated Transcripts in African Americans. J Clin Endocrinol Metab *101*, 1455-1468.

Shin, M.W., Bae, S.J., Wee, H.J., Lee, H.J., Ahn, B.J., Le, H., Lee, E.J., Kim, R.H., Lee, H.S., Seo, J.H.*, et al.* (2016). Ninjurin1 regulates lipopolysaccharide-induced inflammation through direct binding. Int J Oncol *48*, 821-828.

Siegel, R.M., Chan, F., Zacharias, D.A., Swofford, R., Holmes, K.L., Tsien, R.Y., and Lenardo, M.J. (2000). Measurement of molecular interactions in living cells by fluorescence resonance energy transfer between variants of the green fluorescent protein. Sci STKE *38*, L1.

Snapp, E.L., and Hegde, R.S. (2006). Rational design and evaluation of FRET experiments to measure protein proximities in cells. Curr Protoc Cell Biol, 17.19.11-17.19.20.

Sobacchi, C., Schulz, A., Coxon, F.P., Villa, A., and Helfrich, M.H. (2013). Osteopetrosis: genetics, treatment and new insights into osteoclast function. Nat Rev Endocrinol *9*, 522-536.

Steele, D.G., and Bramblett, C.A. (1988). The Anatomy and Biology of the Human Skeleton (Texas A&M University Press).

Sutherland, B.W., Toews, J., and Kast, J. (2008). Utility of formaldehyde cross-linking and mass spectrometry in the study of protein-protein interactions. J Mass Spectrom *43*, 699-715.

Teitelbaum, S.L. (2007). Osteoclasts: what do they do and how do they do it? Am J Pathol *170*, 427-435.

Teitelbaum, S.L. (2011). The osteoclast and its unique cytoskeleton. Ann N Y Acad Sci *1240*, 14-17.

Tusnady, G.E., Dosztanyi, Z., and Simon, I. (2005). PDB_TM: selection and membrane localization of transmembrane proteins in the protein data bank. Nucleic Acids Res *33*, D275-D278.

Vestergaard, P. (2007). Discrepancies in bone mineral density and fracture risk in patients with type 1 and type 2 diabetes--a meta-analysis. Osteoporos Int *18*, 427-444.

Vignery, A. (2005). Macrophage fusion: the making of osteoclasts and giant cells. J Exp Med *202*, 337-340.

Vogel, S.S., van der Meer, B.W., and Blank, P.S. (2014). Estimating the distance separating fluorescent protein FRET pairs. Methods *66*, 131-138.

Wang, X., Kua, H.Y., Hu, Y., Guo, K., Zeng, Q., Wu, Q., Ng, H.H., Karsenty, G., de Crombrugghe, B., Yeh, J.*, et al.* (2006). p53 functions as a negative regulator of osteoblastogenesis, osteoblast-dependent osteoclastogenesis, and bone remodeling. J Cell Biol *172*, 115-125.

Watanabe, C., Morita, M., Hayata, T., Nakamoto, T., Kikuguchi, C., Li, X., Kobayashi, Y., Takahashi, N., Notomi, T., and Moriyama, K. (2014). Stability of mRNA influences osteoporotic bone mass via CNOT3. Proc Natl Acad Sci U S A *111*, 2692-2697.

Whyte, M.P., McAlister, W.H., Novack, D.V., Clements, K.L., Schoenecker, P.L., and Wenkert, D. (2008). Bisphosphonate-induced osteopetrosis: novel bone modeling defects, metaphyseal osteopenia, and osteosclerosis fractures after drug exposure ceases. J Bone Miner Res *23*, 1698-1707.

Wouters, F.S., and Bastiaens, P.I. (2001). Imaging Protein-Protein Interactions by Fluorescence Resonance Energy Transfer (FRET) Microscopy. Curr Protoc Cell Biol, 17.11.11-17.11.15.

Wu, Z.L., Zhou, H., Ethen, C.M., and V, N.R. (2016). Core-6 fucose and the oligomerization of the 1918 pandemic influenza viral neuraminidase. Biochem Biophys Res Commun *473*, 524-529.

Xing, L., Xiu, Y., and Boyce, B.F. (2012). Osteoclast fusion and regulation by RANKL-dependent and independent factors. World J Orthop *3*, 212-222.

Yagi, M., Ninomiya, K., Fujita, N., Suzuki, T., Iwasaki, R., Morita, K., Hosogane, N., Matsuo, K., Toyama, Y., Suda, T.*, et al.* (2007). Induction of DC-STAMP by alternative activation and downstream signaling mechanisms. J Bone Miner Res *22*, 992-1001.

Yin, G.N., Choi, M.J., Kim, W.J., Kwon, M.H., Song, K.M., Park, J.M., Das, N.D., Kwon, K.D., Batbold, D., Oh, G.T.*, et al.* (2014). Inhibition of Ninjurin 1 restores erectile function through dual angiogenic and neurotrophic effects in the diabetic mouse. Proc Natl Acad Sci U S A *111*, E2731-E2740.

Yu, M., Moreno, J.L., Stains, J.P., and Keegan, A.D. (2009). Complex regulation of tartrate-resistant acid phosphatase (TRAP) expression by interleukin 4 (IL-4): IL-4 indirectly suppresses receptor activator of NF-kappaB ligand (RANKL)-mediated TRAP expression but modestly induces its expression directly. J Biol Chem *284*, 32968-32979.

Zou, W., Zhu, T., Craft, C.S., Broekelmann, T.J., Mecham, R.P., and Teitelbaum, S.L. (2010). Cytoskeletal dysfunction dominates in DAP12-deficient osteoclasts. J Cell Sci *123*, 2955-2963.

Zuo, C., Huang, Y., Bajis, R., Sahih, M., Li, Y.P., Dai, K., and Zhang, X. (2012). Osteoblastogenesis regulation signals in bone remodeling. Osteoporos Int *23*, 1653-1663.

요약 (국문초록)

Ninjurin1은 세포막 단백질로 좌골신경 손상 시 신경세포와 신경집세포에서 발현이 처음 확인되었고, 염증상황에서 대식세포와 수지상세포의 이동과 부착에 관여하는 것으로 보고되었다. 하지만 대식세포 및 수지상세포와 동일한 골수계세포에 속하는 파골세포에서는 Ninjurin1의 발현과 기능이 알려지지 않았다. 본 연구에서는 뼈 형성에 중요한 두 가지 세포 중 파골세포에서는 Ninjurin1이 강하게 발현되나 조골세포에서는 발현이 거의 없는 것을 확인하였다. 또한 Ninjurin1은 파골세포의 분화과정 동안 발현량이 증감하는 역동성을 보였다. 그리고 *Ninjurin1* 결핍 마우스의 뼈를 영상의학적으로 분석하여 골석회화증이 발생하였음을 확인하였다. Ninjurin1이 뼈의 구성세포 중 파골세포에서 특이적으로 발현되는 점을 바탕으로 WT 마우스와 *Ninjurin1* 결핍 마우스의 골수세포에서 파골세포 분화를 유도하였을 때 Ninjurin1의 결핍이 파골세포의 발생을 저해함을 확인하였다.

하지만 파골세포의 분화 척도인 *Nfatc1*, *c-Fos*, *itgβ3*, *Oscar*, *Calcr* 등의 발현 정도는 차이가 없었으며, 다른 중요한 분화 과정인 세포이동, 세포결합, actin-ring 형성에서도 차이가 없었다. 대신 *Ninjurin1* 결핍 세포는 전파골세포 시기에 Capase-9을 경유하는 intrinsic apoptosis를 통해 사멸하였다. 또한 Ninjurin1을 과발현한 파골세포전구세포는 정상세포보다 생존능이 향상되었다. 이에 더하여 사람의 뼈질환과 *NINJURIN1*의 상관관계를 확인하기 위해 microarray 데이터를 생물정보학을 통해 분석하였고, 골감소 질환인 류마티스성 관절염과 폐경 후 골다공증에서 *NINJURIN1*의 발현이 증가 해 있음을 확인하였다. 다음으로 Ninjurin1에 의한 세포 내 신호전달기전을 규명하기 위한 첫 단초로써, Ninjurin1의 분자적 특성을 조사하였다. 선행연구에서 보고된 Ninjurin1의 자가친화성 (homophilic affinity)을 바탕으로 FRET (Förster resonance energy transfer) assay를 통해 세포 내에서 Ninjurin1 단백질은 서로 근접해 있음을 확인하였고, formaldehyde를 이용하여 동종다량체 (homomer)로 존재하는 것을 확인하였다.

또한 Ninjurin1의 세포질 영역 중 Leu^{101}에서 Ala^{110}의 아미노산 서열이 Ninjurin1의 동종다량체 형성에 중요하며, 60번 arsparagine 아미노산 잔기에 결합한 *N*-당 (*N*-glycosylation)이 Ninjurin1 동종다량체의 안정성에 기여하는 것을 확인하였다. 이러한 발견을 통하여 골다공증이나 류마티스성 관절염과 같은 골감소 질환의 치료에 Ninjurin1이 새로운 치료표적이 될 수 있으며, Ninjurin1의 동종다량체 형성을 저해함으로써 Ninjurin1의 기능을 억제할 수 있을 것으로 기대된다.

주 요 어 : **Ninjurin1; OC; apoptosis; osteopetrosis; bone destructive disorder; protein complex; homomer; *N*-glycosylation**

학 번 : **2011-30507**